TAMPEREEN TEKNILLINEN YLIOPISTO
TAMPERE UNIVERSITY OF TECHNOLOGY

Joonas Järvelä

Characterization of MgB_2 Superconductors in Conduction-Cooled Systems

Julkaisu 1252 • Publication 1252

Tampere 2014

Tampereen teknillinen yliopisto. Julkaisu 1252
Tampere University of Technology. Publication 1252

Joonas Järvelä

Characterization of MgB_2 Superconductors in Conduction-Cooled Systems

Thesis for the degree of Doctor of Science in Technology to be presented with due permission for public examination and criticism in Sähkötalo Building, Auditorium S1, at Tampere University of Technology, on the 7th of November 2014, at 12 noon.

Tampereen teknillinen yliopisto - Tampere University of Technology
Tampere 2014

ISBN 978-952-15-3387-7 (printed)
ISBN 978-952-15-3400-3 (PDF)
ISSN 1459-2045

Abstract

Superconductivity as a phenomenon was discovered over 100 years ago and the first commercially viable materials have been in use for over 50 years. Today, the truly commercial applications in medical imaging and scientific research are limited to operating temperatures near 4.2 K. However, the discovery of high temperature superconductivity in 1986, and the discovery of superconductivity in magnesium diboride, MgB_2, in 2001, have the potential for changing this. The high temperature superconductors have proven to be useful in many applications including electric machinery and power transfer. However, their wide spread application is in part limited by their steep price. This is not the case with MgB_2. The cheap and easy-to-manufacture material has been shown to be competitive at applications with low to medium strength magnetic fields at an elevated operation temperature of 20 K. The most important commercial application, the magnetic resonance imaging falls within this range. These elevated operation temperatures are cost-effectively reachable with conduction-cooling and mechanical cryorefrigerators, i.e. cryocoolers. Designing and engineering of such dry system requires different approaches than their liquid cooled predecessors. To support these activities, accurate and relevant measurement data on the superconductor properties under the proper operating conditions, is required.

In this thesis, I present the approaches, challenges and solutions for obtaining valid measurement data in a conduction-cooled measurement system, focusing on the measurements of the properties used in characterizing the superconductor performance. I show how measurements in conduction-cooled system differs from ones cooled with liquid or gaseous cryogens. I discuss the importance of a proper sample holder and present considerations on how to make one. While the physical components of the measurement system are important, acquiring valid results requires proper measurement procedures. I analyze the voltage-current characteristic measurement and show how the results are easily effected by improper procedures. I consider, how the quench initiation and propagation experiments are performed, and how the quench dy-

namics MgB_2 and high temperature superconductors differ from low temperature ones. To demonstrate the applicability of conduction-cooling, I present the design, construction and benchmarking a measurement system for determining the magnetization AC-losses in a superconductor.

Preface

It has now been eight years since I started working as a summer trainee/research assistant at the Department of Electromagnetics. Since then, I have written my master's thesis and received my M.Sc. degree, seen much of the change that the Universities in Finland have gone through and today the people from the former Department of Electromagnetics belong to Department of Electrical Engineering.

Now, as my work on this thesis nears its end, I look back and begin to understand the amount of work required for doing experimental research. During the years, I have learned a lot in the fields of cryogenics, superconductivity, electromagnetic modeling and thermal simulation. Also, experimental research often requires that the tests, experiments and sometimes even the measurement apparatus have to be constructed from scratch. Therefore, I have had the opportunity to educate myself on different fabrication methods and materials well suited for low-temperature experiments. I dare to say that I have learned much more than I expected when taking my first steps on this path. I am sure that the skills I have acquired and the knowledge I have obtained will greatly benefit me in my future quests.

I have had the privilege to work with many extraordinarily bright people in our Electromagnetics research group. This work would not have been possible without their guidance and support. I have always found someone who could help me when needed. The spirit and atmosphere of our group are something that is not found everywhere. It has been a great pleasure to work with people who express their thoughts and ideas clearly, who defend their points of view with good arguments, but who are willing to admit of being wrong when it is clearly pointed out. I think I could list here all the people I have worked with and find something to thank them for, but I fear that the list would be too long for the purpose of this preface. Instead, I will have to satisfy in naming only just a few people who have had the most impact on this thesis.

First, I would like to thank Dr. Antti Stenvall for all the guidance and su-

pervision he has provided. Prof. Lauri Kettunen and lecturer Risto Mikkonen, together with Antti, have made it possible for me to pursue my work without having to worry about financial issues. I also appreciate the work Lasse Söderlund and Maija-Liisa Paasonen have done in protecting me from bureaucratic details and keeping the day-to-day things flowing smoothly. The people of our workshop, namely Hannu Nieminen and Pekka Nousiainen, have my gratitude for constructing many of the gadgets I have used in my experiments. Aki is to be commended for being our resident sports enthusiast and conversation starter during coffee breaks. Leena has shared an office with me for several years and she has kindly worked as a proof reader and language police for most of my publications. To the rest of the people in our group, you have not been forgotten, but to prevent this from growing, I wish to thank you all collectively for all the advice you have given and for all the discussions we have had.

I wish to express my gratitude to Dr. Christian Lacroix and Dr. Bertrand Dutoit for pre-examinining my thesis. It is also an honour to have Dr. Dutoit and Dr. Mark Ainslie to donate their time to act as my opponents in the public examination.

Finally, I wish to thank those closest to me, my wife and my parents. My parents Taru and Vesa have given me a home where I could focus my energy on those things I felt were the most interesting. As a child, I always had plenty of food to eat, a large table to do my homework, and other projects, on, and a warm, safe bed to sleep in. I met my wife Marjo during these years of postgraduate studies. Even though she was not in my life during the early stages, she has been there for these strenuous final steps. For that, I am very grateful.

In Tampere, September 8, 2014

Joonas Järvelä

List of publications and author's contribution

Publication 1

Järvelä J, Stenvall, A and Mikkonen, R 2009
IEEE Trans. Appl. Supercond. **19** 3511
"Quench development at supercritical currents in low n-value superconductors"
doi:10.1109/TASC.2009.2018528

Publication 2

Järvelä J, Stenvall A, and Mikkonen R 2010
J. Phys.: Conf. Ser **234** 032026
"Common rectifier diodes in temperature measurement applications below 50 K"
doi:10.1088/1742-6596/234/3/032026

Publication 3

Järvelä J, Stenvall A, Mikkonen R and Rindfleisch M 2011
Cryogenics **51** 400
"Contact resistance simulations and measurements of MgB_2-MgB_2 lap joints"
doi:10.1016/j.cryogenics.2011.04.003

Publication 4

Järvelä J, Stenvall A and Mikkonen R 2013
IEEE Trans. Appl. Supercond. **23** 9500309
"Considerations for designing a conduction-cooled sample holder"
doi:10.1109/TASC.2012.2237511

Publication 5

Järvelä J, Stenvall A and Mikkonen R 2013
IEEE Trans. Appl. Supercond. **23** 9000305
"Common rectifier diodes in thermal stability characterization measurements"
doi:10.1109/TASC.2012.2231453

Publication 6

J. Järvelä, M. Lyly, A Stenvall, R. Juntunen, J. Šouc and R Mikkonen 2014 *IEEE Trans. Appl. Supercond.* Accepted for publication, August 20, 2014. "Design, fabrication and testing of a low AC-loss conduction-cooled cryostat for magnetization loss measurement apparatus"
doi:10.1109/TASC.2014.2357754

Author's contribution

I (later the author) have written all the text in the publications. The author did the simulations and computations for the all of publications, with the exception of **Publication 6** where the AC-loss computations were done by M. Lyly. The general computational model used in **Publication 1** was provided by A. Stenvall and modified to suit the specific situation by the author.

A. Stenvall and R. Mikkonen helped by proof reading and provided comments regarding the presentation of discussed topics. For **Publication 3** M. Rindfleisch provided the MgB_2 samples used in the experiments and helped in finalizing the presentation.

The author designed, prepared and performed all of the experiments and measurements in the publication with the following exceptions. For publication **Publication 6** M. Lyly designed the excitation coil geometry and provided support during the design process and J. Šouc provided the BSCCO sample and the reference measurement data used for benchmarking the system. Jyväskylä University was responsible for constructing the polycarbonate cryostat used in **Publication 6** based on the drawings provided by the author. R. Juntunen from Lappeenranta University of technology designed, constructed and tested the coil power supply used in **Publication 6**. The TUT Department of Electrical Engineering workshop, and its predecessor Protopaja, fabricated components, sample holders and modified existing devices as necessary.

Detailed author's contribution for each publication

Publication 1: The author designed and performed the measurements presented in the publication. Furthermore, I modified the existing 1D-quench simulation model constructed with COMSOL and MATLAB. I reprogrammed significant portions of the existing code to enable the study of operating above the critical current. I was also responsible for analyzing the results and writing

the publication.

Publication 2: The author provided the idea of studying the usability of common rectifier diodes as temperature sensors below 50 K. I was also responsible for designing and performing the forward voltage drop experiments at a conduction-cooled cryostat. For analyzing the transient response of the diode sensors, I developed a technique using a finite element method(FEM) model and a known temperature sensor as a reference. I implemented the computation tool in COMSOL and MATLAB. The author wrote all the text in the publication.

Publication 3: The author provided the idea of analyzing the lap-joint resistance with MgB_2 superconductors. I designed the experiment and performed the resistance measurements. The FEM-model used for computational evaluation of the situation was constructed by the author using COMSOL and MATLAB. A. Stenvall provided technical support in the laborious reparametrization of the model, but the implementation was done by the author. I wrote all the text in the publication including the appendix containing the explanation on the FEM-model reparametrization.

Publication 4: The author provided the idea for defining the key aspects in designing a conduction-cooled sample holder. I constructed the computational FEM-model used for analyzing the sample holder current and cooling contacts with COMSOL and MATLAB. Furthermore, I designed and performed the experiments for testing effects of different surface preparations and interface media on the resistance of pressed copper-copper joints. I also constructed the computational model used for producing the parameters accurately describing the performance of such joints in FEM simulations. I prepared and performed the critical current measurements required for accurately presenting the superconductor in the sample holder simulation. The author wrote all the text in the publication.

Publication 5: The author provided the idea for using the diode sensors presented in **Publication 2** in thermal stability measurements. I invented the method used in improving the transient response of the diode sensors. Also, I prepared and performed the experiments used for analyzing the transient response of the modified diodes, and designed and performed the experiment used for analyzing the effects of external magnetic field on diode sensor output. Furthermore, the author designed, prepared and performed the experiment used for demonstrating the feasibility of the diode sensor the thermal stability measurements. Also, I prepared and performed the critical current measurements required for the computational study of the sample tested with the experiments. The author constructed the 2D FEM-model for analyzing the

transient response of the diode sensors and the 1D FEM-model for evaluating the thermal stability of the superconducting sample used in the corresponding experiment. I wrote all the text in the publication.

Publication 6: The author designed the low AC-loss conduction-cooled cryostat. I also fabricated some of the sample holder components and wound the excitation coils together with M. Lyly and workshop specialist H. Nieminen. I fabricated the pressed cooling contacts for interfacing the flexible cooling cables with the sample holder and fabricated the flexible cooling cables together with M. Lyly. The author measured the eddy-current loss of the conduction-cooled cryostat, performed the benchmarking experiments and measured the magnetization losses for the MgB_2 conductor. The author wrote all the text in the publication, except the part covering the FEM-computations in Section V subsection C: Conduction-cooled AC-loss measurement system.

Contents

Lists of symbols and abbreviations

A	Area of a cross-section
B_c	Critical magnetic flux density
$B_{\mathrm{c},1}$	Lower critical magnetic flux density
$B_{\mathrm{c},2}$	Upper critical magnetic flux density
C	Specific heat
E	Electric field
E_c	Electric field criterion
I	Current
I_c	Critical current
$i_\mathrm{coil}(t)$	AC-loss measurement excitation coil current
J	Current density
J_c	Critical current density
L	Inductance
l	Length
n	Superconductor n-value
Q_init	Quench initiation pulse energy
$\dot{\mathbf{q}}$	Heat flux
$P_\mathrm{theta,xx}$	Heat rate through xx
R	Electrical resistance
$R_{\theta,\mathrm{xx}}$	Thermal resistance of xx
T	Temperature
T_c	Critical temperature
V	Voltage
V_c	Voltage criterion
V_f	Diode forward voltage drop
$V_\mathrm{f,mean}$	Smoothed average forward voltage drop of BAS16 diode
X	Electrical reactance
Δl	Potential tap separation in $V(I)$ and NZPV measurements
ϵ	Electromotive force

λ	Thermal conductivity
ρ	Electrical resistivity
Φ	Magnetic Flux
φ_{i}	Potential tap i in NZPV and MQE measurements
AC	Alternating current
AWG	America wire gauge
BCS	Microscopic theory explaining superconductivity by Bardeen, Cooper and Schrieffer
BSCCO	Bismuth based high temperature superconductors
CAD	Computer-aided design
Di	Diode number i
DC	Direct, i.e. constant, current
DMM	Digital multimeter
FEM	Finite element method
GL	Ginzburg-Landau theory
HTS	High temperature superconductor (or superconductivity depending on the context)
LHe	Liquid helium
LIA	Lock-In amplifier
LN_2	Liquid nitrogen
LTS	Low temperature superconductor (or superconductivity depending on the context)
MLI	Multi layer insulation
MPZ	Minimum propagation zone
MQE	Minimum quench energy
MRI	Magnetic resonance imaging
NZPV	Normal zone propagation velocity
PTFE	Plastic polymer polytetrafluoroethylene i.e. Teflon
PEEK	Plastic polymer polyether ether ketone
RTD	Resistance temperature detector
SMD	Surface Mount Device
SMES	Superconducting magnetic energy storage

Chapter 1

Introduction

Superconductivity, often described as the total loss of electrical resistivity, has been studied for over a 100 years. However, the conditions required for the manifestation of the superconductivity phenomenon are restrictive. Today, the highest temperature under which superconductivity has been shown to exist is 134 K, or -139 °C [65, Sec 4.4]. However, even today, the commercially most viable superconductors still operate at liquid helium temperature 4.2 K, just like in 1911 when the phenomenon was discovered [65, Sec 1.1.1].

These low temperature superconductors formed 99.4% of the global market, worth 5050 M€, for superconductivity in 2011. Currently, the main commercial application utilizing superconductivity is the magnetic resonance imaging (MRI) used in hospitals for diagnosing various illnesses and injuries. The MRI market formed 79.7% of the global superconductivity market. [10]

1.1 Motivation

Utilization of superconductivity in large scale electric applications, like power grid transformers, generators, motors and cables, offers two main advantages over conventional resistive technology. First, the current density in electromagnets, found in MRI, transformers and generators, can be increased resulting in reduction of weight and volume. Second, the absence of resistive losses increases the system efficiency.[56]

In some applications, like MRI and high energy physics, superconductivity is enabling technology. For example, in MRI system the image quality and resolution are improved when the magnetic field is intensified. The first MRI system used resistive electromagnets and were limited to operation at 0.2 T

magnetic flux density. Today, MRI system used in hospitals operate at 1.5 T, some even at 3 T.[65, Sec 10.4].

One of the main challenges preventing mass-production scale utilization of superconductivity is the requirement for very low operating temperatures. The structures used in insulating the superconducting components from the surrounding environment are known as cryostats. As every superconducting system requires some kind of a cryostat, for many applications, a superconducting alternative to conventional resistive technology is more complex. However, the new superconducting materials have the potential to alleviate these obstacles.

As an example, in the MRI application, the new superconducting material magnesium diboride (MgB_2) has been demonstrated successfully. For example, the MROpen MRI-system by Paramed [60, 63] uses dry, conduction-cooled, MgB_2 electromagnets operated at 18 K. While the increase in operation temperature from 4.2 K to 18 K made possible by the use of MgB_2 seems small, the input power required for cooling is 30% of that consumed by a similar system operated at 4.2 K[46].

With the introduction of dry cryogenic systems, the validity of the methods commonly used for analyzing the performance and quality of superconducting wires becomes debatable. This so called short sample characterization is well established technology at 4.2 K, but its fundamentals at conduction-cooled systems have not been widely studied. Are the methods using liquefied gas, such as liquid helium, for cooling, suitable for testing the superconducting materials used in dry systems and in higher temperatures? On the other hand, diverting from the classical techniques can be challenging, as there is little experience on peculiarities and difficulties experienced in applying these alternative approaches. This thesis contributes to the knowledge of the field by exploring short sample characterization at conduction-cooled environment. Means for successful construction of measurement stations and their operation are presented. Focus is on critical current, minimum quench energy, normal zone propagation and magnetization loss measurements.

1.2 Structure of the thesis

The thesis begins with a brief look into the history of superconductivity presented at the beginning of Chapter 2. This very short review aims to present how the experiments performed on the superconducting materials provided insight in to the nature of the phenomenon. The historical outlook also intro-

duces the main concepts and quantities related to the superconducting state.

Chapter 2 is then continued by introducing the concepts used in analyzing and designing superconducting systems. The discussion then proceeds to presenting the different options for cooling superconducting devices. Finally, the Chapter ends with an overview of the different experiments used for characterizing superconducting wires. These experiments are then detailed in the rest of the thesis.

This thesis is of compilation type. Correspondingly, the chapters after the background are based on published, and one submitted, peer-reviewed articles. Many details are available only in the publications, but the chapters form independently readable ensembles.

Chapter 3 discusses the tangible corner stones of conduction-cooled systems. The first part, sections 3.1-3.4 scrutinizes the issues related to designing and constructing a conduction-cooled sample holder for different types of experiments. The second part lays out the tools for proper planning and realization of instrumentation connections. Near the end of the second part, special attention is given to temperature measurements.

Once the issues related to sample holder design, and other hardware related aspects are carried through, Chapter 4 analyzes how the actual measurements are performed in a conduction-cooled system. In the first part of the Chapter, it is examined how the current transport properties of a superconducting sample should be measured and how conduction-cooling can effect the result. The second part discusses the thermal stability measurements in a similar fashion.

Planning a cryogenic system used for characterizing superconductors is a multidisciplinary task. Therefore, Chapter 5 presents a complete workflow, from specifications to benchmark measurements, using an AC-loss measurement system as an example case. The first part of the chapter illustrates how the specifications and measurement principle restrict the available materials and construction options. Then, the system components are introduced along with considerations on their fabrication. Finally, the resulting measurement apparatus is demonstrated along with discussion on the experienced challenges.

At the end of the thesis, final conclusions are drawn and contribution of each publication is shortly summarized.

Chapter 2

Technical superconductors and their characterization

Superconductivity is not a new phenomenon, as it was discovered over 100 years ago. Today, there are still very few applications for superconductivity as because the operating conditions of commercially viable superconductors, or technical superconductors, are restrictive. The first part of this Chapter introduces superconductivity with a brief historical review. In the second part, different methods for cooling superconducting components are presented. Finally, the third part introduces the main properties used for assessing superconductors.

2.1 Phenomenon called superconductivity - History and introduction

2.1.1 Over 100 years of zero resistance

Early days

The prelude of the history of superconductivity was written in 1908 by Heike Kamerlingh Onnes. Professor Onnes was a Dutch physicist working in the Leiden University in the field of physics and metrology. One of his main interests was to study the resistance of metals at low temperatures and on July 10, 1908 he succeeded in liquefying helium. This achievement allowed experiments to be made at lower temperatures than ever before as the boiling point of liquid helium is only 4.2 K. From there on, the discovery of elemental

superconductors was only a matter of time. [65, Sec 1.1.1]

Superconducting state was first observed in mercury on 8th of April 1911, but at this time the true nature of superconductivity was not noticed. Onnes and his team did further experiments and on 26th of October 1911, the sudden shift from zero to observable resistivity at critical temperature (T_c), was recorded. In the experiment performed that day, the temperature of the mercury test sample was slowly increased while the resistance of the wire was monitored. This method allowed the resistance-temperature curve to be measured accurately. The data from this measurement showed that at 4.20 K the resistance was less than 10^{-5} Ω and when the temperature was increased by 0.2 K the resistance jumped to 0.1 Ω. [65, Sec 1.1.1]

In the following years, experiments were continued and new discoveries followed. New superconductors, tin and lead, were identified and new phenomena were observed. In 1913 the critical current (I_c), the maximum amount of current that can be carried by a superconductor, was first observed. The discovery of I_c was followed by the discovery of critical magnetic flux (B_c) in 1914. This last critical quantity to be discovered revealed the main challenge of using elemental superconductors. The B_c of elemental superconductors[1] is so small, that it prohibits their use in most applications. The strong electromagnets envisioned by prof. Onnes were not possible until the discovery of superconducting alloys. [65, Sec 1.1.1]

The second effect unique to superconductivity, in addition to the zero resistivity, was discovered in 1933, when Meissner and Ochsenfeld discovered the Meissner[2] effect. They discovered that, as opposed to an ideal conductor, with just the property of zero resistivity, a superconductor expels external magnetic field from itself during the superconducting transition. The effect and the difference between an ideal and superconductor is illustrated in figure 2.1.[65, Sec 1.1.2]

Evolution of theories and materials

While the Meissner effect is less interesting from the electrical engineer's point of view, the discovery provided a major step towards a better understanding of superconductivity. Now, any theory used for describing superconductivity also had to predict the magnetic interaction correctly. The discovery of the Meissner effect promoted the postulation of the London equations in 1935, that, for a macroscopic case, predict the relationships between magnetic fields

[1] Excluding niobium (Nb)

[2] The term Meissner Ochsenfeld-effect is also used.

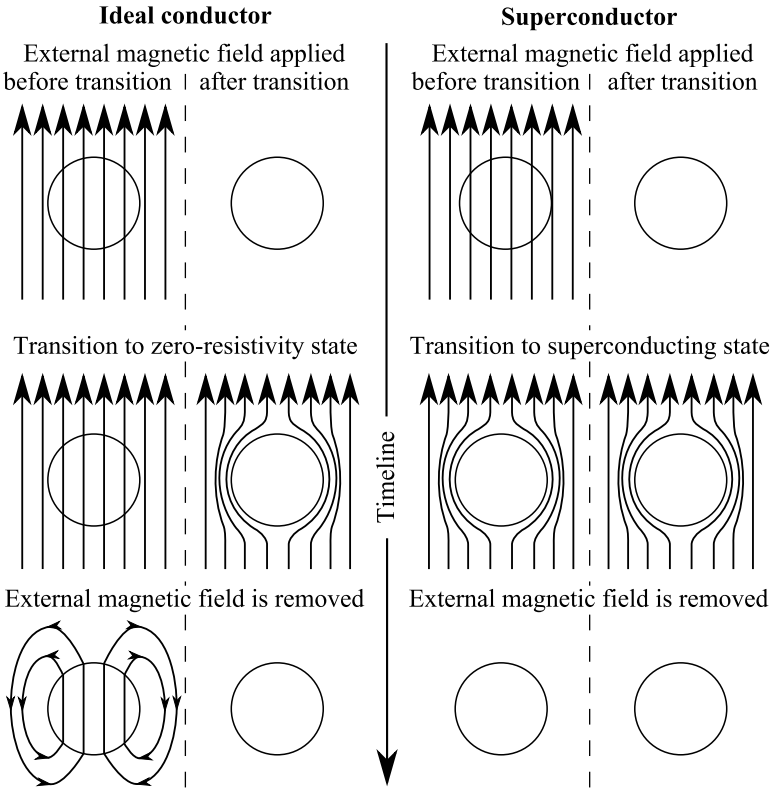

Figure 2.1: Illustration outlining difference between superconducting Meissner state and ideal conductor in external magnetic field. Left side of figure shows how ideal conductors can shield interior of zero resistivity bulk material from external magnetic applied only after transition. On right side, superconductor expels applied magnetic field regardless of initial state. Also note how ideal conductor becomes permanently magnetized in the case far left.

and currents in superconductors.[65, Sec 1.1.2]

Today, the Meissner effect is used to divide superconductors into two types, Type-I and Type-II. The first superconductors discovered, the elemental superconductors, mostly belong to the Type-I category[3]. Type-I superconductors exhibit the full exclusion of external magnetic field from the superconducting bulk, i.e. the Meissner effect, until B_c is reached. Above this limit, the superconducting state is lost completely. The modern commercial superconductors are in the Type-II category and they too remain in the Meissner-state when a low external magnetic field is applied. However, when the external magnetic flux density increases above the lower critical flux density ($B_{c,1}$), they enter a

[3]For example Nb is a Type-II material.

state known as the mixed state. In the mixed state, the superconducting material is partly in the normal conducting state allowing the external magnetic field to pass through, while the ability to carry lossless transport current remains.[4] The material remains in this state until the upper critical flux density ($B_{c,2}$) is reached and the superconducting state is completely lost. For engineers working with superconductivity, it is common to denote the $B_{c,2}$ simply with B_c for the Type-II materials.[65, Sec 1.1.3 & 2.1][84, Sec. 12.1.2] This convention is followed also in thesis, if not otherwise stated.

The division of superconductors into two distinct categories took place along the development of the Ginzburg-Landau (GL) theory. The GL theory formulated to extent the London equation was first published in 1950. It was further refined by Abrikosov in 1957 to demonstrate the existence of Type-II superconductors. As it happens, the mixed state had been experimentally detected originally in 1937 by Shubnikov. However, due to unfortunate events preceding World War II, the discovery did not receive the deserved attention until the Abrikosov's 1957 publication.[65, Sec. 2.1]

Somewhat parallel to the GL theory, a microscopic theory explaining the superconductivity phenomenon was developed by Bardeen, Cooper ans Schrieffer. The first version of the BCS theory was published in 1957. Finally, there existed a theory that correctly predicted the observations related to superconductivity. The GL theory, that was known to successfully predict the behavior of superconducting materials, was shown to be derivable from the BCS theory in 1959. According to BCS theory electrons, that normally repulse each other, in the transition to superconducting state, condense and form Cooper pairs. These pairs are able to flow through the superconducting material without experiencing resistance.[65, Sec 2.2&2.3]

Commercial superconductors and high temperature superconductivity

First of the commercially viable alloys Nb_3Sn was initially discovered in 1954. After a few years of experimentation, in 1961, the niobium based material was reported to exhibit both high I_c and B_c in [39]. The problems in using Nb_3Sn even today arise from the fact that it is a very brittle intermetallic compound. Using this material is therefore limited to high field-high current applications where other superconductors cannot be used. [65, Sec 11.3]

Today, the most common superconductor found in commercial applications is NbTi, a ductile alloy that is able to withstand deforming and handling much

[4]The description of the mixed state given here, outlines only the fundamental idea. For a complete exposition please see e.g. [65, Sec 2.1&2.6].

better than the brittle intermetallics. This workhorse of superconductivity was discovered in 1962. It is used to manufacture e.g. the magnets to almost all of the superconducting MRI devices.[65, Sec 11.2]

Before the year 1986, the highest observed critical temperature was 25 K (Nb_3Ge). The cuprate material (LaBaCuO) discovered by Müller and Bednorz in 1986 increased the T_c to a new record 35 K [5]. After this discovery, known today as high temperature superconductivity (HTS), the T_c record has climbed to 134 K. [65, Sec 4.2&4.4]

While the BCS theory correctly predicted the observations associated with low temperature superconductivity (LTS), i.e. the superconductivity observed prior to discovery of HTS, the theory predicted 25-30 K as an upper limit for T_c. Today there are candidate theories describing the superconductivity in HTS, but a widely accepted theory on the origins of high temperature superconductivity, has not been found. The question if superconductivity is possible in room temperature is yet to be answered.[65, Sec 2.4&4.4]

Superconductivity has gained several Nobel prices in physics for the people involved in the field. The first Nobel laureate was Heike Kammerlingh Onnes in 1913 for the discovery of superconductivity. The second person to get awarded with the price was Lev Landau in 1962 for the development of theories for condensed mater. Third Nobel in the field went to John Bardeen, Leon Cooper and John Schrieffer in 1972 for the formulation of the BCS-theory.[57]

Fourth Nobel was jointly awarded to Brian Josephson for the theories on supercurrent tunneling through an insulator known as the Josephson effect, and Leo Esaki with Ivar Giaver received their share on the prize for the experimental studies conducted on the tunneling effect in superconductors and semiconductors. The discovery of high temperature superconductivity was recognized by awarding the fifth Nobel related to superconductivity to Georg Bednorz and Alexander Müller. The sixth, and currently the last, Nobel prize was given in 2003 to Alexei Abrikosov, Vitaly Ginzburg and Anthony Legget for their contribution to the theories of superconductivity.[57]

Applications and recent discoveries

Today, the applications of superconductivity can be divided into two branches. The first branch is based on the utilization of superconductivity in electronics. Often, the applications in this group utilize the Josephson effect in one way or another. The second branch uses the lossless flow of electricity and the Meissner effect. Within this group, the superconducting material is formed to wires, tapes and cables and used for creating e.g. strong magnetic fields for

medical and scientific applications, or, as another example, for improving the efficiencies of conventional electrical machinery. In this thesis, I reside solely within this later branch.

The most recent additions to the superconducting materials family are magnesium diboride (MgB_2) [54] and iron based p-nictides [38]. The research done for this thesis focuses on the MgB_2 superconductor. In one experiment, HTS material $Bi_2Sr_2Ca_2Cu_3O_{10}$ (BSCCO) was also used.

2.1.2 Introduction to electrical engineering with superconductors

For most engineering tasks, the superconducting material is formed into wires or tapes. These wires and tapes are often fabricated as composites containing the superconducting material in fine strands surrounded by a metallic matrix. The matrix can contain several different normal metals or alloys and it serves two purposes. First, it provides reinforcement for the superconducting filaments. Many of the superconducting materials listed in the previous subsection are brittle and handling them during e.g. coil winding, would be difficult without the matrix. Second, the matrix provides fault tolerance and stabilizes the operation of the superconducting device.[34, 84] Figure 2.2 illustrates the cross-sections of some composite superconductors.

Critical quantities and transfer of electric current

In the previous subsection, the three critical quantities: current (I_c), temperature (T_c) and magnetic flux density (B_c), were presented. The three quantities depend on each other, e.g. I_c is a function of both temperature and flux density, and thus the critical surface presented in figure 2.3 can be defined. Below the surface, the superconducting state is maintained, but if the surface is punctured, resistive transition occurs and the superconducting state is lost. Therefore, the critical quantities set the boundaries inside which the superconducting system has to operate. One could state, that the critical quantities form the foundation of superconductive engineering.

In an ideal case, a superconductor has zero resistance until the I_c is exceeded. Above I_c the resistance discontinuously jumps to some value, typically considerably higher than that of copper, and heat begins to dissipate due to resistive losses. With a real, non-ideal, superconducting composite wire, the change in resistance is continuous and even before the measured I_c is reached,

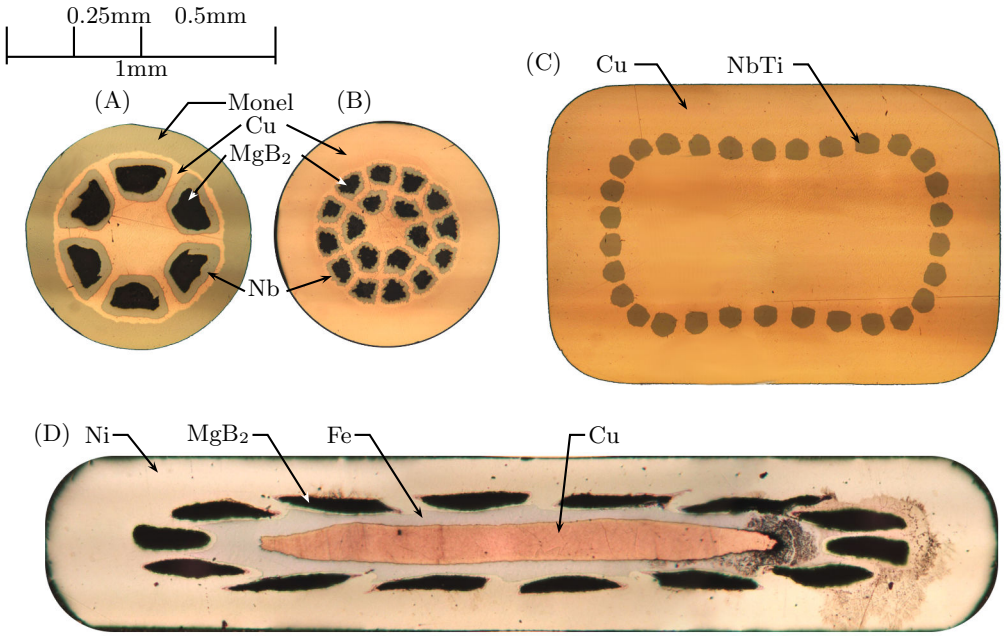

Figure 2.2: Cross-sectional photomicrographs of multifilamentary superconducting wire composites. Dimensions of conductors are as follows: (A) and (B) ⌀0.83 mm, (C) 1.1x1.67 mm and (D) 0.65x3.65 mm.

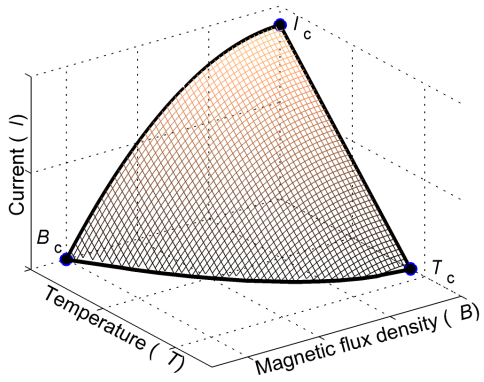

Figure 2.3: Critical surface of a superconductor. Maximum values of critical quantities are highlighted.

some resistive losses are present. To effectively predict the characteristics and behavior of a superconducting device, a mathematical model describing the situation has to be constructed.

This situation is often described with the empirically developed power

law [84, p. 236]

$$E = E_{\mathrm{c}} \left(\frac{J}{J_{\mathrm{c}}} \right)^{n}, \tag{2.1}$$

where E is the electric field observed in a superconductor, E_{c} is the critical electric field, n is the n-value, J and J_{c} the operation and critical current densities, respectively. Note that different selections of E_{c} lead to different values of J_{c}. Typically, 0.1 and 1 μV/cm are used as the E_{c} [18, Sec. 10.1][25]. Since E and J are difficult to measure in practice, a power law relation between current (I) and voltage (V) is used instead:

$$V = V_{\mathrm{c}} \left(\frac{I}{I_{\mathrm{c}}} \right)^{n}. \tag{2.2}$$

The n-value in (2.1) is the parameter used to describe the steepness of the resistive transition. An ideal superconductor would have an infinite n-value to exhibit the properties described in the previous paragraph. With real superconductors, the n-value is finite and the superconductor starts to gradually exhibit resistance until at J_{c} the electric field criterion reached.

The power-law does not describe the $V(I)$-relation for all the values of I, but it typically holds only near I_{c}. This is related to constant current loss mechanisms in superconductors such as flux creep and flux flow.[Sec. 2.4][52]

A key aspect in designing superconducting system is to ensure adequate stability[5] for the given task. The dependencies between the critical quantities I_{c}, T_{c} and B_{c} indicate, that if e.g. the I_{c} is locally reduced due to change in operation temperature, a local transition to normal conducting state could occur. If this transition happens and the cooling of superconducting component is not sufficient, the disturbance begins to spread. This loss of stable operation is called a quench.[34, Sec. 6.2][84, Sec. 5.3-6]

A quench needs to be detected and the system must include adequate protection so that normal operation can be continued after the incident. Typically this means de-energization of the system and some recovery time for re-cooling.[34, Chap. 8][84, Chap. 9]

Stability

Depending on the system, it is possible to ensure stable operation in all conditions, but achieving this so called cryostability [84, Chap. 6] often requires

[5]The term "stability" in superconductive engineering is commonly used for referring to thermal stability.

the system to operate well below the critical surface. It is more common to design a system to cope with disturbances below a certain magnitude and in the event of a large disturbance, to quench safely. This later meta-stable approach allows the designer to optimize the operation parameters: I, T and B, and stability to the requirements of the application at hand.

One commonly used parameter in defining meta-stability is the minimum propagation zone (MPZ) introduced by Martinelli an Wipf [48] and demonstrated with computations and experiments by Wilson and Iwasa [85]. In principle, the volume of the smallest ellipsoidal normal zone leading to a quench is determined. It can then be computed what is the energy required for creating such ellipsoid leading to the concept of minimum quench energy (MQE).

The energy required for the formation of a MPZ can originate from the wire itself and from external sources. Microyielding of the superconducting filaments is a potential source of localized heat releases in a superconducting wire. Frictional heat caused by a movement due to Lorenz force is an example of a potential external source. In applications involving high energy particles, e.g. a particle accelerator, stray particles colliding to the superconducting wires can also deposit the energy required for the formation of a MPZ.[6][15][34, chap.6]

When a MPZ is created into a superconductor, it will propagate through the conductor at a certain speed. This normal zone propagation velocity (NZPV) can be used in analyzing the evolution of the quench event. The NZPV can be used in determining if there is a risk of damage to the superconducting components during quench. If the NZPV is low in comparison to the energy dissipated in the propagating normal zone, it is possible that the temperature in the hotspot reaches a level where the superconductor is damaged either due to the temperature or mechanical stresses caused by thermal expansion. Further discussion on this topic is beyond the scope of this thesis and further reading providing insight into this field can be found in e.g. [34, 73, 84].

Considering the characterization measurements of superconductors, it is worth noting that if a given conductor or coil operated with constant current in constant T and B, the magnitude of MQE is not necessarily constant. If the heat diffusion in a superconducting wire or a coil is considered, the magnitude

[6]Some of the MQE sources listed here can originate only once from a single location. For example, once a filament has yielded or epoxy has cracked, the same location will not release energy again under the same conditions. This effect known as training, is present with nearly all superconducting magnets, and usually once a magnet is trained, most of these one time energy releases have been triggered.

and duration of the disturbance can be seen to effect the MQE.

Other aspects

In electrical applications, superconductors are often used as cables to transfer electric power, or they are wound in to coils to form an electromagnet. Whichever the application, firm attachment of the wire to a support is required as wire movement was listed as one of the sources of a MPZ leading to loss of stable operation. Therefore, eliminating the possibility of wire movement is necessary in the design and fabrication of a superconducting device.

In the case of superconducting coils, the turns and layers are impregnated with a binding agent or otherwise mechanically supported, or both depending on the shape of coil. With smaller superconducting magnets found in e.g. MRI, rotating electric machinery and research apparatus, the windings are often impregnated with epoxy resin. In the case of a simple solenoid, the resin impregnation and the superconducting wire together form the necessary support structure. With other coil configurations, such as a racetracks, external support is often necessary.

With any superconducting system, care must also be taken when the cryogenic structures are designed. Maintaining the specified operating temperature is vital in preventing the loss of stability. On the other hand, if the cryogenic specifications are too loose, the volume and weight savings obtained from using superconductors in the first place can be reduced. Designing a superconducting system is therefore a multidisciplinary task and requires knowledge from several different areas of engineering.

2.2 Cooling methods for superconducting applications

The temperatures required for utilizing superconductivity can be reached with different cooling methods. Similarly to the setup used by Onnes in his discovery of superconductivity, the use of liquefied gas, such as helium or nitrogen, is still one of the most common methods for cooling superconducting devices. Today, there are also other cooling options available. In this section, I briefly present two cooling methods, bath and gas flow cooling, that require the use of liquid cryogen. The third option, conduction-cooling, is presented in more detail as superconductor characterization measurement in such a system are the main

topic of this thesis.

2.2.1 Cryogenic bath

The simplest setup for performing the $V(I)$ measurement discussed in the previous section, is illustrated in figure 2.4. It consist of a sample holder immersed in a bath of liquid cryogen. The most common cryogenic liquids used with superconductors are liquid helium (LHe) and liquid nitrogen (LN_2). The liquid bath can also include a background field magnet, also shown in figure 2.4. Depending on the coolant, the liquid bath cryostat can be as simple as a styrofoam thermal box, photographed in figure 2.5, used for housing the LN_2 cooled excitation coil for the magnetization AC-loss measurement system discussed in Chapter 5. The use of LHe requires a better cryostat, but still, the setup can be very simple as shown in figure 2.6.

The major advantage of the bath cooling method, in addition to simplicity, is good thermal stability. The temperature of the setup is determined by the boiling point of the coolant. It is known that the boiling point of a liquid depends on the ambient pressure and thus the temperature of the coolant bath is determined by the pressure of the cryostat. If the pressure is held constant, the temperature of liquid reservoir remains constant. Therefore any liquid boiling of at the locations of heat generation is replaced by fresh coolant and the sample remains at constant temperature.

On the negative side, the temperature of a bath cryostat is not easily changed. The only way to change the temperature notably is to use a different cryogen to change the boiling point. Using different cryogenic fluids allows the temperature to be set coarsely to some level. The different cryogenic liquids are listed in table 2.1 along with the atmospheric pressure boiling points. Fine control can be achieved by pumping or pressurizing the liquid reservoir. However, this method is highly inefficient as the entire liquid volume needs to chilled or warmed. For example, subcooling a LHe cryostat to 2.2 K by pumping, requires 25-35% of the initial LHe volume to boil off for the rest of fluid to cool down.[18, p.11][4, p.24]

In a system using LHe, the problem can be circumvented with a lambda point refrigerator. The lambda point refrigerator is a device used for partially subcooling a LHe bath from 4.2 K to just above the lambda point at 2.17 K. The design and operation of the lambda point refrigerator is however beyond the scope of this thesis. These topics are discussed in more detail in e.g. [4][18, p.33].

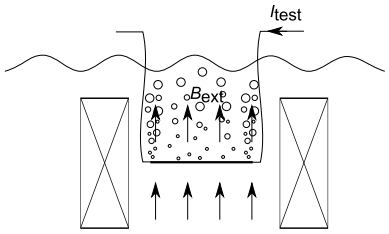

Figure 2.4: Principle of cryogenic bath cooling. Sample is fixed on sample holder and immersed into liquid cryogen. Electromagnet for producing variable background magnetic field is also illustrated.

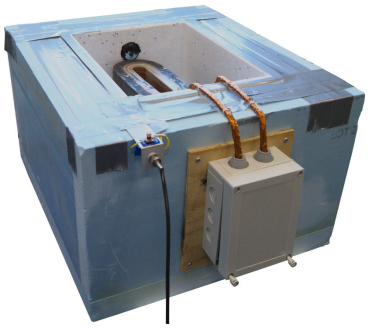

Figure 2.5: Photograph of styrofoam LN_2 cryostat. Coil inside cryostat is used for excitation in AC-loss measurement(see Chapter 5).

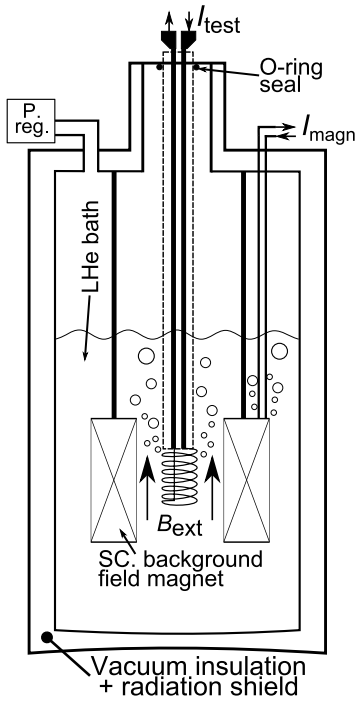

Figure 2.6: Bath cryostat for in-field sample characterization suitable for use with LHe. Vacuum and radiation shielding are used for reducing heat influx and cryogen boil-off.

The lambda point refrigerator uses the properties of liquid helium to efficiently cool down only a part of the cryogenic bath. The refrigerator consists of a heat exchanger, needle valve and a vacuum pump. The exchanger coil is place above the superconducting device and continuously evacuated with the vacuum pump. Using the needle valve, a small amount of LHe is allowed to pass into the heat exchanger coil where the reduced pressure causes it to evaporate and cool down. The ambient pressure LHe bath surrounding the superconducting component and the lambda point refrigerator is cooled by the heat exchanger. The lambda point refrigerator is efficient, as due to the properties of liquid helium two layers are formed into the bath. The upper layer consist of LHe at 4.2 K while in the bottom layer, at and below the lambda point refrigerator the temperature can be reduced to just above the lambda

Table 2.1: Boiling points of common cryogenic liquids. Price estimates for three common cryogenic fluids are from [58].

Substance [Abbreviation]	Boiling point at atm.pressure	Remarks
Oxygen(O_2) [LOx]	90.19 K	Powerful oxidizer, fire hazard
Argon(Ar) [LAr]	87.30 K	Inert
Nitrogen(N_2) [LN_2]	77 K	Inert ($\sim$ 3€/l)
Neon(Ne) [LNe]	27.07 K	Inert ($\sim$ 230€/l)[a]
Hydrogen(H2) [LH2]	20.28 K	Highly flammable
Helium 4(^{4}He) [LHe]	4.2 K	Inert, superfluid below 2.17 K, ($\sim$ 42€/l)
Helium 3(^{3}He)	3.2 K	Inert, rare and expensive

[a]The cost of gas only, liquefaction will increase the price.

point, 2.2 K. The thermal conductivity of LHe is low, and the bulk of these two layers are nearly isolated from each other creating a large temperature gradient at the border. [4][18, p.33]

2.2.2 Gas flow cooling

To overcome the temperature control limitations of the bath cryostat, a gas flow system can be used instead. In this setup, illustrated in figure 2.7, the sample is cooled by flowing gas extracted from the main cryogen reservoir. The gas temperature can accurately be controlled by manipulating the flow rate, the sample space pressure and the power dissipated in the heating element. This can also be done automatically by a temperature controller adjusting the needle valve position and the heating element power.

The temperature of a gas flow cryostat can be set in a wide range. For example, a gas flow system from the portfolio of Oxford instruments allows the temperature of the sample to be set freely from 2 to 300 K [59]. Depending on

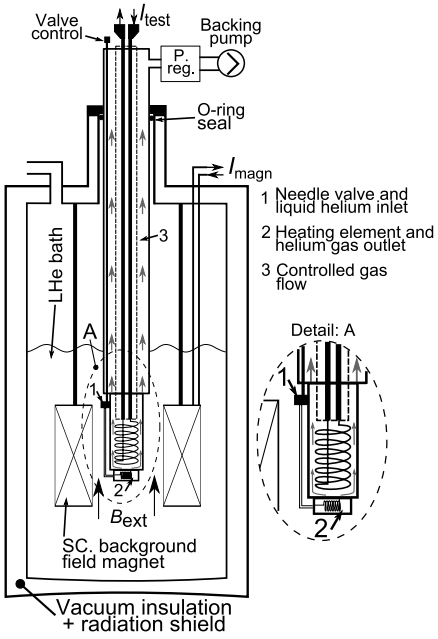

Figure 2.7: Basic structure of gas flow cooled measurement system. Gas flow control is achieved by controlling sample space pressure with pressure regulator (P.reg.), needle valve position and heating element output. Detail A shows LHe flow from reservoir, through needle valve (1) and heating element (2) into the sample space.

the the sample holder setup, the test currents in such system can reach 1500 A.

On the negative side, the gas flow system is the most complex of the three options presented here. The type of system illustrated in figure 2.7 must contain two interconnected cryostats if the temperature of the sample space is higher than that of the LHe bath. The two cryostat structure is necessary in preventing heat from the sample space from transferring to the main LHe bath. With high operation currents, large flow of He gas is required for removing the heat dissipated in the normal conducting components and a large backing pump is therefore required. The needle valve is also a problematic component. If the system runs continuously, a small amount of impurities can accumulate into the main LHe bath and freeze. These frozen impurities can clog the needle valve and thus impair the operation. A heater placed to the needle valve solves the problem but adds complexity by introducing one more item to control.

2.2.3 Conduction-cooling with cryocoolers

With the previous two methods, the entire length of the sample is cooled directly by either the liquid cryogen or the flowing cold gas. While this is desirable in e.g. I_c testing, there are some measurements that would benefit from an alternate approach. Further, when new superconducting applications are pushed to markets where people are not familiar in dealing with cryogenic fluids, the market penetration can be eased with these plug-and-play devices.

As discussed in the previous section, a superconducting coil can be impregnated to prevent winding turns from moving and causing a quench. A tightly wound, impregnated coil without any additional cooling structure is refrigerated only from the outer surface. Thus, the turns and layers inside the coil experience a rather different environment than the ones on the surface. In [84, Sec. 9.3][34, Chap.6] it is noted, that in this case, the heat transfer inside the coil from turn to turn is considerably weaker than along a single turn. Therefore, the data obtained by measurements done with bath or gas flow systems can be optimistic when compared to the conditions of a wire in an impregnated magnet. Optimistic measurement data can in turn cause unreliability when the stability of a superconducting system is analyzed.

Also the advent of HTS and the improvements in the performance of mechanical refrigeration units, cryocoolers, have allowed superconducting systems to operate at temperatures significantly above 4.2 K even in magnet applications. Instead of immersing the superconducting components to a liquid cryogen, the component is connected to a thermal interface. The interface conducts the heat from the superconductor to a refrigeration unit e.g. a cryocooler. This type of a setup is illustrated in figure 2.8. These conduction-cooled system are often housed in vacuum for thermal insulation. For fast transients, like a quench, the situation at the circumference of the superconducting wire resembles adiabatic conditions.

Performing characterization measurements in a conduction-cooled system is more complicated than in the previously presented classical setups. At best, the cooling capacity available for protecting the sample and removing the heat dissipated in the ohmic parts, is limited to a few watts. With a modern cryocooler, like the one shown in figure 2.9, the maximum cooling capacity is usually 4-14 W at 10 K [12, 76].

Keeping the limitations in mind, the data obtained in a conduction-cooled measurement is more accurate for superconductors operating in adiabatic conditions. The greatest differences between adiabatic and classical measurements can be found in the stability parameter characterizations. For example, min-

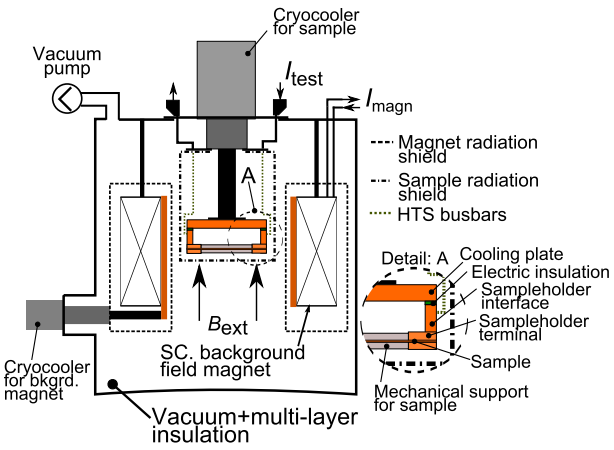

Figure 2.8: Basic components of conduction-cooled measurement system with background field magnet. Note actively cooled radiation shields around sample space and background magnet. In detail A, note how thermal pathway must be insulated from electric contacts.

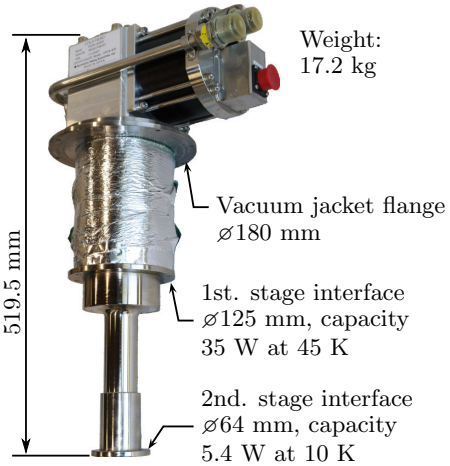

Figure 2.9: Modern 2-stage Gifford-McMahon cryocooler model RDK-408S2 from Sumitomo Heavy Industries. Dimensions, weight and capacity values are from [76].

imum quench energy measured in a conduction-cooled system is significantly different when compared to measurements done in neon vapor [50].

The main advantages of a dry, i.e. the refrigeration is done using a mechanical cryocooler, measurement system, is the simplicity of operation. Only electric power and coolant[7] are required for operating the compressor unit of the cryocooler. In addition, the temperature of the sample space is easy to control with an electric heater. As with the gas flow cooling, an automatic controller unit can be used to achieve precise operating temperatures.

The simplicity of operation comes at a price. The limited cooling capacity of such a dry system poses challenges in designing the experiments. The power dissipation in normal conducting components and during a quench need to be dealt with. Also, as the sample is not immersed in a liquid at nearly constant temperature, the uniformity of the temperature distribution in the sample needs attention.

[7]Water circulation is often used, but there are system that can operate with forced air cooling.[12, 76]

2.3 Typical characterization measurements

Before introducing three common test used for characterizing composite superconductors, the quantities of interest require further consideration. The quantities presented in the previous sections, can be divided into two groups. First, quantities like critical temperature T_c and superconductor critical magnetic flux density B_c depend on the chemical composition of the superconducting material itself. Second, conductor specific properties like critical current I_c, n and MQE depend also on the layout and materials used in the superconducting wire.

The acknowledgment of this division is necessary, as the conclusions that can be drawn from measured quantities in the two categories are significantly different in range of applicability. For example, the measurement of T_c in the absence of transport current and external magnetic field, is valid for all conductors using the same superconducting material. However, two multifilamentary superconducting strands with different matrix material, but otherwise identical in e.g. I_c and n, can have significantly different MQE and NZPV. The explanation lies in the differences in thermal conductivity and specific heat of the conductor composite. Additionally, in HTS coated conductors[8] the conductor architecture and interfacial resistance between superconductor and stabilizer have been shown to have an effect on these parameters.[40]

If the design process of a superconducting system, and the associated modeling tasks, are considered, the parameters used for studying superconductors can be divided into three categories

1. electrical,
2. thermal and
3. mechanical properties.

The first of these contains quantities like $I_c(T, B)$ and $n(T, B)$ that are used primarily in the electromagnetic simulations. The second group has quantities like thermal conductivity $\lambda(T)$ and specific heat $C(T)$ required in the thermal modeling. The third category includes properties like stress/strain characteristics and yield strength measurements.

[8] To manufacture a flexible conductor from Rare Earth-Barium-Copper-Oxide HTS material, where e.g. Yttrium is used, the superconducting material is formed to a very thin layer, usually with a thin film deposition process e.g. pulsed laser deposition or chemical vapor deposition, on a normally conducting substrate. The resulting HTS tape is referred to as a coated conductor.[65, sec. 11.5]

Quantities like MQE and NZPV create interconnections between the categories e.g. MQE depends on both the electrical and thermal behavior of the superconducting composite conductor. Similarly, interaction between electrical and mechanical properties is required as variation in I_c is observed when the stress/strain applied to the superconductor is changed [20, 68].

The most common tests used to asses the performance of a superconducting wire are

- I_c and n-value testing as a function of B and T,
- minimum quench energy measurement,
- normal zone propagation velocity measurement and
- I_c stress/strain-measurement.

Specific heat and thermal conductivity are not mentioned in the list above, as they can be adequately approximated from tabulated values of the component materials when the cross-section and sample composition is known [45, 74]. If it is foreseen that rapid changes in the operation current are required, AC-loss should also be measured.

Measuring thermal and mechanical quantities, along with I_c stress/strain-measurement, are not discussed further as they are beyond the scope of this thesis. For those interested in these experiments, see e.g. [18, chap. 9][19, 68].

2.3.1 Measuring critical current I_c and n - The $V(I)$-measurement

Using superconductors in applications involving the transport of large electrical currents requires information on the current carrying capacity of the superconducting wire. Often this information is required at various temperatures and under various magnetic fields.

The common way to determine the current carrying capacity of a superconducting wire is to study the resistance of the sample as a function of the transport current. Resistance (R) is defined by the Ohm's law as the ratio of V and I , i.e. $R = V/I$. Measuring the voltage across the sample as a function of the current flowing through the specimen provides the required information. In the field of superconductivity this test is known as the $V(I)$-measurement.

Since the resistivity of superconducting materials is very non-linear, and depends highly on the temperature and magnetic field, the analysis of the results of the $V(I)$-measurement requires a more sophisticated approach than with normal conducting metals. Two basic properties can be extracted from the $V(I)$-measurement, the critical current I_c and n-value. As discussed earlier, these two parameters describing the performance of a superconductor are commonly used in designing systems with superconducting components. Measuring these parameters is more involved than it initially appears, and the $V(I)$-characteristic measurement is discussed in more detail in Section 4.1.

2.3.2 Minimum quench energy and normal zone propagation velocity measurements

The $V(I)$-measurement provides the data required in the electromagnetic design of a superconducting device. To ensure stable and reliable operation of the device, stability and tolerance to external disturbances must also be considered. Often this stability analysis includes the determination of the minimum quench energy as well as the design of the quench protection scheme.

Numerical modeling with Finite Element Method (FEM) can be used in the stability analysis [86, 7, 8, 45, 73]. To increase the reliability of the modeling results, experiments are required. For example, if the V(I)-characteristic, specific heat, thermal conductivity, normal state resistivity and the internal structure are known for a superconducting composite wire, a coupled electro-thermal FEM modeling tool can be used to predict the minimum quench energy [49, 50, 74, 75]. Comparing this predicted value to measurement data is a good benchmark in assessing the validity of the approach.

The measurement of minimum quench energy and normal zone propagation velocity is inherently more demanding than the $V(I)$-measurement. The heat transfer conditions, i.e. is the sample insulated or convectively cooled with a gaseous or liquid cryogen, have a significant effect on the measurement results. Also, the normal zone in a quench can expand very rapidly placing stringent requirements on sampling rate of the measurement instruments. These thermal stability measurements and their challenges in a conduction-cooled system are discussed in more detail in Section 4.2.

2.3.3 AC losses measurement

Alternating current(AC) losses in a superconductor are present in nearly all superconducting applications. Whether the application is to transfer energy using AC or to produce a stable magnetic field with direct current(DC), both applications require the consideration of AC losses.[9]

The AC losses in superconductors are divided into three types: hysteresis, eddy current and coupling losses.[29][84, Chap. 8] Depending on the application, the magnitudes and prominence of each source varies greatly. Hysteresis losses are due to changes in magnetic field and/or current density profiles in superconducting regions. Eddy current losses are caused by induced currents in the normal conducting domains of the system. The resistivity in the superconductor is orders of magnitude lower than that of the matrix metals. Thus, superconducting filaments may look like galvanically isolated wires to each other. However, if this is not the case, it is said that the filaments are coupled and consequently, coupling losses arise.

AC loss measurement methods can be divided into two categories. The calorimetric methods determine the magnitude of total AC loss by determining the heat input into the system. For example, with a bath cryostat, it is possible to monitor the cryogen boil off rate. By computing the volume of the liquid evaporated due to AC loss, it is possible to determine magnitude of the electrical losses. Another alternative is to use the changes in sample temperature for determining the energy input into the system.[47]

However, with the calorimetric method it is not possible to differentiate the losses caused by the transport current from the losses caused by variations in the external magnetic field. Also, this approach works best with LHe system as the heat of evaporation of LHe is low in comparison to other cryogens.[62] For example, 1 W of power dissipation will change the boil off rate by 16.05 $\frac{\mathrm{l}}{\mathrm{min}}$ for LHe, by 1.505 $\frac{\mathrm{l}}{\mathrm{min}}$ for LH_2 and by 0.243 $\frac{\mathrm{l}}{\mathrm{min}}$ for LN_2 [18, App. A1.6].

To overcome the challenges of the calorimetric method, electrical methods can also be used. Hysteresis losses can be considered to be caused by applied field and transport current. The losses due to the applied field are typically referred to as magnetization losses. The electrical methods allow the measurement of both transport and magnetization AC-loss separately. In the transport AC-loss measurement, the dissipation caused by an alternating transport current are measured. Common way for realizing the measurement

[9] Even with DC-applications, the current has to be increased or decreased if the magnetic field has to be changed. Changes in the current and magnetic field cause AC-losses similarly to an AC-application.

is to use a lock-in amplifier and potential taps for detecting the voltage component in-phase with the current. The AC-loss is then obtained by multiplying the in-phase voltage with the transport current. The magnetization AC-loss is more challenging to measure. Common approach is to use pick-up coils for sensing the sample magnetization. However, this approach requires calibration as the pick-up coil output depends on the coil geometry and position of the sample relative to the coil.[62]

The calibration free method, proposed in [79], also uses a lock-in amplifier, but instead of sensing the sample magnetization directly, the change in the electric power supplied to the excitation field is detected. The measured signals are therefore directly related to the power dissipated due to the AC-losses and calibration is not required. In Chapter 5 AC-loss measurement using this technique is described in detail.

Chapter 3

Conduction-cooled sample holder design, instrumentation and sensors

In this Chapter, I present a definition for the technical term 'Sample holder', the specific requirements imposed by conduction-cooling and considerations on how to design a functional sample holder. After this, I discuss what are the requirements for the instrumentation of basic short sample characterization measurements and present two options for analyzing the heat leak through instrumentation wiring. In the final section different temperature sensor options are considered and a cheap alternative for commercial temperature sensors is presented and its feasibility is studied.

The sections discussing the sample holder design are based on **Publication 3** and **Publication 4**. The computation results for analyzing the shape and length of sample holder contacts are presented and scrutinized in **Publication 4**. **Publication 3** constructs the foundation and justifications for using the simplified computation models of **Publication 4**. Furthermore, in **Publication 3**, the total resistance of a solder joint between two composite superconductors was measured and the obtained result was applied into the computation model of **Publication 4**.

The silicon diode temperature sensors presented as an alternative for commercial temperature sensors were studied in **Publication 2** and **Publication 5**. **Publication 2** discusses the accuracy and sensitivity of the BAS16 Si-diode in sensing constant temperatures and also the suitability of the component for sensing temperature transients. In **Publication 5**, the effects of external magnetic field to the sensor output is measured and analyzed. Addi-

tionally, in **Publication 5**, method for improving the transient response was tested.

3.1 What is a sample holder?

There are many different ways to define what the term 'sample holder' means. One solution is to look up both words from a dictionary for a definition. In this case one would read something like "sample - a small part of anything or one of a number, intended to show the quality, style, or nature of the whole" and "holder - something that holds or secures" [16]. By combining these definitions, and the context of superconductivity characterization measurement, a sample holder is a device that holds and secures a small piece of a superconductor. Another definition can be obtained from the literature related to the field of research. For example, in his book *Experimental techniques for low temperature measurements* Ekin states that "The holder supports the sample against the magnetic Lorentz force, and has a thermal contraction that matches that of the sample, eliminating the stress of the differential thermal contraction."[18, p.274] As surprising it might be, the dictionary reference correctly defined the most important property i.e. a sample holder needs to secure the sample to prevent movement during measurement.

The sample holders used in characterizing superconductors come in a variety of shapes and sizes. Some possible sample holder types are schematically presented in figure 3.1. Each of these sample holders is designed for a specific task, e.g. the VAMAS [83] type barrel in figure 3.1(A) is often used for characterizing high I_c LTS conductors in a background magnetic field. However, the fiberglass composite plate in figure 3.1(B) has been used e.g. in measurements studying the magnetic flux density distribution of an HTS tape [51]. The arc shown in figure 3.1(C) is an adiabatic, conduction-cooled, sample holder used in e.g. contact resistance and quench propagation measurements. The conduction-cooled, adiabatic, sample holder in figure 3.1(D) has been used for $V(I)$-measurement. The comb-like device in figure 3.1(D) has evenly spaced potential taps and it can be used in combination with the sample holder for measuring e.g. quench propagation.

Before proceeding further into the details of designing a good sample holder for a specific type of measurement, it is prudent to list some key aspects. The following list is based on [18, pp.273-315] and on personal experience. A sample holder must:

- provide mechanical support. The sample must not move during the mea-

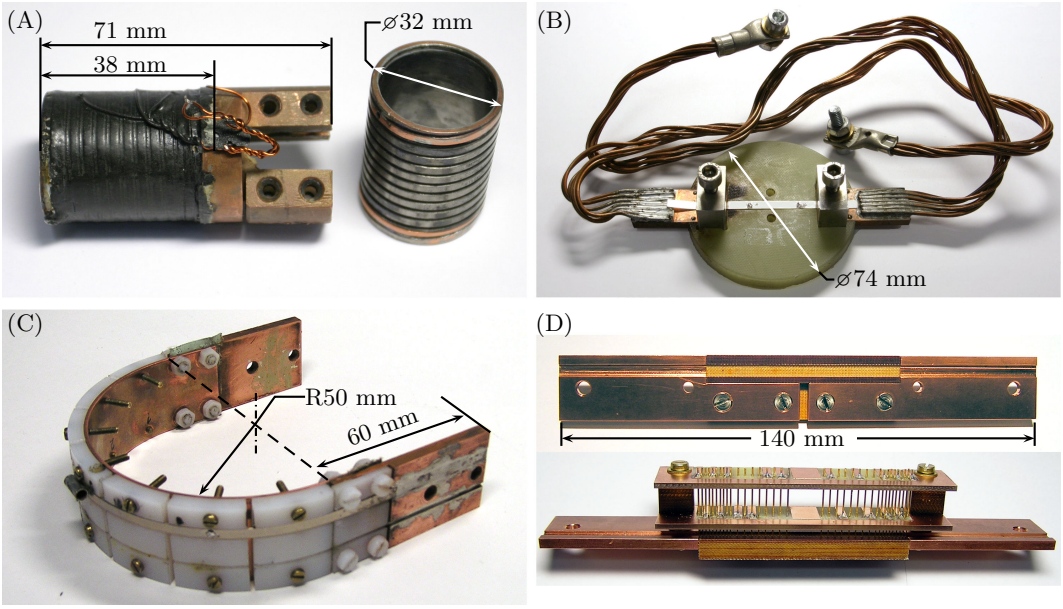

Figure 3.1: Different types of sample holders. (A) is used in liquid helium system with gas flow cooled variable temperature sample space. (B) is used in Hall magnetometer system with liquid nitrogen bath as coolant. (C) and (D) are adiabatic, conduction-cooled sample holders for a mechanically cooled system.

surement e.g. due to Lorenz force.

- not damage the sample mechanically e.g. due to differences in thermal expansion/contraction.

Additionally, it is often required that the sample holder

- has contacts for interfacing with the sample e.g. terminals for a connection to a current supply.[1]
- can easily be installed and removed from the measurement system.
- provides passive protection against sample burnout during a quench. E.g. the VAMAS barrel in figure 3.1(A) provides an alternate path for test current, when the superconducting sample becomes increasingly resistive.[2]

[1]For some measurements, like the AC magnetization loss, current terminals are not needed.

[2]With experiments like MQE or NZPV measurement, an alternate current path will distort results, and should therefore be avoided.

In a conduction-cooled system the absence of external coolant poses new challenges. With conduction-cooling, the sample is only cooled via the sample holder structure. The limited cooling capacity of a conduction-cooled system also places tight constraints on the power dissipated e.g. in the current terminals soldered to the sample.

3.2 Conduction-cooled sample holders

Designing a conduction-cooled sample holder should be done in a top-down fashion. In the top-down approach, the design process begins by defining the general outlines of the experiment, i.e. what are the properties/quantities that are to be studied. Then the process can proceed into defining the details, planning the sample holder geometry and drawing the fabrication schematics.

The design of a sample holder should aim for the elimination of external effects and therefore establish a good basis for characterizing the intrinsic properties of the superconducting sample. For example, in the previous Chapter it was discussed, that with impregnated superconducting coils, the measurement of MQE and NZPV should be done in a system allowing adiabatic condition at the sample circumference. On the other hand, in the $V(I)$ measurement used for studying I_c and n-value, thermally anchoring the whole sample to the holder will help to control the self-heating issues.

Next the length of the sample needs to be determined. For studying the critical current, it is fairly simple to visualize how increasing the distance of the potential taps also increases the sensitivity. This is illustrated in figure 3.2, where the larger potential tap separation yields a larger voltage signal at I_c for a given E_c. However, when the tap separation is increased, the sample must also extended as placing the taps too close to the current terminals can cause measurement errors [18, pp.290-296].

In adiabatic thermal stability measurements, the sample length affects the accuracy of the measurement in two ways. First, similarly to the $V(I)$-measurement, a long sample makes it possible to place measurement instrumentation further apart. Increasing the separation increases the temporal resolution of the propagation velocity measurement as illustrated in figure 3.3. Also, increasing the tap separation decreases the relative error caused by absolute error in the tap separation. Also, like in the $V(I)$-measurement, when potential taps are used to measure quench ignition and propagation, placing the taps too close to the current terminals can interfere with the measurement.

Second, the sample length also affects the validity of the assumption of

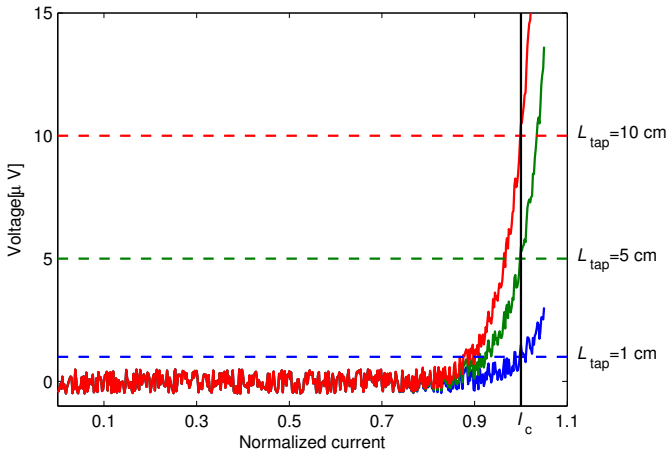

Figure 3.2: $V(I)$-curves computed using power law with ± 0.5 μV noise. E_c was set to $1\frac{\mu V}{cm}$ while potential tap separations were set to 1, 5 and 10 cm. For 1 cm tap separation, observe how determining I_c is difficult as noise makes detecting critical voltage obscure.

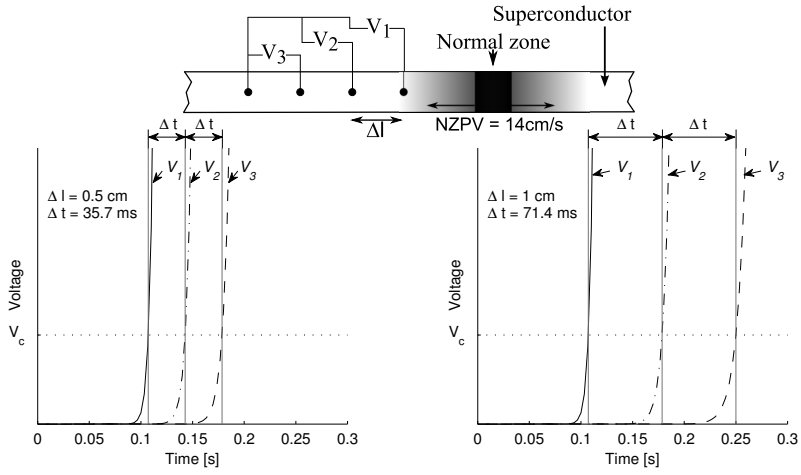

Figure 3.3: Sketched voltage-time graphs typical to normal zone propagation velocity measurement. Increasing tap separation increases measurement accuracy in time domain, since recording voltages with high accuracy reduces sampling rate.

adiabatic conditions. If the sample is too short, the initial normal zone created by the quench ignition system might reach the current/cooling terminals. In this case, energy dissipated in the normal zone bleeds directly to the cooling system and the assumption of adiabacy is no longer be valid.

One solution for estimating the necessary sample length in a thermal stability measurement is to use the concept of a MPZ, discussed in Chapter 2.1.2 as a reference. In an adiabatic MQE measurement, propagating normal zones, i.e. equal to or larger than MPZ, must be distinguished from collapsing ones, i.e. smaller than MPZ. Therefore the MPZ must fit between the sensors/potential taps used in monitoring quench initiation and propagation.

At this point, it should be defined what is the measurement system that is going to be used. Options for cooling and current supply depend greatly on the choice of the measurement system. In a conduction-cooled system, cooling the sample relies on the conduction of heat away from the sample. Therefore, minimizing the thermal resistance of the cooling interfaces, as well as minimizing the dissipation in the current contacts, is important. This in turn implies, that all the components need to fit precisely together, and have adequate contact areas, for ensuring low thermal and electrical resistances. Therefore, the mechanical constraints set by the measurement system need to be incorporated into the design process at an early stage.

When the constraining dimensions set by the sample and the measurement system are known, the sample holder can be sketched and its behavior during the measurement must be simulated. A thorough thermal and electrical analysis of the sample holder is useful as it allows one to avoid constructing sample holders that are sure to fail. Modern computer-aided design (CAD) software have built in simulation capabilities for making basic structural and thermal analysis [3, 14]. For more detailed simulations, such as a coupled electro-thermal model, commercially available FEM software typically offer a CAD interface or are able to import CAD models [2, 9]. Using these tools to gain information on the expected behavior of the sample holder helps in defining e.g. the maximum safe operating current.

3.3 Connecting the sample to the holder - Current and cooling contacts

In literature [18, pp.290-296][24], the minimum length of the current contact is usually defined via the twist pitch of a composite superconductor. While nearly all LTS wires are twisted, this is not the case for HTS or MgB_2. As suggested in [18, pp.341-346], the current contacts for HTS and other untwisted samples should be studied using the contact resistance of the joint. It is also emphasized, that conservative, i.e. worst case, approximations are the proper way of estimating the power dissipation in a resistive joint. While these state-

ments also apply to conduction-cooled sample holders, the absence of cooling fluid poses additional challenges. This fact is also noted, and some general advice is given, in [18], but in depth analysis is not presented.

3.3.1 Defining the properties and requirements

With conduction-cooling, the dissipation in the current contact needs to be removed either by

- directly conducting the heat to a thermal pathway,
- by conducting the heat to the thermal pathway via the superconductor and/or via the current leads used for supplying the operation current.

These configurations are illustrated in figure 3.4. In the left figure, the thermal pathways connected to the sample holder terminals provide cooling for both the sample and the dissipation in the current contacts. In the right figure, the sample is cooled from the middle and the terminals are cooled by allowing heat to flow through the current leads and through the sample. Any combination of these two options is also possible, e.g. cooling the setup by connecting thermal pathways to both the terminals and the sample.

The thermal and electrical resistances of different types of contacts are listed in table 3.1. It is obvious, that a solder joint is the best way to fabricate both thermal and electrical contacts among these alternatives. Now, if a high

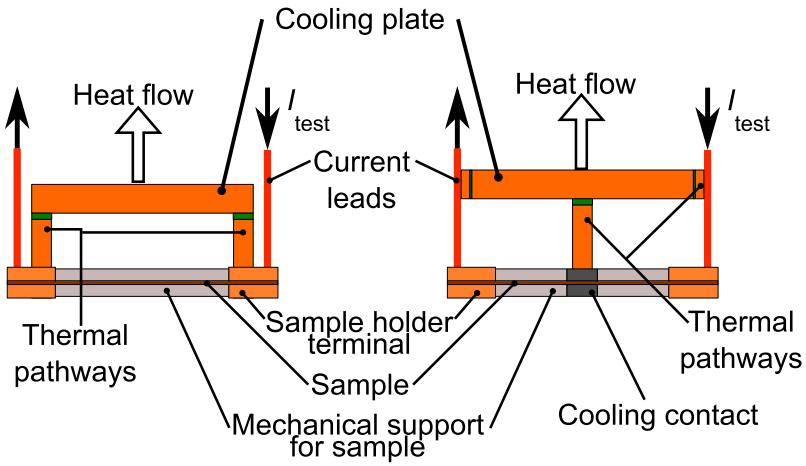

Figure 3.4: Illustration for outlining two different approaches to conduction-cooling.

Table 3.1: Thermal and electrical contact resistances of various contact types at 20 K. Thermal data are from [18] and electrical data from [18, 61, 37].

Contact	Thermal conductance $\left[\frac{\mathrm{W}}{\mathrm{cm^2K}}\right]$	Electrical resistance $[\Omega\mathrm{cm}^2]$
Solder, Pb-Sn	9	$0.004 \cdot 10^{-6}$
Low pressure (≈100 N)	0.01	$4300 - 6.45 \cdot 10^{-6}$
Low pressure, with grease	0.05	-
Moderate pressure (≈500 N)	0.05	$0.3 \cdot 10^{-6}$

current composite superconductor is tested in a conduction-cooled system, it is sensible to use the solder joint for interfacing the sample to the current terminal also as a cooling pathway. One such configuration is shown in figure 3.5.

Fast and straightforward sample changeover is often desired for a short sample testing setup. The setup illustrated in 3.5 contains a combined current/cooling fixture onto which the sample holder is mounted with pressed contacts. Changing the sample is fast as no soldering is required when the sample holder is mounted to the cryostat. For example, if two identical sample

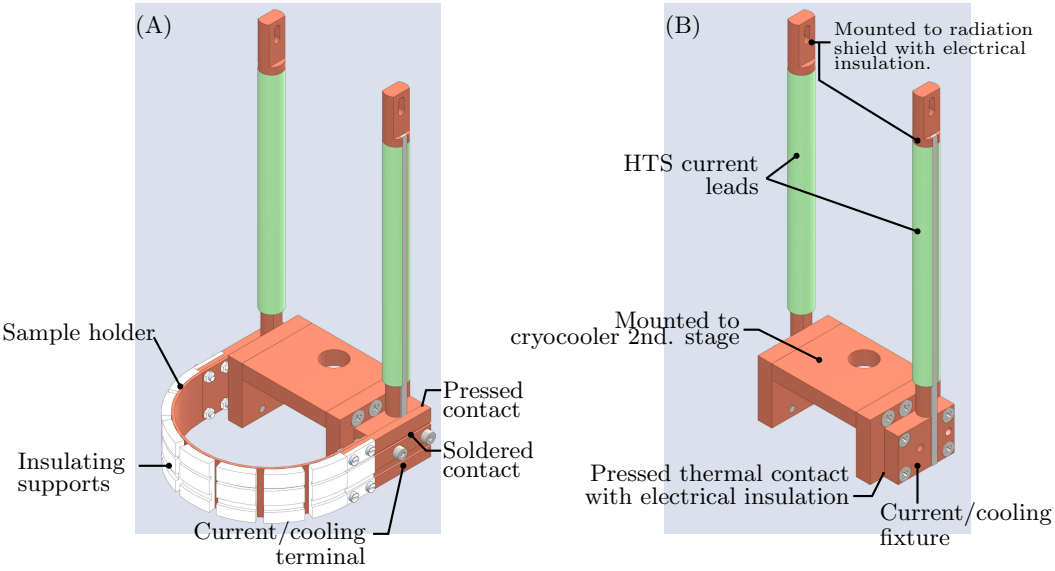

Figure 3.5: (A) Illustration of conduction-cooled sample holder with combined current and cooling terminals mounted onto corresponding fixture. In (B) sample holder mounting base is shown in more detail.

holders are used, one sample holder can be prepared with a new sample, while the other holder is cooling down for experiments with a previously prepared specimen.

An additional advantage for this kind of an arrangement is the added flexibility. When new experiments are considered the contacts for providing both current and cooling are already in place. Thus, it is easier to design a sample holder as it is not necessary to design also the interfaces to the cooling system or to the current terminals.

3.3.2 Designing the contacts

Several factors need to be considered when the current/cooling contact is designed for a conduction-cooled sample holder. One of these is the aspect ratio of the contact. Figure 3.6 shows a rectangular current/cooling contact, similar to that seen in figure 3.5, as a simplified domain suitable for numerical simulation. Here, the aspect ratio is defined as $\frac{\text{length}}{\text{width}}$. Studying different shapes of rectangular contacts and two similar MgB_2 composite superconductors with different sheaths[3] using FEM computations provided the data shown in figures 3.7 and 3.8. In the computations, it was assumed that a constant current of 200 A flowed through the superconductor at 20 K operating temperature. Material properties of copper were used for the terminal and fixture and contacting surfaces were assumed to be cleaned from oxidation giving an interface resistance of 300 $n\Omega cm^2$.

The results in figures 3.7 and 3.8 indicate that increasing the length of the contact decreases the dissipated power. When the simulated power dissipation with the two studied sheath materials are compared, it is clear that the significantly higher resistivity of the Monel sheath[4] results in increased resistive losses. It is also evident, that depending on the conductivity of the superconductor sheath material, changing the width of the contact has only a limited effect.

While modeling the current/cooling contact seems straightforward, it is worth mentioning that the interface resistance of the pressed copper-copper contact between the sample holder and the cryostat can be significant. Table 3.2 lists the measured contact resistances of a pressed contact when different surface finishes are applied to the mating surfaces. Comparing the values

[3]With MgB_2 wires, the outmost part of the matrix is often called sheath due to the fabrication process.

[4]For example in 20 K temperature the resistivities used in computations were $1.7 \cdot 10^{-10}$ Ωm and $3.65 \cdot 10^{-8}$ Ωm for the copper and Monel sheaths, respectively.

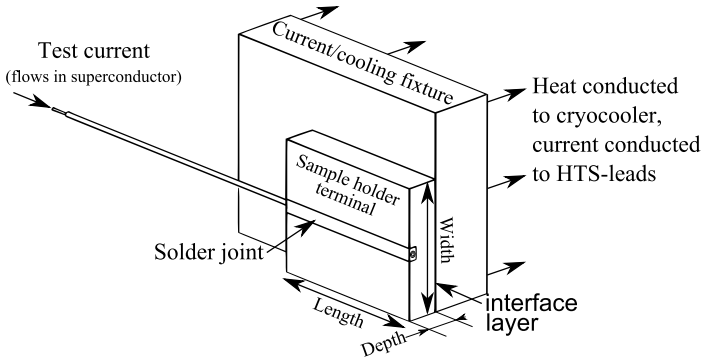

Figure 3.6: Current/cooling contact simplified for computational modeling and definitions of dimension naming.

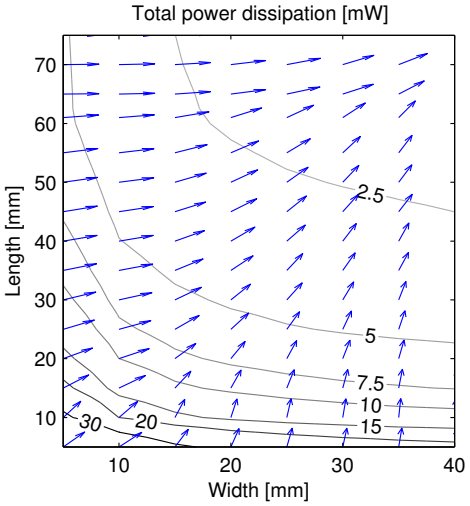

Figure 3.7: Total ohmic losses in current/cooling contact with Cu sheathed MgB_2 composite conductor.

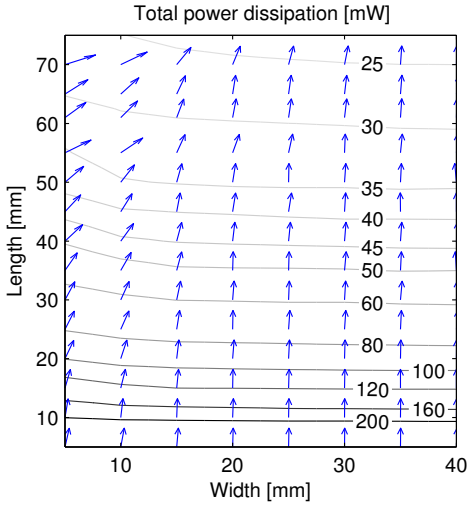

Figure 3.8: Total ohmic losses in current/cooling contact with Monel sheathed MgB_2 composite conductor.

in table 3.2 show that if the contact terminal cannot be polished after soldering the sample, the increase in interface resistance should be taken into consideration.

Based on these notions, it can be determined, that

- the sample, especially the sheath material, has a significant effect on the dissipation in the contact,
- the contact should be made as long and wide as possible, emphasizing

Table 3.2: Measured contact resistivities (R_{int}). Values for soldered contacts were taken from [31].

Interface type	R_{int}[nΩcm^2]	Interface type	R_{int}[nΩcm^2]
Cu,ox	2700	Cu, cleaned	300
Ag-grease	2270	Ag-grease, cleaned	$\sim$270
N-grease+Cu dust	1980	Soldered, 96.5Sn/3.5Ag	121
		Soldered, 90In/10Ag	45

the length over width and

- if a pressed contact is used, e.g. between the holder's contact and the cryostat's fixture, it should be polished as it can reduce the interface resistance by an order of magnitude.

3.4 Mechanical support

Supporting the sample against Lorentz, and other, forces occurring during a measurement was listed a key function for a sample holder. The support structure can, at first, look like a simple component. In reality, it has to be as carefully designed as any other component in a sample holder.

The support structure is often fabricated from a material with poor electrical conductivity to prevent low resistivity current paths in parallel with the sample form interfering with the measurement. However, composite superconductors often contain large amounts of copper or some other low resistivity metal such as silver. Using different materials in the sample and holder can cause challenges during cooldown as the thermal contraction of the components might be different. For example, during cooldown from 290 K to 20K, a one meter long solid rod made from copper, brass or nylon would contract 3.2, 3.9 and 12.6 mm, respectively [36]. From this point of view, the best material for the support structure would be to use the same metal that is used in the composite superconductor. In such case, the support structure would have to be carefully insulated from both the sample and the current terminals. However, this has proven to be a challenge, and therefore the use of insulating supports is preferred whenever possible.

Designing the sample holder to withstand mechanical stresses is thoroughly discussed by Ekin in [18, pp.296-298]. Also, matching the differences in thermal

contraction is analyzed in detail in [18, pp.282-288,303].

3.5 Instrumentation

3.5.1 The Basics

Once the sample holder has been designed and constructed properly, the next step is to mount and connect the necessary measurement instruments. Depending on the measurement that is to be performed, the quantity of instrumentation can vary significantly. Based on the discussion so far, the required instrumentation in the very basic $V(I)$-measurement consists of sensors for both temperature and current plus a pair of potential taps. The applied magnetic field is typically known beforehand as a function of magnet's current. This configuration, known as the four-lead arrangement[5], is outlined in figure 3.9(A).

When MQE and NZPV are measured, more information is required. In these measurements the propagation of the normal zone needs to be confirmed and monitored. The configuration illustrated in figure 3.9(B) shows a setup capable of monitoring quench propagation by both thermal and electrical signals. This is achieved by increasing the number of potential taps and temperature sensors, the central potential tap across the quench heater is used to verify proper heater operation and the presence of a normal zone.

The potential taps and sensors are separated by a known distance Δl. Also, as the NZPV measurement is performed in time domain, acquisition time of each data point must be recorded as well. In figure 3.9(B) the voltage and temperature meters are connected to a multiplexer. This reduces the number of the expensive measurement instruments, i.e. in figure 3.9(B) only one voltage meter is required for monitoring the five potential taps. On the downside, this limits the highest sampling frequency per channel to $\frac{1}{5}$ of the maximum frequency of the instruments. The same applies also for the temperature instrumentation. Thus, the most accurate results are achieved, if each potential tap and temperature sensor is monitored with a dedicated instrument.

Wiring and connecting the instrumentation requires care and planning. There are several sources of interference that can effect the low level signals often present in the characterization of superconductors. The possible sources

[5]The name four-lead arrangement can be derived from the fact, that four leads are connected to the sample. The test current is provided through a pair of wires, and the voltages are measured with a different pair of wires.

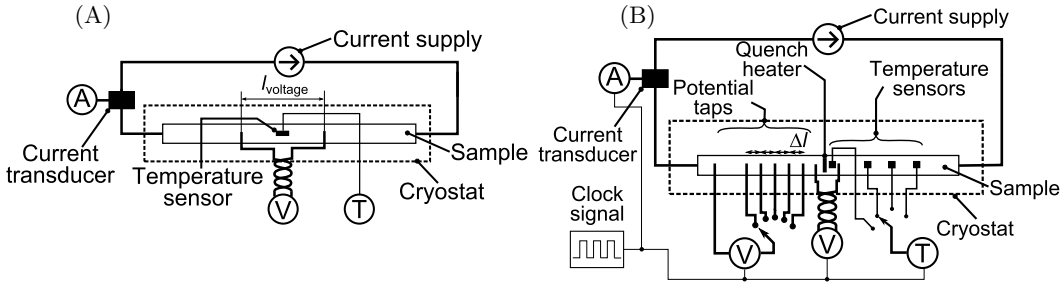

Figure 3.9: Schematic presentation of measurement setups used for studying $V(I)$-curve (A) and thermal stability (B). Ⓐ, Ⓥ and Ⓣ denote measurement instruments for current, voltage and temperature, respectively.

of interference listed in [18, pp.150-151,161-166,288-289] include e.g.

- thermoelectric voltages,
- magnetic coupling,
- rf-noise from laboratory equipment,
- ground loops and
- artifacts from superconducting solder joints.

The techniques for managing these interferences in [18, chap. 4] also apply to conduction-cooled systems. The thermoelectric potentials are best managed by avoiding joints, especially soldered, in wiring used for sensing low voltages. If joints are necessary, they should be heatsinked carefully. Magnetic coupling and other forms of electromagnetic interference are reduced or eliminated when tightly twisted and shielded conductors are used. Ground loops are prevented by using a single grounding point.

In addition to electrical interference, the instrumentation wiring can leak heat into the sample space. Using a wire with small cross-section and poor thermal conductivity is a good choice in most cases. In some cases, the instrumentation wiring is used to transport larger excitation currents, from few mA to a few A. In these situations, a case by case study of the necessary wire cross-section should be made. Also, a rough estimation of the heat leak should also be done, if measurements where even small heat leaks can effect results, such as determining thermal conductivity, are to be made.

3.5.2 Estimating heat leak through instrumentation wires

The length of an instrumentation wire is considerably greater than the diameter. Therefore, the heat flow through the conductor can be modeled using one dimensional approximation i.e. it is assumed that each radial cross-section of the wire is at constant temperature and thermal gradient is only present along the wire. In such a case, an easy solution for estimating the heat influx is to use the tabulated thermal conductivity integrals found in literature. Table 3.3 lists the thermal conductivity integrals for copper and phosphor bronze as these two materials are often used in instrumentation wiring. If the wire has a cross-section of A [m^2] and a length of l [m], the heat flux $\dot{q}$ [W] through the wire is

$$\dot{q} = \frac{A}{l}\int_{T_1}^{T_2} \lambda(T)\mathrm{d}T = \frac{A}{l}\left\{\int_{4\,K}^{T_2} \lambda(T)\mathrm{d}T - \int_{4\,K}^{T_1} \lambda(T)\mathrm{d}T\right\}, \tag{3.1}$$

where T_1 and T_2 are the cold and warm end temperatures, respectively and $\int_{T_{\mathrm{lower}}}^{T_{\mathrm{upper}}} \lambda(T)\mathrm{d}T$ are the thermal conductivity integrals. For example, the heat leak from 300 K to 10 K through a copper conductor having the length of 1 m with the diameter of 0.5 mm is 31.2 mW. The computed heat leak was for one wire only and e.g. in a simple measurement system with two temperature sensors, two pairs of potential taps, and temperature control heater, 10 to 14 wires are required depending on the temperature sensors used. Therefore, the heat leak needs to be multiplied by the number of wires. Thus, the total heat rate of 310 to 440 mW flows into the sample space through the instrumentation wiring.

A phosphor bronze wire with the same dimensions would leak 2.3 mW per wire. The bundles with 10 and 14 wire would thus leak 23 and 32 mW, respectively. By selecting the instrumentation wiring material correctly, the stray heat flux into the sample space can be significantly reduced.

Table 3.3: Thermal conductivity integrals for ETP copper [18, App. A2.1] and phosphor bronze [44, 36].

Temperature T [K]	ETP Copper $\int_{4\,K}^{T} \lambda(T)\mathrm{d}T$ [kW/m]	Phosphor bronze $\int_{4\,K}^{T} \lambda(T)\mathrm{d}T$ [kW/m]
10	3.32	0.0186 - 0.0194
77	68.6	1.07 - 1.13
300	162	9.36 - 11.8

The allowed heat leak depends greatly on the application, but as a rule of thumb 1% of the available cooling power has been found to work adequately. For example, the RDK-408S2 [77] cryocooler in our laboratory has a capacity of 5.4 W at 10 K and with this cryocooler, the maximum allowed total heat leak through the instrumentation wiring is 54 mW. I have often used 25 pin D-subminiature connectors in vacuum thight feedthroughs and with 25 instrumentation leads, the allowed heat leak per wire is 2.2 mW.

In addition to limiting the quantity of heat conducted through the instrumentation wiring, the point into which it is deposited in the cold end also requires consideration. For example, to ensure accurate temperature readouts, the temperature sensor wires need to be heat sinked. If this step is not taken, the heat conducted through the wiring connection is deposited into the sensor resulting in too high temperature readings.

Some effective ways of thermally anchoring the wires are illustrated in figure 3.10. The figure illustrates three options for routing the instrumentation wires. In the option A), the wires are directly connected to their targets e.g. temperature sensors etc. without any heatsinking. In the option B) the instrumentation wires are heatsinked near their targets, e.g. at the cooling plate. In the option C) the wires are heatsinked to both the radiation shield and near end points.

If the cryostat in figure 3.10 was equipped with 25 instrumentation wires with a minimum length of 1 m and 15 cm of additional wire required for each heat sinking post, the resulting heat leaks for each case are listed in table 3.4.

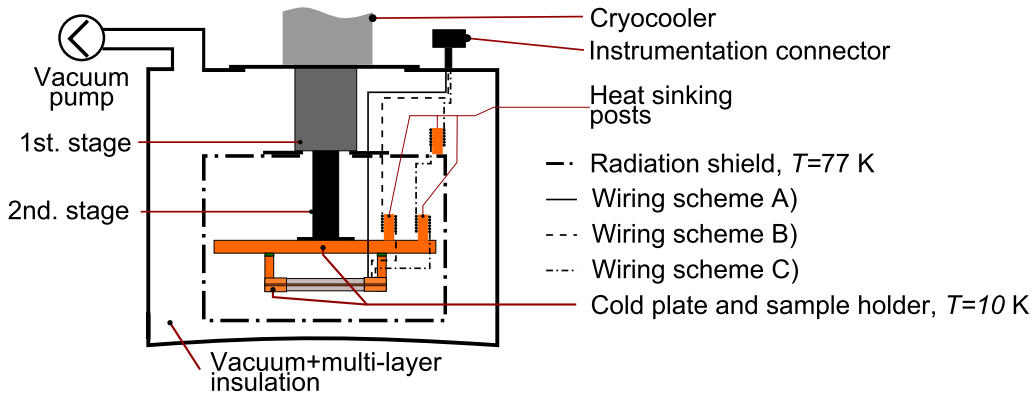

Figure 3.10: Different options for routing and thermally anchoring instrumentation wires: A) Direct connection from terminal to target, B) Thermal anchoring to cold plate just before target, C) Dual thermal anchoring to radiation shield and to cold plate.

Table 3.4: Estimated heat leaks for the wiring schemes illustrated in figure 3.10. Heat sinking length assumed to be at constant temperature. Therefore, conduction length listed in table was reduced by heatsinking length for computations.

Wire material $A_{\text{wires}} = 25 \cdot 0.0181$ mm^2	Case A) $L_{\text{wire}} = 1.15$ m $L_{\text{heatsink}} = 0$ m	Case B) $L_{\text{wire}} = 1.3$ m $L_{\text{heatsink}} = 0.15$ m	Case C) $L_{\text{wire}} = 0.5 + 0.5$ m $L_{\text{heatsink}} = 0.15 + 0.15$ m
ETP Copper	72 mW	72 mW	85 mW (300 → 77 K)
			59 mW (77 → 10 K)
Phos.bronze	5.3 mW	5.3 mW	9.7 mW (300 → 77 K)
			1.0 mW (77 → 10 K)

Based on the results, options B) and C) are both efficient ways for controlling the heat seepage into the sample space, but the best option depends on the wire material and how the length of the wiring is distributed between the three temperature levels. Note, that the advantage with option B) over A) is that the heat leak through the instrumentation wires flows to the heatsinking post and not to the sample.

In some experiments, heat leak from the sample into the instrumentation wiring must also be taken into account. For example, in a minimum quench energy measurement, a precise amount of energy needs to be deposited into the sample under test. In such a measurement, it is possible that a non-negligible part of the quench initiation pulse energy flows through the heater wiring into the heat sinking post. Figure 3.11(A) shows a schematic illustration of a conduction-cooled setup with a quench heater attached to the sample along with the heat sinked wiring. All other sensors and wires are omitted for clarity.

A rough estimation whether the heater wiring will have an effect on the measurement results or not, can be made using a steady state thermal network model. For the case shown in figure 3.11(A), if it is assumed that

- heat conducts in one dimension only,
- the changes in temperature are small and
- the material properties are constant,

the corresponding thermal network is shown in figure 3.11(B). If the quench heater is mounted to the sample midpoint and the length of the heater wiring

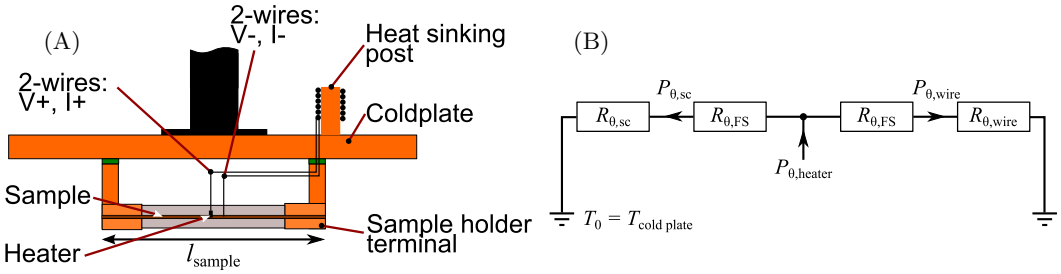

Figure 3.11: One option for realizing quench heater wiring in MQE measurement. Schematic illustration of sample space components and heater wiring is shown in subfigure (A) (for further details, see figures 3.4 and 3.9(B)). In subfigure (B) thermal pathways connected to quench heater are presented as thermal network. Legend: $R_{\theta,\mathrm{sc}}$ =thermal resistance through superconducting sample, $R_{\theta,\mathrm{wire}}$ =thermal resistance of heater connection wiring, $R_{\theta,\mathrm{FS}}$ =thermal resistance from heating element to soldered terminals, $P_{\theta,\mathrm{sc}}$ =heat rate to sample, $P_{\theta,\mathrm{sc}}$ =heat rate to connection wiring and $P_{\theta,\mathrm{heater}}$ =heat rate dissipated in heating element.

is l_{wire}, the thermal resistances $R_{\theta,\mathrm{sc}}$ and $R_{\theta,\mathrm{wire}}$ in figure 3.11(B) are defined as: from the perspective of the heater,

- the sample forms two equal thermal paths connected in parallel, thus $R_{\theta,\mathrm{sc}} = \left(\frac{\frac{1}{2}l_{\mathrm{sample}}}{A_{\mathrm{sc}}\lambda_{\mathrm{sc}}}\right)/2$
- the two heater connection wires, one for heater voltage measurement and the other for supplying current, form two equal thermal paths connected in parallel, thus $R_{\theta,\mathrm{wire}} = \left(\frac{l_{\mathrm{wire}}}{A_{\mathrm{wire}}\lambda_{\mathrm{wire}}}\right)/2$.

The thermal resistance $R_{\theta,\mathrm{FS}}$, i.e. the thermal resistance from the heating element to the heat flow paths, depends on the type of the heater and how the heating element is connected to the other components.

As an example, the sample holder shown in figure 3.1(C) was used in the MQE measurements presented in the next Chapter. A surface mount device(SMD) resistor, size 0805, was used as the quench heater with one end soldered directly to the superconductor. The heater wiring was soldered to the other end. The thermal resistance from the resistive element to the casing is 38 K/W and the thermal resistance of each solder joint is 1 K/W [80]. The length and diameter of the sample were 300 mm and 0.83mm, respectively. The copper wires connected to the heater were 0.1 m in length, measured from the heat sinking post, with a diameter of 0.152 mm. The system operated at 20 K temperature.

With this data, the thermal resistances of the two conduction paths can be calculated

$$\begin{aligned} R_{\theta,\mathrm{sc.tot}} &= \frac{\frac{\frac{1}{2}l_{\mathrm{sample}}}{A_{\mathrm{sc}}\lambda_{\mathrm{sc}}}}{2} + R_{\theta,\mathrm{FS}} = \frac{0.5 \cdot 0.3}{(0.5 \cdot 0.83 \cdot 10^{-3})^2 \cdot \pi \cdot 2100} + (38+1) \\ &\approx 104 \text{ [K/W]} \\ R_{\theta,\mathrm{wire.tot}} &= \frac{\frac{l_{\mathrm{wire}}}{A_{\mathrm{wire}}\lambda_{\mathrm{wire}}}}{2} + R_{\theta,\mathrm{FS}} = \frac{0.1}{(0.5 \cdot 0.152 \cdot 10^{-3})^2 \cdot \pi \cdot 1500} + (38+1) \\ &\approx 1900 \text{ [K/W]}. \end{aligned}$$

If the heater connection wires were replaced with a flat ribbon cable, typically fabricated with 26 AWG[6] (⌀0.405 mm) strands, the thermal resistance of the two wires would be approximately 300 K/W. With the thin wire the ratio of thermal resistances is 18.3, but with the slightly thicker 26 AWG ribbon cable, the ratio drops to 2.9.

For one of the data points in the MQE experiment, the heater resistance was 437 Ω and current 40 mA resulting in a heat rate of 0.7 W. The heater was energized for 15 ms and thus the energy of the pulse was 10.5 mJ. With the thermal resistances computed above, the energy injected into the superconductor can be estimated to be 9.9 mJ and 7.8 mJ for the 0.152 mm and 26 AWG wires, respectively. This final analysis of quench pulse energy distribution into the two thermal paths violates the steady state assumption made at very beginning. Therefore, the obtained result does not accurately describe the situation, but it gives a first order estimation where the energy of the heat pulse will eventually end up. It is obvious that with the 26 AWG wire, too much of the pulse will bleed to the heat sinking post resulting in optimistic MQE values.

3.5.3 Temperature measurements

In general, there are two common approaches to thermometry. One is based on the thermal expansion and contraction of a solid, liquid or gaseous sensing material, e.g. bimetal, mercury and helium gas thermometers. The other depends on the changes in the electrical properties of a sensing element as a function of temperature. Today, calibrated, accurate and robust electrical temperature sensors are readily available from several commercial vendors. These components are simple to use and small in size, and therefore have become the

[6] America wire gauge, a North American standard for current carrying round wires

standard method for sensing cryogenic temperatures in most applications.[18, pp.185-202]

There are three main categories of electrical sensors: Resistance temperature detectors (RTD), diodes and thermocouples. Here, the different categories of sensors and their features are only briefly reviewed as discussing cryogenic thermometry in detail is beyond the scope of this thesis. For further reading on this topic see [18] and product literature of sensor suppliers.

As the name implies, the resistance of an RTD changes when temperature changes. A large temperature coefficient of resistivity is desired as it increases sensitivity and accuracy. For cryogenic applications, a negative temperature coefficient is preferred i.e. it is desirable that the sensor resistance increases as the temperature decreases. With such a sensor, the resistivity is high in cryogenic temperature range making it easier to measure. Constant direct current excitation is often used, but in an electromagnetically noisy environment it is possible to use lock-in techniques and AC excitation for noise rejection. [18, pp.185-196][44].

Diodes are similar to negative temperature coefficient RTDs as the output signal, the forward voltage drop(V_f), increases with decreasing temperature. Different from RTDs, the diodes however require excitation with a predefined constant direct current as the V_f also depends on the forward current. The calibration curves must therefore be accompanied by the excitation used in the calibration process.[18, pp.185-196][44].

The thermocouple is a sensor that does not require excitation. Instead, the sensor operation is based on the difference of thermoelectric voltages between wires made from different metals. When the thermocouple wires are joined from the ends to form the sensing element, one end is fixed at a known temperature.The potential difference between the two wires then depends on the temperature of the other end.[18, pp.185-196]

Each of these sensor types has it own advantages and drawbacks. Table 3.5 lists the most common types of temperature sensors, their strengths and weaknesses.

Depending on the application, different properties are required. For example, if the temperature is measured in a magnetic field, the only viable option of sensors in table 3.5 is the Cernox. On the other hand, if the sensor is not exposed to a magnetic field and very high accuracy is required, the Germanium sensor is the best choice. Applications requiring fast response to thermal transients, a sensor with small thermal mass and fast response time is required and the thermocouple is a viable option. What almost all of the sensor types

Table 3.5: Sensors for measuring temperature.[18, pp.185-196][44]

Sensor	Pros	Cons	Price (Uncal.-Cal.)
Platinum (RTD)	Cheap, interchangeable, standard curve	Sensitive to magnetic field, usable above 14 K.	∼$85-1300
Rhodium Iron (RTD)	Stability over time, wide temperature range, secondary standard	Sensitive to magnetic field, expensive, requires calibration	∼$2906-3539
Germanium (RTD)	Stability over time, high sensitivity, secondary standard[a]	Sensitive to magnetic field, expensive, requires calibration	∼$457-1300
Cernox™ (RTD)	Insensitive to magnetic field, good accuracy and sensitivity	Expensive, requires calibration, not a secondary standard	∼$100-1700
Silicon diode	Cheap, interchangeable, standard curve, high output signal	Sensitive to magnetic field, less accurate, long term stability is moderate, self-heating	∼$200-800
Thermocouple wire	Cheap, standard curve, very small	Sensitive to magnetic field, low signal, low accuracy	∼$17/m

[a]The sensor can be used for accurate, certifiable, calibration of other sensors as its accuracy and reproducibility are very good.

presented in table 3.5 have in common, is their high price and the requirement of individual calibration.

3.5.4 Alternative for the commercial sensors

One of the most interesting sensors listed in 3.5 is the Si-diode. These sensor are not that expensive and they are interchangeable to a high degree, e.g. the type DT-670A by Lake Shore has an interchangeability of $\pm$ 0.25 $°K$ between $2-100$ K [44]. The drawbacks, as listed in table 3.5, are the poor tolerance to a magnetic field and the above average self-heating. However, for an application where the number of sensors is more important than these two downsides, the Si-diode is a viable choice. In such a case, the interchangeability allows all the sensors to be monitored with a single display/recording unit and a multiplexer unit thus reducing the total cost of the temperature instrumentation.

While the commercially available Si-diodes are from the cheaper end of cryogenic temperature sensors, the price of a single unit is still quite high. The

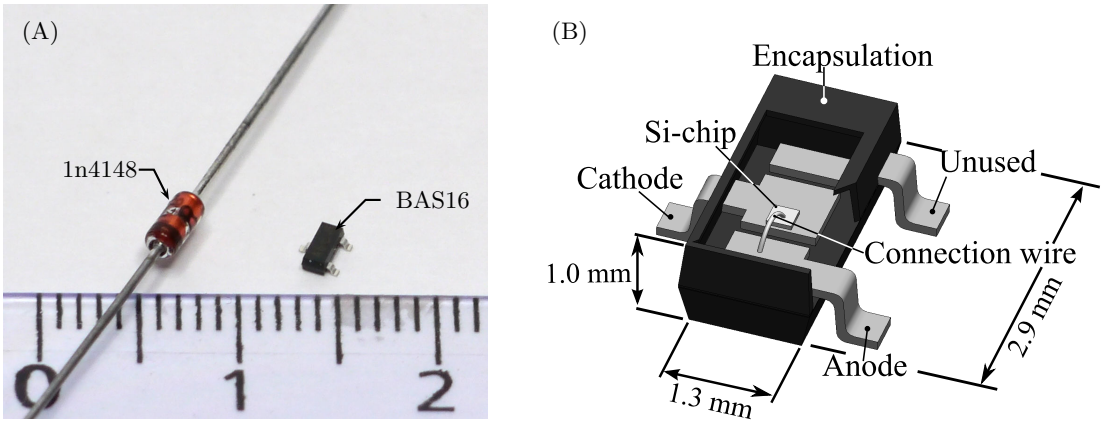

Figure 3.12: On the left (A): Silicon rectifier diode 1n4148 pictured with surface mount alternative BAS16. Minor tick marks of the scale at the bottom of figure are 1 mm apart. On the right (B): Internal structure of the BAS16 diode in SOT-23 case is shown. Note: Distance from the top of the case to Si-chip (0.5mm) is considerably longer than from bottom (0.3)mm. Total height 1mm contains also thickness of the lead wires (0.1 mm) and 0.1 mm gap from bottom to mounting surface.[69]

Si-diode for thermometry is electrically similar to a standard rectifier diode such as the 1n4148. Both have a pn-junction and the forward voltage drop across the junction varies when the temperature is changed. This raises the question, if a standard rectifier diode used in electronics could be used as a cheap substitute for the commercial cryogenic diode sensor. The 1n4148, and its SMD equivalent BAS16, have been successfully used as a very low cost temperature sensor in temperature range of 50-300 K [64]. The two components are pictured in 3.12(A). However, to be able to use the component in conduction-cooled measurements with MgB_2 superconductor, the lower end of the temperature range needs to be extended to begin from 20 K or below. Also, for the sensor to be useful in a variety of superconducting applications, the response to thermal transients and external magnetic fields needs to be determined.

First, the suitability of the BAS16 component as an absolute temperature sensor was studied. Four samples were mounted into a conduction-cooled cryostat and the changes in V_f were recorded as a function of temperature. In the measurements, a calibrated Cernox CX-AA[7] type sensor was used as a reference. The resulting $V_f(T)$-curves are shown in figure 3.13(B) along with

[7]Copper can package, ⌀3.048 mm and length 10.032 mm.[42]

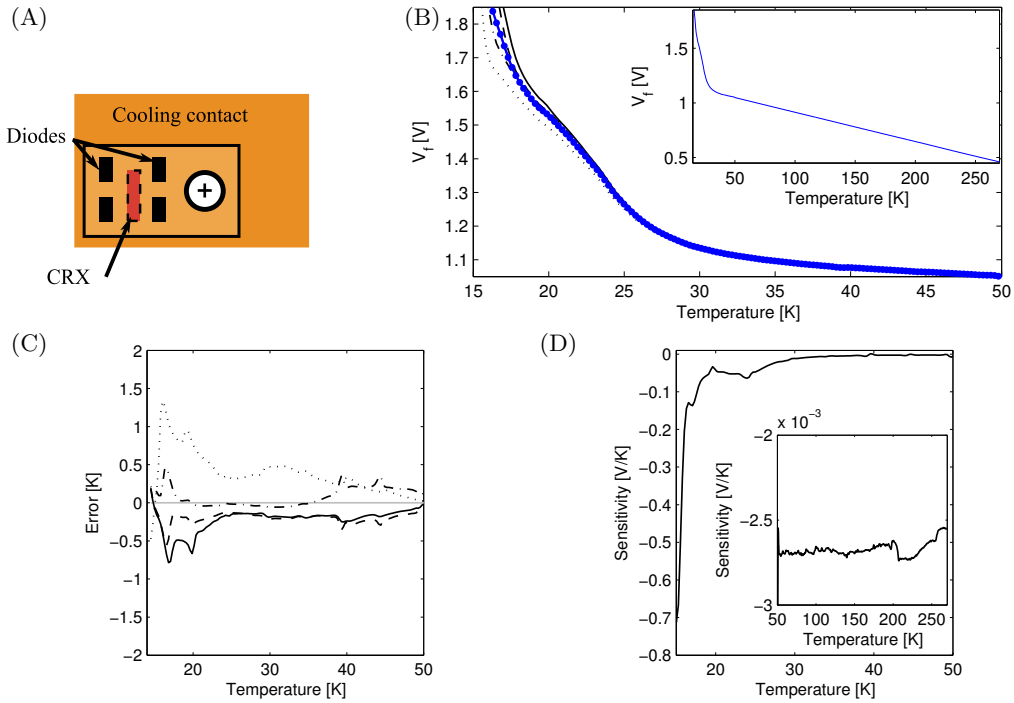

Figure 3.13: BAS16-diode V_f temperature dependence measurement setup and results obtained between 15-270 K. In subfigures (B) and (C) different line types indicate different BAS16 units: — D1, – · – D2, - - - D3, ··· D4, —●— $V_{\mathrm{f,mean}}$ fit. Subfigure (D) presents sensitivity $\frac{V_\mathrm{f}(T)}{T}$ computed from $V_{\mathrm{f,mean}}$ fit

the curve $V_{\mathrm{f,mean}}(T)$ representing the smoothed average response of the four tested units. Figure 3.13(C) shows the error in temperature readout of each specimen with respect to $V_{\mathrm{f,mean}}$. That is, if the temperature display unit was calibrated with $V_{\mathrm{f,mean}}(T)$, the data in figure 3.13(C) shows the error in measured temperature vs. actual temperature.

The data shown in figure 3.13(C) suggests, that the BAS16 sensor can be used as a temperature sensor with ±0.8 K accuracy above 20 K. Below 20 K, the error increases significantly.

Further processing of the fitted curve $V_{\mathrm{f,mean}}(T)$ provides the sensitivity graph presented in figure 3.13(D). The data shows, that the sensitivity of the BAS16 diode begins to increase below 30 K. The sensitivity at 30 K was measured to be 10 $\frac{\mathrm{mV}}{\mathrm{K}}$ and it was observed to increase to 50 $\frac{\mathrm{mV}}{\mathrm{K}}$ at 20 K. High sensitivity allows the sensors to be used for monitoring fluctuations in temperature. This property is useful e.g. in thermally monitored quench initiation

and propagation measurements. However, monitoring changes in temperature in such an application also requires a fast response time in addition to high sensitivity. Further experiments are therefore required.

The following conclusion can be made from the results of the steady state $V_{\mathrm{f}}(T)$-measurement:

- Absolute accuracy is sufficient for monitoring temperature above 20 K to within ± 0.8 K. Below 20 K the variation between specimens increases significantly and individual calibration is required.
- The sensitivity of the sensor increases with decreasing temperature and the value 10 $\frac{\mathrm{mV}}{\mathrm{K}}$ obtained at 30 K temperature is sufficient for monitoring temperature fluctuations in the order of 10 mK.

By combining FEM computations with measurements, the setup shown in figure 3.14 was used for determining the response time of the BAS16 diode. The CX-AA sensor with known response time was used as a reference. The results from the response time measurement are shown in figure 3.14(A) and (B). For these tests, the detection of 16 mK shift in temperature was used in determining the response time. First, it should be noted that an unmodified BAS16 diode in SOT-23 casing performs poorly with respect to the reference sensor. Thus, by studying the structure of the SOT-23 case shown in figure 3.12(B), the component was modified by removing some of the black plastic encapsulant. The component encapsulation was sanded with fine grit sandpaper exposing the terminals from below. The procedure notably improved the transient behavior as the results in figure 3.14(C) and (D) show.

However, further testing of the modified BAS16 diode in a quench propagation measurement showed poor results. The response time of the modified sensor was too long for accurately monitoring the fast thermal transients of a short sample quench propagation experiment. The measurement setup is illustrated in figure 3.15(A). Figure 3.15(B) shows the data obtained from potential taps, labeled $\varphi_{1\to 5}$, and the BAS16 temperature sensors labeled D1 $\to$ 3. When the data from the potential taps is compared to the data from the diodes D1 and D3, two problems can be observed. First, the observed increase in temperature is significantly delayed when compared to the voltage signals. Second, the temperature of D3 is greater than that of the D1 sensor from the power supply cutoff to 4 seconds of elapsed time. This indicates that producing consistent transient properties by sanding down the encapsulation of the BAS16 diodes is challenging.

Three conclusions can be made from the transient experiments:

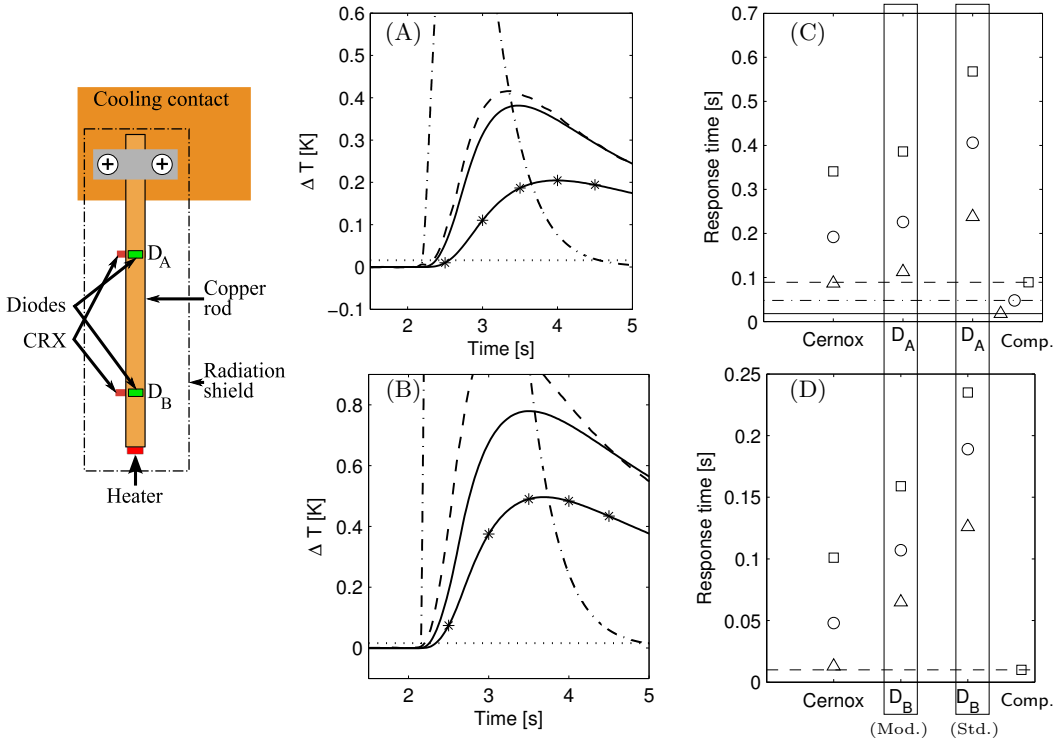

Figure 3.14: BAS16-diode V_f transient response measurement setup and results. Subfigures (A) and (B) show the response of different sensors measured near cooling contact and heater, respectively, at T_{init} = 25 K. Legend: —∗— diode in standard casing (Std.), — diode in modified casing (Mod.), - - - Cernox (CRX),– · – Computed, ··· 16 mK criterion. Subfigures (C) and (D) show the measured response times at T_{init}= 30 K(□), 25 K(○), 18.5 K(△).

- The transient response of a standard BAS16 diode is slow.
- It can be significantly improved by reducing the thickness of the encapsulation material and properly orienting the SOT-23 case.
- Producing sensors with consistent transient properties by sanding down the case is problematic.

As listed in table 3.5, one of the major weaknesses of the diode sensors is the sensitivity to external magnetic fields. Therefore, the in-house diode sensor was subjected to external magnetic field at different orientations. Four temperatures (16, 20, 25 and 30 K) and three magnetic flux densities (0.5, 1 and 1.5 T) were used in the experiments. The testing setup is illustrated in figure 3.16(A) and the measurement results in figure 3.16(B).

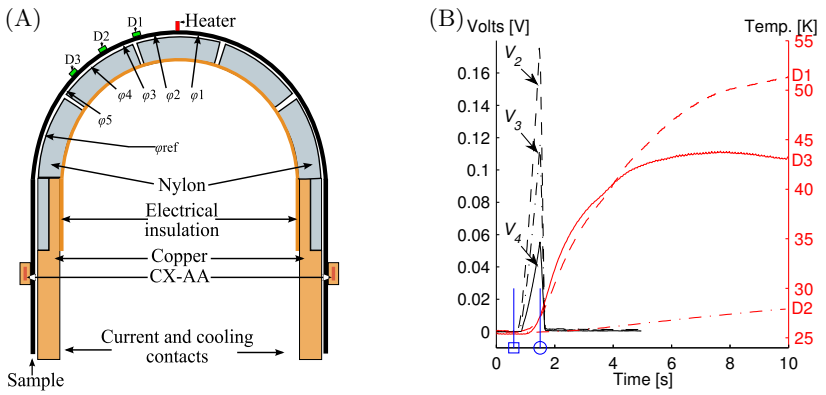

Figure 3.15: Setup and results used for evaluating BAS16 diode sensor in quench propagation measurement. Measurement setup with instrumentation is illustrated in subfigure (A) and results in subfigure (B). Voltage-time graphs V_{2-4} in (B) were measured between potential taps φ_{3-5} and φ_{ref}, respectively. Diode D2 did not register quench event properly as it had detached from sample during cooldown. The blue vertical lines with □ and ◯ indicate times of quench initiation pulse and power supply cutoff, respectively.

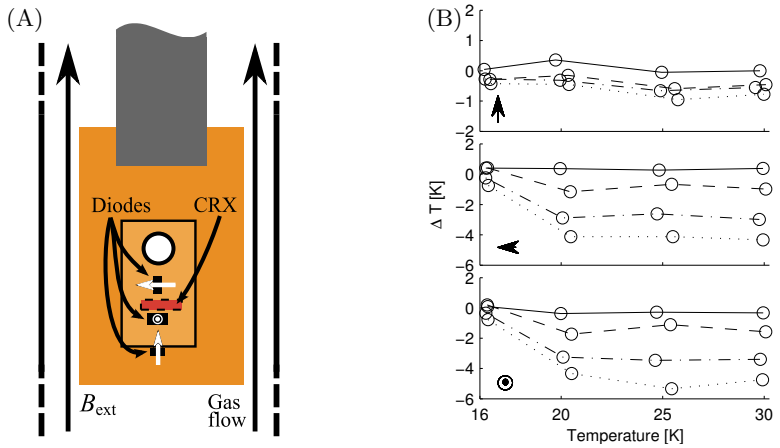

Figure 3.16: BAS16-diode magnetic field error measurement. Measurement setup is illustrated in (A) and results in (B). White arrows in (A) and black arrow in (B) show the direction of current flow in the pn-junction. For computing the error, $V_{\mathrm{f,mean}}(T)$ was used as a reference. Legend: $B_{\mathrm{Ext}} = 0$ T(—), 0.5 T(- - -), 1 T(– · –) and 1.5 T(· · ·).

The results show, that when the current flowing through the pn-junction was aligned with the external magnetic field, no error was introduced to the temperature measurement. In the worst orientation, when the current and

the external magnetic field were perpendicular to each other, the error was found to depend from both the temperature and the magnetic flux density. Thus, if the sensor is properly aligned, it is possible to use the BAS16 diode in an external magnetic field. However, this requires *a priori* knowledge of the magnetic fields present in an application.

3.6 Remarks

Sample holder in a conduction-cooled system has more functions than those found in conventional liquid or gas flow systems. In conduction-cooled systems, the sample, and its thermal and electrical properties, need to be taken into consideration when the holder is designed. The current contacts can be used also as the thermal interface, but in such cases it is essential that the heat transfer aspect is included into the design process from the beginning. It is possible to produce an adequate electrical connection while the thermal connection remains poor.

The stray heat flux flowing through the instrumentation wiring can cause challenges in achieving and maintaining the desired operation temperature. The limited cooling capacity inherent to conduction-cooled system calls for at least a first order estimate of the heat leak to be made, if measurements which are sensitive to temperature are performed. Planning the heat sinking of the instrumentation wiring requires care. It is possible to increase the heat load to the sample space, if the wire length between the sample connection and intermediate temperature is not sufficient.

Commercial temperature sensors are necessary for ensuring the reliability of temperature measurements. However, for some applications the expensive commercial sensor can be replaced with a cheap in-house option. For example, if a large amount of sensors is required and high accuracy is not the main requirement, such cheap alternatives can reduce the cost of the temperature instrumentation significantly.

In this Chapter, I have shown what are the aspects that separate a conduction-cooled sample holder form others. I presented tools and measurement results to be used in the designing such a sample holder. Furthermore, I showed how planning the instrumentation connections is important in controlling the stray heat flux into the sample space. Finally, I demonstrated how cheap alternatives for commercial temperature sensors can be used in applications requiring multiple sensors, but in which limited measurement accuracy is not a challenge and where fast response is not important.

Chapter 4

Short sample measurements in conduction-cooled system

In this Chapter I discuss how critical current and thermal stability parameters are measured in a conduction-cooled system. The previous chapter focused on designing a sample holder suitable for such measurements. The topics of self-heating and instrumentation were covered from the perspective of constructing a functional sample holder. Now I present, how these two topics connect to the measurement and data processing.

First, the $V(I)$-measurement is scrutinized. The discussion on the factors effecting measurement accuracy and on the challenges in using conduction-cooling is based on **Publication 4**. Most of the measurement data presented in this section was measured for **Publication 5**. In the second section, the thermal stability measurement is analyzed based on the results from **Publication 1** and **Publication 5**.

4.1 Measuring critical current and n-value - The $V(I)$-measurement

The determination of the characteristic voltage-current dependence of a superconductor is known as the $V(I)$-measurement. This measurement is a very common method for studying and comparing the quality and performance of superconducting wires. Performing the $V(I)$-measurement is simple in principle, as it only involves cooling the sample to superconducting state and then increasing the current passing through the sample until I_c is

reached. However, the measurement has proven to be more involved than it initially seems and Goodrich and Ekin, for example, have done extensive work in analyzing and developing the $V(I)$-measurement and procedures [18, 21, 22, 23, 24, 25, 27, 26, 28]. However, they have focused on measurements in liquid and gas flow cooled systems. Most of the challenges also apply to conduction-cooled systems, but some of these are an even greater in them. For example, the self-heating due to AC-losses in the sample, or the resistive losses in the normal conductive components, such as the current terminals, are more challenging to control [33, 82].

The work presented in [33] show that by varying the rate at which the test current is increased has a significant effect on the n-value and I_c. For example, at 2 A/s the n-value and I_c were reported to be 19-41 and 165-170 A, and at 30 A/s 19-25 and 175-166 A for a 14 filament MgB_2 /Ni/Fe/Cu tape. Also in [33] a method for correcting the effects of self-heating presented in [32] was demonstrated and the corrected results were shown to be more consistent. Combining the correction method with a properly designed sample holder, these effects of self-heating and AC-loss can be controlled, but not eliminated. Proper measurement procedures are therefore required.

Maintaining stable operating conditions, i.e. temperature and background magnetic field, during a $V(I)$-measurement is crucial for obtaining valid data. In a conduction-cooled system, the operation temperature is often controlled with a closed loop controller including an electric heating element, temperature sensor and a controller. Like any other real world system, this system has a finite response time. This means, that if a disturbance shifts the prevailing balance in the input and output of heat, a change in temperature occurs before the control system can compensate and re-stabilize the operating conditions. The idea is demonstrated in the following experiments, where a copper sheathed multifilamentary MgB_2 superconductor was studied. The sample cross-section is shown in figure 2.2(B).

In the first experiment, the control loop was not allowed to stabilize during the measurement. The results are illustrated in figure 4.1 where two different current ramps were used in measuring the $V(I)$-characteristic. In the figure 4.1(A) the recorded current ramps along with the measured $V(I)$-data is shown. In the first measurement, the ramp was divided into two parts and in the second into three. A slight difference in the recorded $V(I)$-characteristics can be observed at a glance. To enhance the difference between the two measurements, an enlargement of the section near I_c is shown in figure 4.1(B). The critical current in this example measurement was determined using 10 μV as the voltage criterion. This corresponded to 3.33 μV/cm in the sample. In

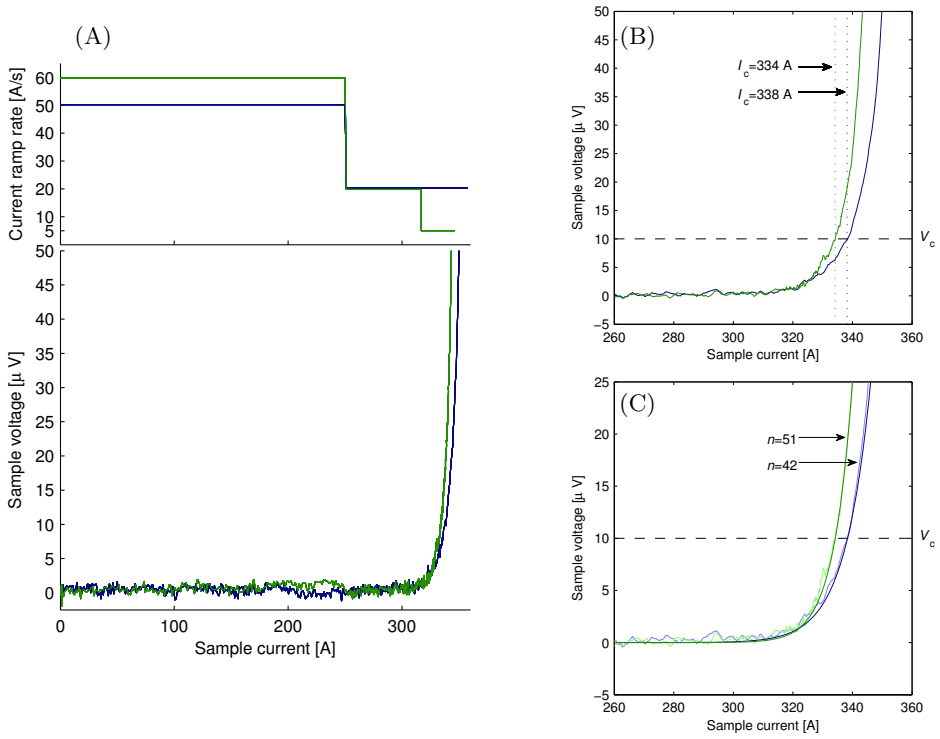

Figure 4.1: $V(I)$-measurement data for copper sheathed multifilamentary MgB_2 conductor. In (A) ramp rates and recorded $V(I)$-characteristics are shown. Critical current I_c is determined in (B) with voltage criterion $V_c = 10\ \mu V$. Subfigure (C) shows results fitted with power law and corresponding n-value.

figure4.1(C) the power law (2.2) is fitted to the data using least squares-method and the n-value is obtained. The observed increase in n-value from 42 to 51 is significant e.g. in the design of persistent mode superconducting coils. For example, if the allowed resistivity in the superconducting wire is $10^{-15}\ \Omega m$, with the tested MgB_2 sample, this limit is reached at current of 288 A and 296 A for the n-values 42 and 51, respectively.[1]

To study the effects caused by self-heating and the finite response time of the control loop, the $V(I)$-curve shown in figure 4.2(A) was measured. During the measurement, the current ramp was put on hold for 45 seconds at 330

[1]The resistivity of the superconductor in a coil varies significantly as the magnetic flux density is not constant within the coil. The example is therefore not realistic, but only meant to underline the significance of n-value. With real persistent mode superconducting coils, the current decay rate and total coil resistance and current decay rate are often used as the design criteria[84].

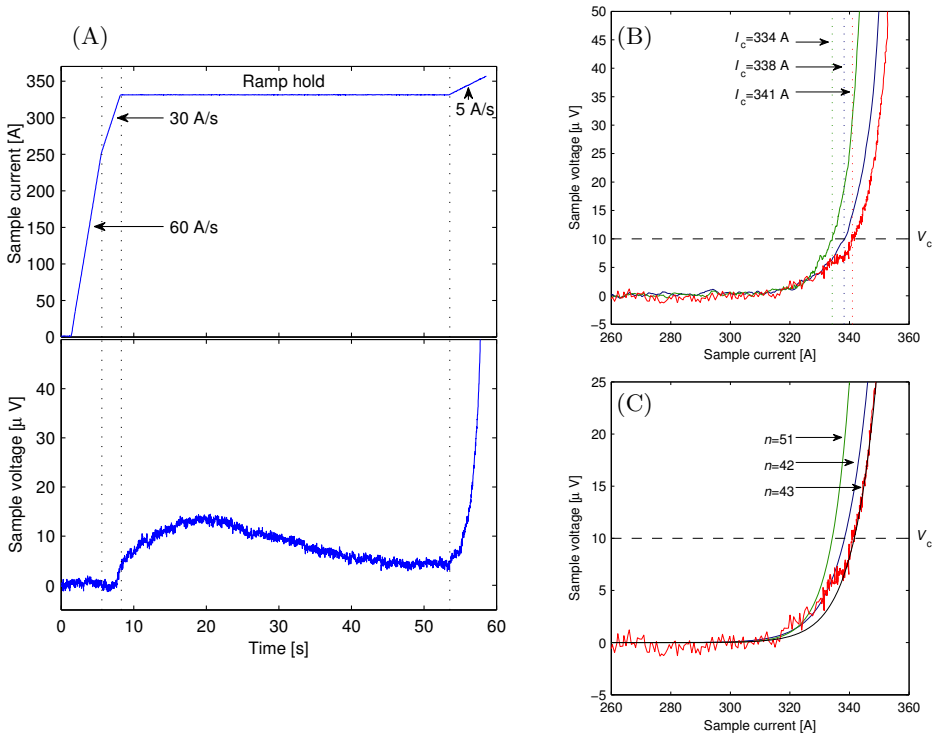

Figure 4.2: $V(I)$-characteristic measured for MgB_2 conductor with ramp-hold-ramp -method. Subfigure (A) illustrates recorded current and voltage signal in time domain, subfigures (B) and (C) show post-processing steps for determining I_c and n. In (B) and (C) red and black lines are used for ramp-hold-ramp -data, and for comparison, measurement data and post-processing results from figure 4.1 are reproduced with green and blue.

A, 98.8% of the lowest I_c in the previous experiment. The voltage measured from the sample started to decrease during this hold period as the temperature controller compensated for power dissipated in the resistive components. After the temperature had again stabilized, the ramp was resumed until the I_c was reached. Figures 4.2(B) and (C) show the post processed result of the experiment along with the previous results. The measured I_c can be seen to increase by 2.1% when the ramp-hold method was used instead of the slow three-part ramp. At the same time, the measured n-value decreased by 15%. The differences between the ramp-hold method and the two part ramp were smaller, the I_c increased by 0.89% and the n-value increased by 2.4%.

The previous experiment provides two important conclusions:

- Both I_c and n are sensitive for the measurement procedure. On one hand,

based on [32] the faster the current ramp, the better the results as the amount of energy deposited into the system by dissipation in the form of resistive losses is smaller. On the other, if the ramp rate is too high the AC-losses in the sample become an issue and effect the measurement results. Solving this dilemma requires a properly designed sample holder for removing the power dissipation, and controlling the resistive losses, along with proper measurement methods for limiting the AC-loss.

- Stable operation can be achieved in a conduction-cooled system even at operation current close to I_c. In the example, it was demonstrated that operating at 98.8% I_c was possible. Stable operation is achieved, when the system is properly designed to take into account the properties of the sample and the desired operating current. Additionally, the temperature control system needs time to compensate the change in the power input into the cryogenic system.

4.2 Quench propagation and initiation measurement

The often used setup for measuring MQE and NZPV illustrated in the previous Chapter (figure 3.9(B)) can be combined with a straight forward measurement procedure. First, data acquisition is started, the sample is then energized with the desired transport current and a known amount of heat, the quench initiation pulse, is injected into the sample using a resistive heater. The quench initiation pulse is increased and decreased until the MQE is determined with the desired accuracy. Data for determining the NZPV is provided each time, when the injected heat results in a quench.

In practice, similarly to $V(I)$-measurements, there are some aspects that should be discussed in more detail. Here, the discussion regarding MQE and NZPV measurements is focused to the electrical method. Quench propagation measurement using the thermal signals illustrated in 3.9(B) was studied e.g. in [49, 50].

Before performing the MQE and NZPV measurements, it is good practice to do a $V(I)$-characteristics measurement in advance. This helps in determining the transport current values used for the data points. Also, knowing the critical current aids in making an educated guess on the magnitude of the MQE. With this information the futile attempts to measure MQE too near I_c and unnecessary cooldowns, or sample burnouts, due to too high quench

initiation energy can be avoided. Also, repeating the $V(I)$-measurement after the quench propagation and initiation tests is advisable as detecting I_c degradation, and thus permanent damage to the sample, aids in analyzing the results.

During the measurements, the quench initiation pulse shape should be monitored. As demonstrated in [74] introducing the same amount of energy in a short or a long pulse yields different results. To obtain comparable results, the pulse duration should remain constant during the measurement set.

4.2.1 Measuring minimum quench energy

One common way to determine MQE is to use a small resistive heating element. A known amount of energy, Q_{init}, is deposited into the specimen carrying a known transport current. Voltages and/or temperatures are then monitored to determine if quench occurred or not. To determine MQE accurately, several measurements are required. One way in achieving good results is to use the up-down-method used in high voltage engineering [17, 35]. In the up-down method, Q_{init} is increased when quench did not occur. Correspondingly, after each consecutive quench, Q_{init} is decreased until a recovery is observed. The procedure is repeated until sufficient amount of data has accumulated, e.g. 5-10 completed up-down cycles.

The following stability measurements were performed with the same MgB_2 sample as the $V(I)$-measurements. The main properties of the sample are listed in table 4.1. The sample was mounted to the arc shaped sample holder presented in the previous Chapter and instrumentations used in the experiment are shown in figure 4.3(A). Subfigure (B) presents to voltage graphs recorded in case of a recovery to stable operation and in a quench. The Q_{init} used in obtaining the two graphs differed by 1 mJ, i.e. 2.5% of the MQE.

Table 4.1: Superconductor composition and transport properties.

Dia. Out [mm]	0.83	I_c(20 K) [A]	305
Cu [%(vol.)]	86.667	I_c(25 K) [A]	191
Sc. [%(vol.)]	10	I_c(30 K) [A]	76
Nb [%(vol.)]	3.333	n(25 K)	35
No. filaments	18	Mono sheath	Cu
Outer sheath	Cu		

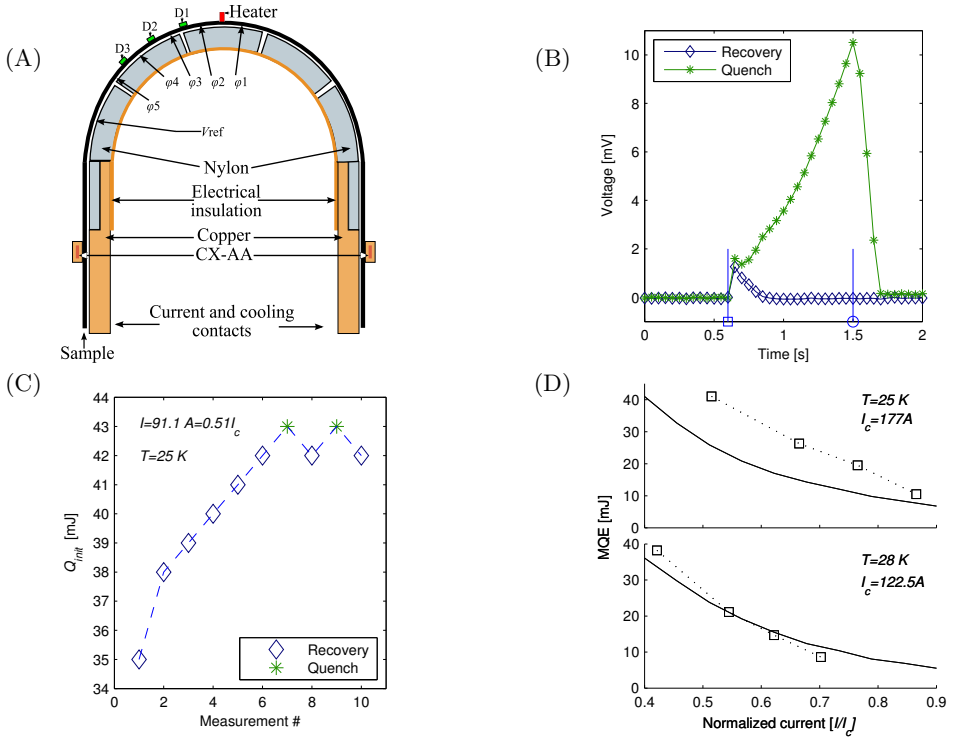

Figure 4.3: MQE and NZPV measurement setup illustrated in (A). MQE measurement details and results are shown in (B), (C) and (D). Subfigure (B) shows potential difference V_1 between taps φ_1 and φ_2 when Q_{init} <MQE (recovery) and Q_{init} ≥MQE (quench), □ show quench initiation pulse and ◯ power supply termination. In (C) MQE is determined with up-down-method for a single operating point. Subfigure (D) shows results of MQE measurement (□) and simulation (—).

Determining MQE using the up-down method is illustrated in figure 4.3(C). The increment used in the measurement was 1 mJ and for each recovery or quench, Q_{init} was increased or decreased by one increment. It is clear, that for the operating point $I = 91$ A and $T = 25$ K, the MQE is just above 42 mJ with very little variation. Reducing the increment would improve accuracy, but 1 mJ accuracy was deemed adequate for this experiment.

Using the presented method, the MQE of the sample was measured at two operation temperatures for four operation currents. The results are shown in figure 4.3(D). Along with the measurement results subfigure (D) also shows the predicted MQE obtained with FEM-simulations as verification of simulation models is one of the motivations for obtaining experimental data. The

simulation of MQE is discussed in more detail at the included publications and also in [74].

Errors in MQE measurement are mostly related to determining energy deposited into the superconductor. If the energy dissipated in the heater does not flow into the superconductor, the measured MQE values are too high. In designing a superconducting system, with its inherent instability, optimistic results can lead into problems. In an adiabatic measurement, the heat flux from the quench heater has three likely paths to follow:

1. from the heater to the superconductor,
2. from the heater to the instrumentation wiring used for carrying the excitation current,
3. from the heater via radiation into the surrounding cryostat structures.

The first of these options is the preferred one and the two others must be limited if not eliminated. Radiative heat transfer is quite inefficient, when temperature differences are small. This can easily be determined from the equation of radiative heat transfer, where the temperatures of the source and destination surfaces are raised to the fourth power and subtracted.[18, pp. 55-6] Therefore, if the heater is not significantly hotter than the surroundings, radiation can be omitted.

The second option, conduction to the instrumentation wiring can be a problem. If the instrumentation wires are too thick, a significant amount of heat can leak into those and reduce the energy transferred into the sample. The thickness of the wires can be evaluated with the methods described in Section 3.5.2. Finally, it is important to mount the heater to the sample in a way that maximizes heat conduction. There are several ways to fabricate the MQE heater. Two common approaches are to use resistive wire wrapped around the sample [66, 85] or to use a resistive paint/paste that is applied on to the specimen surface [49, 70].

In the experiment presented here, a third option was used. A small SMD resistor mounted by soldering one end directly to the sample, has proven to be an effective quench heater. In the configuration shown in figure 4.4, the heater excitation current flows through the resistor into the superconductor and then back to the instrumentation wiring. With this approach, the heater resistance can be chosen freely and high resistances can be utilized. This in turn allows the excitation current to be smaller and thus the wiring used for the circuit can be smaller for limiting the stray heat flux. Also, the SMD resistor is designed

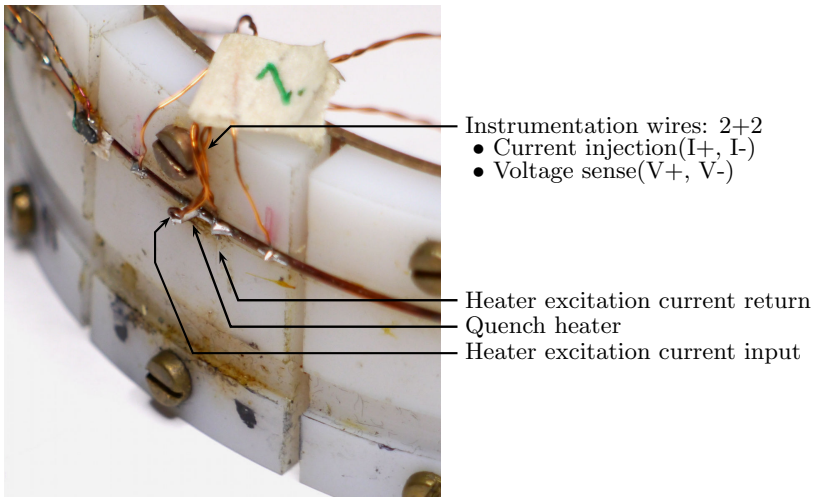

Figure 4.4: SMD resistor (size:0805 i.e. 2x1.25x0.5 mm) used as quench initiation heater. Annotations show locations of solder connections to instrumentation wiring.

to dissipate heat through the solder contacts [80] thus ensuring good thermal conductivity from the resistive element into the superconductor.

The SMD resistor has some finite heat capacity and therefore it can have an effect on the heat flux and energy deposited into the superconductor. To evaluate the magnitude of the effect, the smallest MQE, 8.6 mJ, and the associated initial temperature 28 K and operation current 86 A provide the worst case estimate. The critical current at this temperature was 122.5 A and if it is assumed that it linearly decreases to zero at T_c=39 K, the operation current 86 A can be calculated to exceed the critical current at 31.25 K. The energy stored in the heat capacity of the SMD resistor, when the temperature increases from 28 to 31.25 K, is 36 μJ.[2] This corresponds to 0.5% of the measured MQE suggesting only a minimal effect on the measurement accuracy.

4.2.2 Normal zone propagation velocity measurement

With the setup illustrated in figure 4.3(A), data for determining the NZPV is collected each time when Q_{init} is large enough to cause a quench. The additional potential taps φ_3,φ_4,φ_5 and φ_{ref} in 4.3(A), were used for recording

[2]The bulk of the SMD resistor formed by the aluminium oxide ceramic substrate and therefore the heat capacity can be estimated from the specific heat of Al_2O_3 [36] and the dimensions of the resistor.

the voltage-time graphs required in determining the NZPV.

Figure 4.5(A) shows an example of the recorded $V_{\mathrm{x}}(t)$-graphs during a quench. From the graphs, the time at which resistivity is observed, i.e. voltage increases from zero, is noted. For example, in figure 4.5(A) resistivity was observed between potential taps φ_3 and φ_{ref} at $t_{\mathrm{V2}} = 0.917$ s, between taps φ_4 and φ_{ref} at $t_{\mathrm{V3}} = 1.049$ s and φ_5 and between taps φ_{ref} at $t_{\mathrm{V4}} = 1.140$ s. The distance Δl of two adjacent taps in this experiment was 1.5 cm. Now, the normal zone propagation velocities of $v_{\varphi 4 \leftarrow 3} = 11.36$ cm/s, $v_{\varphi 5 \leftarrow 4} = 16.48$ cm/s and $v_{\varphi 5 \leftarrow 3} = 13.45$ cm/s can be computed from equation

$$NZPV = \frac{\Delta l}{\Delta t} = \frac{15\mathrm{cm}}{t_{\mathrm{Vi+1}} - t_{\mathrm{Vi}}}. \tag{4.1}$$

The increase in propagation speed from $v_{\varphi 4 \leftarrow 3}$ to $v_{\varphi 5 \leftarrow 4}$ is not a measurement error.

Here, the MgB_2 sample was operated at 51% $I_{\mathrm{c}} = 90$ A at 25 K temperature in self-field. Assuming, that $I_{\mathrm{c}}(T)$ can be approximated to drop linearly to 0 at $T_{\mathrm{c}} = 39$ K, the operation current of 90 A corresponds to I_{c} at 29.4 K temperature. This indicates, that the temperature of a given point of the superconductor has to increase 4.4 K before any resistance, and therefore quench propagation, can be observed. Now, by the time when the first potential tap pair φ_3 and φ_{ref} registers the resistance increase, the heat dissipated in the normal zone has already diffused further along the conductor. At the next potential tap φ_4, the temperature has now already increased from the inital 25 K, and therefore quench is observed sooner than the previous interval indicates resulting in the obseverd propagation velocity acceleration. The topic is further discussed and analyzed in [30] and it is worth noting, that the propagation velocity will eventually reach a constant value, but it can take more than 10 cm of propagation along the conductor before the constant value is reached.

Figure 4.5(B) presents the average NZPVs measured for the same sample that was used for the MQE example results in the previous subsection. The same data set with two temperatures and four operation currents were used in the propagation velocity analysis.

The sources of error in the NZPV measurement can be found from two places. First, the placement of the voltage taps and accurately measuring their distances from each other can be challenge. If the taps are close to each other, even a slight error in measuring the separation can be have a significant effect on the NZPV measurement accuracy. For example, if the taps were placed 5 mm apart, ± 0.5 mm absolute error would correspond to a relative

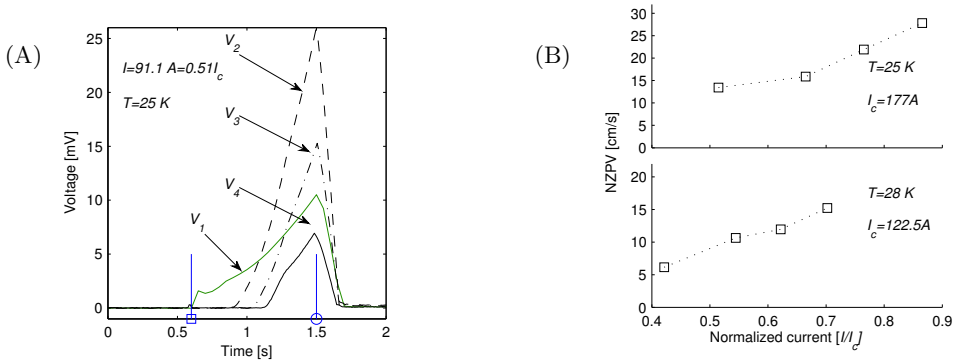

Figure 4.5: Voltage-time graphs measured during quench are shown in (A). Potential taps used in the experiment are illustrated in 4.3(A). Recorded voltages were obtained with potential tap pairs as follows: V_1 between φ_1 and φ_2, V_2 between φ_3 and φ_{ref}, V_3 between φ_4 and φ_{ref} and V_4 between φ_5 and φ_{ref}. Measured normal zone propagation velocities are presented in (B).

error of 10%. The same absolute error with a tap spacing of 10mm would correspond to 5% and so on. Thus increasing the tap separation is an effective tool in reducing error in the NZPV measurement.[3]

The second error source in the quench propagation experiment is the timebase accuracy. However, compared to the errors caused by the displacement of the potential taps discussed earlier, problems with timebase are unlikely. The required sampling frequency in the NZPV measurement, based on the previous example with 15 mm tap separation resulting in approximately 100 ms of delay in normal zone detection, is in the range of 1 kHz or 1000 samples/s. Even the low end commercially available digital storage oscilloscopes have their upper band with limits above 1 MHz [1, 78]. The challenge in using an oscilloscope is their low accuracy in detecting small voltages. To overcome this challenge a high accuracy, high speed digital multimeter (DMM) with a digital function generator for providing the sampling trigger signals can be used. In such a configuration, the upper frequency is limited by the DMM and the required accuracy. For example, 750 samples/second can be measured using the Agilent 3458A DMM in 6.5 digit mode and 1 V range, giving an accuracy of 10 μV [1].

[3]One way of improving the accuracy of the tap separation measurement is to assume an evenly distributed resistance on the sample and measure the separation and resistance of the longest tap at room temperature. The separation of the shorter taps can then be computed by measuring their respective resistances. For example, if a tap separation of 10.00 cm yields a resistance of 0.100 Ω, it can be estimated that a 1 cm piece of the wire has a resistance of 0.01 Ω/cm. Now, if the observed resistance between two taps is e.g. 0.0145 Ω the corresponding separation is 1.45 cm.[41]

Reducing the number of digits would further increase the sampling speed.

4.3 Remarks

The common $V(I)$-measurement has proven to be anything but simple to perform. A thorough understanding of the measurement system is essential in ensuring good quality results. Measurement procedures should be designed to cope with the systems limitations. Failure to do so results usually in under estimated I_c and over estimated n-value.

The discussion presented in this Chapter shows how measurement setup can effect the outcome of the experiment. I demonstrated this by showing the results of $V(I)$-measurement done with different current ramps. I analyzed how the conduction-cooled setup, controlled with a closed loop temperature controller, responds to the heat generated during the experiment and how the response can effect the measurement result. Also, I showed how a superconducting short sample in a conduction-cooled system can be operated for extended periods of time near the I_c.

Compared to the $V(I)$-measurement, the thermal stability test is more demanding. First, more instrumentation is required as monitoring the normal zone propagation requires good resolution in both spatial and temporal domains. Second, to accurately determine the MQE, a small heater with solid connection to the sample is required.

I presented a simple and systematic approach to the measurement of the MQE and its variation. Furthermore, I illustrated how measuring the NZPV can be challenging with short sample and discussed what caused the acceleration of the measured NZPV. As a conclusion, with HTS and MgB_2 materials, the actual NZPV might not be reached until after several centimeters of quench propagation and this should be taken into account in the experiment preparation.

Chapter 5

Magnetization AC-loss measurement with a conduction-cooled system

In the previous chapters, I have presented challenges and solutions in performing short sample characterization in a conduction-cooled system. In this research project, my duty was to develop a conduction-cooled magnetization loss measurement station with a variable operating temperature from 6 to 30 K. Here, I present the whole process from specifying the requirements to verifying the operation of the finished system.

First, I discuss the requirements and working principle of a magnetization AC-loss measurement. Then these definitions are applied to design and construct the different components of the measurement system. Finally, the proper operation is verified by performing measurements on control samples and the system is demonstrated by studying the AC-losses of multifilamentary MgB_2 superconductor.

The results presented in this Chapter are based on **Publication 6**. Especially the method to simulate AC-losses in superconductors is entirely left for the publication.

5.1 Specifications and requirements

Cryocoolers and HTS conductors have made it feasible for SC magnets to operate at temperatures between 10-20 K using conduction-cooling. Compared

to the LTS conductors often cooled with LHe, there is a significant gain to be made in the cooling costs of these new systems. However, in all magnet applications AC-losses arise in some phase. With these conduction-cooled systems, the limited cooling capacity discussed in Section 2.2 creates challenges in the management of the AC-losses.

One of the most important form of AC-loss is the hysteresis loss of a superconductor. In this form of loss, the energy dissipated is almost independent of the frequency during one cycle of a periodic stimulus. In contrast, the dissipated energy per cycle in the eddy current losses, induced to the normal conducting domains of the superconducting wire, depends significantly on the frequency.[29] One approach to studying these losses experimentally is to position a superconducting sample into a time varying magnetic field. Such a setup does not need current injection into the sample making conduction-cooling a viable option.

A simple but effective measurement principle presented in [79] was chosen as the basis of the measurement system. The setup uses two coils, one for hosting the sample and the other for providing a reference, to detect the change in power input required to overcome the magnetization AC-loss in the superconductor. The principle is discussed further in the next section, but for specifying the initial requirements, it should be noted here, that it is necessary to achieve a relatively homogeneous magnetic field into the sample.

The system presented here needs to operate with LTS placing a stringent condition on the operation temperature. Furthermore, it was also decided, that the system needed to operate at higher temperatures enabling the study of MgB_2 samples at 20 K and operation should be possible for a non-expert in cryotechnology. Therefore, conduction-cooling with a closed loop temperature control system was chosen. It is known, that the losses in the multifilamentary LTS conductors are low, e.g in [67] measured hysteresis losses are in the range of $10^{-4} - 10^{-5}$ J/m per cycle. Therefore, sensitivity of the measurement will be an issue. Great care must be taken in choosing the construction materials and in installing the instrumentation.

The initial specifications and requirements can be summarized as follows:

- sample temperature is adjustable and it should enable operation with both LTS and MgB_2 ,
- sensitivity needs to be high, the expected loss levels for a 10 cm long sample fall in the range of $10^{-3} - 10^{-5}$ W at 50 Hz frequency,
- sample is cooled with a cryocooler,

- magnetization AC loss is studied by monitoring the power balance between the two excitation coils,
- several measurement frequencies must be available, one of them must be close to 50 Hz,
- the maximum amplitude of the excitation magnetic field is 250 mT and
- the field needs to be homogeneous within ±3% at the sample [81, pp.64-5].

5.2 Measurement principle

The operating principle has a significant effect on possible construction materials. The time varying magnetic fields induce eddy currents to any electrically conductive material near the excitation coils. This in turn creates background signals that interfere with the measurement. To better understand the challenges present in constructing the measurement system, the operating principle needs to be discussed.

5.2.1 Calibration free magnetization AC loss measurement

The approach used here for measuring the AC loss was presented in [79]. The main components of the measurement setup are illustrated in figure 5.1. In principle, the system measures the difference of the induced voltages in the two coils. To avoid measuring the resistive losses in the winding, the coil system uses a pick-up co-wound with the main coil. Thus, the voltage induced to the pick-up exactly matches that of the main winding, but the voltage due to resistive losses is excluded. Therefore, the resistive losses in the main winding are only relevant for the coil power supply.[79]

Due to the chosen co-wound geometry of the pick-up and the main winding, the difference in the induced voltages is directly proportional to the losses in the superconducting sample. In an ideal case of the described setup, the induced voltages of the coils are identical, if neither of the coils has the superconducting sample placed within the bore. Consequently, the sample's losses can be determined by measuring the coil current i_{coil} and the difference in the induced voltages across the pick-up coil terminals. Connecting the two pickup coils in anti-series, the difference in the induced voltages, and thus the loss component, can be extracted. This process is visualized in figure 5.2.[79]

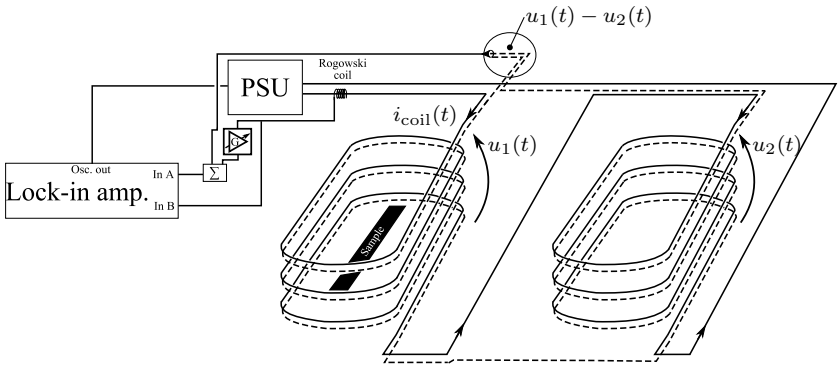

Figure 5.1: A diagram illustrating main components and instrumentation of AC-loss measurement. The analog summing block Σ and variable gain amplifier G are used for compensating residual inductive voltage remaining after anti series connection of pick-up coil voltages $u_1(t)$ and $u_2(t)$. Coils' current, $i_{\mathrm{coil}}(t)$, magnitude and frequency are controlled with lock-in amplifier's internal oscillator.

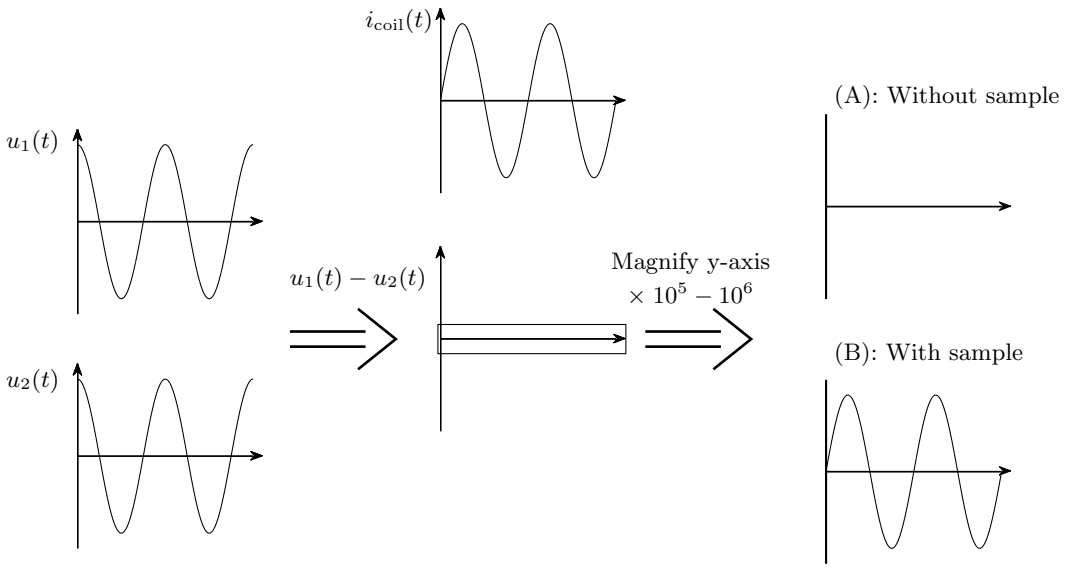

Figure 5.2: Illustration of obtained output signals from AC-loss measurement. Pick-up coil voltage subtraction $(u_1(t) - u_2(t))$ is achieved with anti-series connection. Y-axis magnification is achieved using LIA and high amplification. Note that signal with sample is in phase with excitation coil current, this indicates power dissipation in sample.

A key component of the system is the Lock-In Amplifier (LIA). The LIA offers excellent noise rejection from the ambient electromagnetic interferences as it amplifies only the signal at the specified frequency. Therefore, high amplification of the measurement signal is not a challenge. High sensitivity to signals at the specified frequency is thus achieved making it possible to extract the low level signals associated with the magnetization AC-loss.

However, the setup contains several components that cause error and interference in the real world, non-ideal, setup. The most significant source of such errors are the minor differences in the two excitation coils. It is very difficult, if not impossible, to manufacture two coils that are exactly identical. Therefore, in the balanced case i.e. without a sample, the output signal is not zero. Fortunately, the inductive part of the signal can be compensated electrically as shown in figure 5.1. The compensation circuit uses a voltage signal proportional to $i_{\mathrm{coil}}(t)$ from the Rogowski coil. The output of the Rogowski coil is at a $\frac{\pi}{2}$ phase shift to the $i_{\mathrm{coil}}(t)$, and therefore in phase with the inductive component of the voltage induced to the pick-up coil. Connecting the output of the Rogowski to an adjustable gain operational amplifier allows the signal amplitude to be varied. This compensation signal can then be subtracted from the anti-series connected pick-up coils to reduce the total signal magnitude without modifying the loss component.

The second source of error can be found from the surroundings. Basically, the system measures the difference in the resistive losses sensed by the two coils. However, the system cannot distinguish the losses dissipated in the superconductor from losses dissipated in any conducting object placed in close proximity to the coils. Therefore, the measurement system must be constructed from electrically insulating materials. Also, the surroundings of the measurement system must be non-conductive as the system is very sensitive. For example, the steel reinforcements in concrete flooring can cause interfering background signals. At the same time, the conductor used in the coils should be such that the self-field does not induce currents to the conductor itself i.e. the power dissipation in AC and DC use should be the same.

5.3 System design and construction

There are three main components in the system:

- coils and their power supply,
- conduction-cooled cryostat for the sample and

- instrumentation and auxiliary devices.

To begin the design process, the sample dimensions were fixed. It was decided that a sample length of 90 mm would be sufficient. To ensure the option of measuring round wires and 4 mm wide tapes, the maximum width was set to 7 mm to allow some flexibility. With these parameters, it was possible to determine the dimensions of the sample space and internal dimensions of the two excitation coils.

5.3.1 Excitation coils

It was specified, that the system must be able to operate near power line frequency. Therefore, the lowest operation frequency was chosen to be 36.75 Hz in order to avoid power line noise at 50 Hz. To simplify the power supply design, the maximum operation frequency was defined to be 147 Hz i.e. four times greater than the lowest. A Litz-type copper cable was chosen for fabricating the coils. The Litz cable consists of insulated copper wires that are transposed. Consequently, its average loss in corresponding AC and DC conditions (rms current vs. constant current) are the same. Also, the subdivided structure of the Litz cable allows one of the strands to be used as the pick-up coil.

The excitation coil design was guided by the maximum magnetic field density and homogeneity requirements. To achieve the required homogeneity while limiting the coil dimensions and volume, a race-track type coil geometry was chosen. The chosen geometry was simulated and fine tuned to reach the specified homogeneity, while limiting the resistive losses and induced voltage. With the final coil geometry, the peak magnetic flux density 250 mT is reached at a current of 204 A. If a sinusoidal current is used, the peak flux density equals to 144 A_{rms} coil current. The corresponding copper current density is 9.6 A/mm^2 and the coil current density is 6.1 A/mm^2.

The resistive losses in the copper coil were computed to be significant, and it was therefore decided to cool the coils with liquid nitrogen. The LN_2 cooling offers the advantages of both lower resistivity and more efficient heat transfer, than the natural convection at room temperature would provide. Thermal simulation was used to verify the stability of the coil when placed in LN_2 bath and operated at the maximum current. Multiphysics FEM software Comsol [9] was used in these simulations.

The coils were manufactured by hand in an in-house workshop using a wet-layer winding technique. Strong impregnation of winding turns and layers is crucial, as there will be significant time varying Lorenz forces acting on the

coils' wire during the operation. Two different epoxies were used as the small bending radius on the inside of the coil made winding the initial few layers a slow process. The winding process was started with Hysol 9466 as the impregnation resin, as it offered a long pot life of 120 minutes. After a few full layers, Stycast 2850FT epoxy was used as it offers better properties, such as matched thermal expansion, better adhesion and improved thermal conductivity. The shape, dimensions and electrical properties of the constructed coils are shown in figure 5.3.

During operation, the coils were placed in two separate open bath cryostats. The cryostats were manufactured from closed cell polystyrene foam. This approach was chosen as the cryostats must be manufactured from electrically insulating material. The cryostats were equipped with a junction box containing the terminals for coil current supply and a shielded connector for the pick-up signal. One of the cryostats was shown photographed in figure 2.5.

5.3.2 Coil power supply

The starting points of the power supply specification were the simulated inductance and resistance. The total expected resistance and reactance of the series connected coils were $R = 0.024\ \Omega$ and $X = 2.77\ \Omega$, respectively, at the 147 Hz frequency. At the maximum operation current 144 A_{rms}, the resulting voltage across the power supply terminals is $\sim$400 V_{rms}. Thus the total power requirements are 500 W resistive and 57 kVAr reactive.

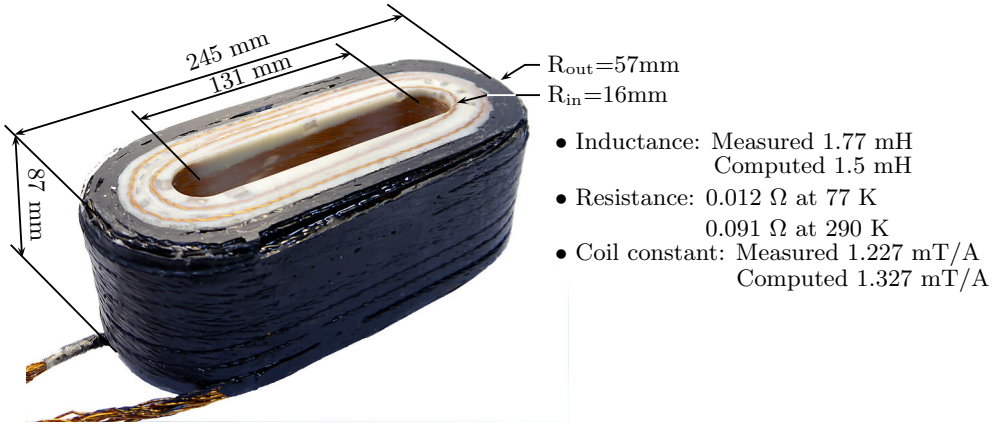

Figure 5.3: Photograph of AC-loss measurement system excitation coil. Associated dimensions and electrical properties are provided for reference. Using two different epoxies Hysol 9466 and Stycast 2850FT during winding resulted in light and black colored segments, respectively, visible in photograph.

The required reactive power can be produced by introducing additional capacitance to the circuit. In the best case, the reactive power demand and supply are balanced in a resonance condition and the power supply only needs to provide real power to overcome the resistive losses in the coils. Note, that the AC-loss in the sample is on the order of few mW and thus negligible when compared to this. However, the capacitance required for reaching resonance depends on the frequency. To limit the complexity of the power supply, three harmonic operation frequencies 147, 73.5 and 36.75 Hz were selected as the starting point. The required capacitances are therefore 0.325, 1.302 and 5.214 mF for these frequencies, respectively.

The operation frequencies chosen for the system are in the range of low frequency audio amplifiers. Using such a device offers the benefit of commercially constructed, reliable and easily replaceable units. For this application a 1.5kW audio amplifier was chosen. The optimal load impedance[1] for the unit was between 4 and 8 Ω. However, with the listed capacitances, the impedances of the coil-capacitor parallel connection are 460, 120, 29 Ω for each of the operation frequencies, respectively. To match the impedances, a transformer with two secondary windings, each with a turns ratio of 2, was introduced between the amplifier and the load circuit. Connecting the secondary windings in parallel provides a total turns ratio of 2 and an impedance transform ratio of 4. A series connection provides a turns ratio of 4 and an impedance transform ratio of 16. The transformer also offers the benefit of galvanic isolation from ground potential improving electrical safety of the system.

During construction of the power supply, it was chosen to shift the desired operation frequencies slightly. The new frequencies were 139.25, 72 and 43.4 Hz This provided the advantage of reduced capacitance requirement at the lowest operation frequency and simplified the capacitor wiring arrangements. The capacitors were connected to form two 1000 μF banks, one 1400 μF and one permanently connected 367 μF bank. The capacitor banks were connected to circuit as required using micro processor controlled contactors. Simplified circuit diagram of the power supply is shown in figure 5.4 along with the capacitance values for each operation frequency.

5.3.3 Conduction-cooled cryostat

Preventing eddy currents and magnetization losses in the system components is vital as the system cannot differentiate losses dissipated in the surrounding

[1]By definition, impedance $\overline{Z}$ is a complex number, but here, and in audio applications, the term impedance is used for referring to the absolute value, i.e. $|\overline{Z}|$, of $\overline{Z}$

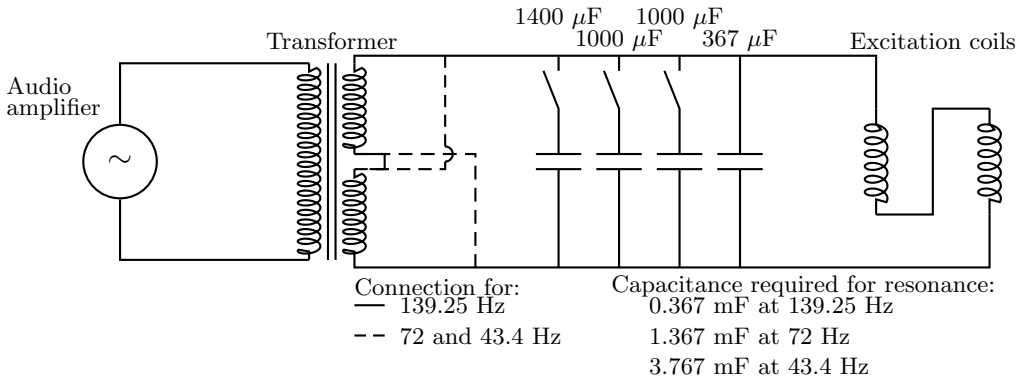

Figure 5.4: Simplified connection diagram of excitation coil power supply and resonance circuit.

objects from those dissipated in the sample. Therefore, the sample housing cryostat has to be constructed from electrically insulating material. The same applies to the internal structures e.g. thermal pathways and sample holder.

The material options available for constructing the vacuum vessel of the system were limited to two classes: polymer composites and plastics. These two classes contain electrically insulating materials while retaining the possibility to manufacture intricate details and shapes with conventional metal working tools. The vacuum vessel is partly immersed in the LN_2 bath when the sample space is placed inside the measurement coil bore. The system must therefore withstand thermal shocks and cryogenic temperatures and this requirement reduces the number of available materials to only a few. Of the polymer composites G10 fiberglass epoxy laminate is commonly used in cryogenic systems and would perform well also in this application [18, Sec 3.2.2]. Plastics such as Teflon (PTFE), Nylon and Polycarbonate are, by experience, known to endure the stresses present in cryogenic applications.

In designing the cryostat the following list was used for a guideline:

- high factor of safety in material thickness should be used as plastics often break without warning,
- all joints should be made with face flanges and use O-ring seals,
- glued or welded joints should be avoided as achieving leak tightness is difficult,
- joints (with or without o-ring) in close proximity to LN_2 are to be avoided and

- the cryocooler should be placed as far away as possible from the sample space.

The design of the cryostat is illustrated in figure 5.5. The cryostat contains four main components, the cryocooler, the vacuum and instrumentation connections flange, the cryocooler support tube and the base structure. The sample space lid provides easy access to the sample space. The base divides into two components for easier access to the cryocooler 2nd stage during service and assembly. All the seams between the various components are sealed with o-ring seals and held together by either plastic screws, in the components nearest to the sample space, and stainless steel bolts in those further away.

The base structure of the cryostat was manufactured from clear polycarbonate. Polycarbonate was chosen over fiberglass as it was available in sheets with greater thickness. Initially, the base structure was to consist of only the

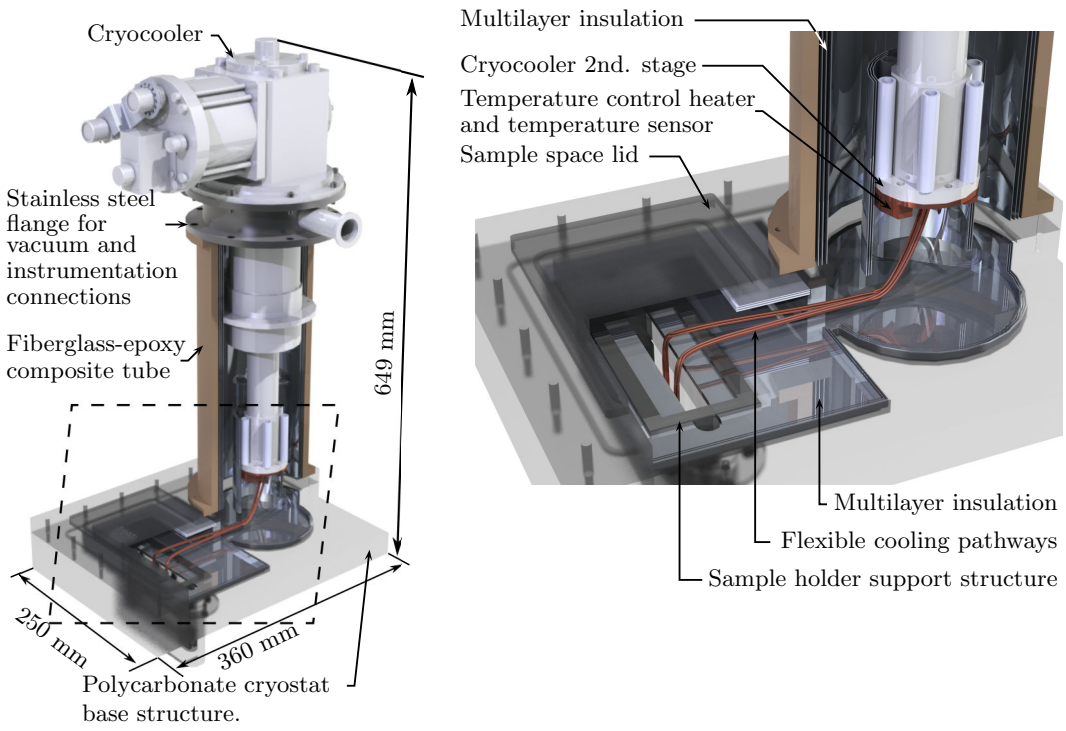

Figure 5.5: Conduction-cooled, mostly non-conductive cryostat used for cooling superconductive sample. Whole cryostat is illustrated on left side and area within dashed trapezoid is shown magnified on right. CAD-model used for rendering both images has been cut open to reveal internal components.

two sections. One section fabricated with openings for the sample space access and mounting the cryocooler support tube, and the other with the sample space. However, the thickness of the polycarbonate sheet available was not sufficient to manufacture the bottom of the cryostat, seen in figure 5.6, from a single blank. Therefore, it had to be manufactured from two components causing a violation of the design guidelines. This later resulted in a vacuum leak when the system was tested with the sample space immersed in LN_2. The troublesome component was modified to include a solid PTFE seal instead of a standard rubber o-ring and the fastening screws were replaced with larger ones. The screws were fabricated in house from solid PEEK [13] plastic as commercially available nylon screws proved to be both elastic and prone to failure during assembly.

The tube supporting the cryocooler proved to be challenging to obtain. The flanges had to be vacuum tight, and therefore it was a requirement that the entire component was manufactured from a single blank. However, obtaining a blank with adequate dimensions proved challenging if not impossible. As a solution, the tube was manufactured by filament winding in a workshop specialized in polymer composite fabrication. The resulting part was then machined to ensure the surface finish of the vacuum flanges.

The only component fabricated from metal can be seen between the cryocooler and the support tube. The flange was specified to

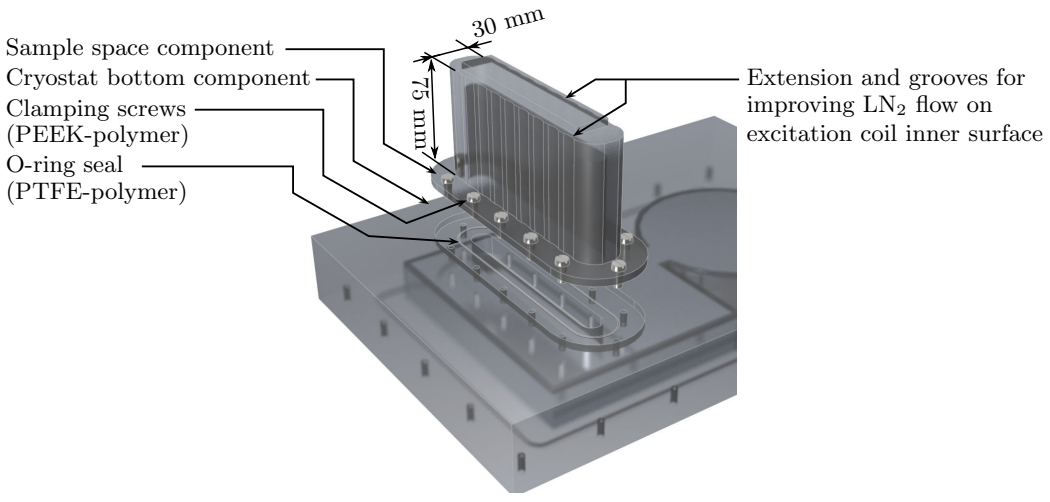

Figure 5.6: Bottom side of cryostat base structure viewed from below. During operation sample space is partly immersed in LN_2, rest of surface is cooled by gaseous N_2 boil off.

- contain the connections for vacuum pumping system and instrumentation and
- adapt the mounting of the cryocooler to the mounting of the composite support tube.

The component was manufactured from stainless steel, as it is a relatively poor electrical conductor, non-magnetic and fabrication of vacuum tight welds is a known process. However, even with the poor conductivity and non-magnetic nature of stainless steel, the flange was placed as far away from the sample space as possible to minimize possible eddy current losses.

Conduction-cooled system often employ an active radiation shield for thermal insulation in addition to the convection preventing vacuum.[11, 53, 87] In this system, metallic radiation shield thermally anchored to the 1st stage of the cryocooler was not an option. The eddy currents in such structures would be challenging to manage and they increase the background level in the output signal. Instead several layers of nylon netting and reflective metalized mylar foil were used for controlling the radiative heat transfer. This multi layer insulation (MLI) is often used in conjunction with an active radiation shield. But when the number of layers is large, it has proven to be and effective solution also on its own. For this system we used 20 to 40 layers of this MLI depending on the location. For example, surfaces facing liquid nitrogen are significantly cooler, and thus require fewer layers of MLI, than those exposed to ambient room temperature.

The thermal pathways used for cooling the sample were designed to minimize losses caused by the alternating magnetic field. Controlling the eddy current loss was achieved with a fine coil wire bundled and twisted together. One cooling conductor bundle contained 10 wires and each conductor contained four bundles braided to form a flexible and compact cooling pathway. Four such cooling pathways were used and one end of each pathway was soldered to an interface piece mounted to the 2nd stage of the cryocooler. The other end was soldered to an interface piece for establishing thermal connection to the sample holder.

The pressed cooling contacts used for interfacing with the sample holder were manufactured from brass formed to a rectangular 1x2 mm U-profile. Brass was chosen for this task as the eddy current loss had to be minimized also in this component. One pressed contact contained four 7 mm long pieces of the brass profile. On to each piece, one bundle of 10 strands of the braided cooling wires was soldered to provide best possible thermal contact. The four profile pieces connected to the cooling wires were then mounted to a polycarbonate

support structure. The resulting pressed cooling contact is shown in figure 5.7.

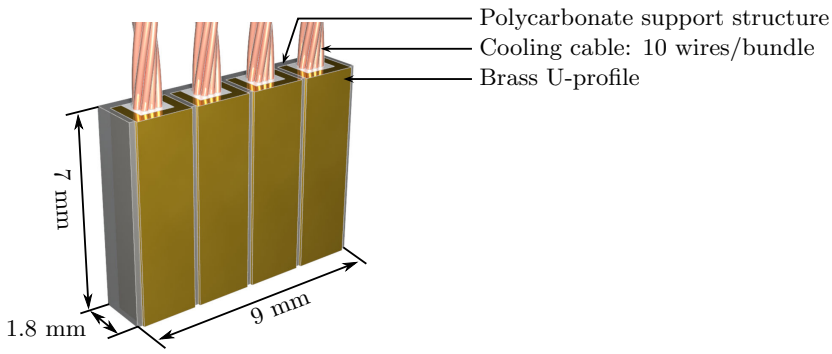

Figure 5.7: Pressed cooling contact. Four identical contact assemblies were used for thermally connecting ceramic sample holder to cooling pathways.

The sample holder was manufactured from an electrically insulating, machinable ceramic BNP-2 [6]. The material offers good thermal properties and it is machinable using standard metal working tools. The sample holder support structure was fabricated from polycarbonate and it was designed to place the sample at the coil centerline. Also, to study the effects of magnetic field direction to the experienced losses, the support structure allows the sample holder to be placed at 0, 45 and 90 degree angles with respect to the excitation magnetic field. The sample holder and support structure are shown in figure 5.8. Also, the polycarbonate clamps used for securing the pressed cooling contacts are shown.

All of the components were analyzed with FEM simulations to determine possible weaknesses in structural and thermal designs. Structural analysis with static loading was done to ensure the integrity of the vacuum chamber components against vacuum loading. Thermal modeling was done for all of the components with direct contact to the ceramic sample holder. Of these components, the sample holder support structure was simulated to verify that only a negligible amount of heat would leak to the sample holder. The ceramic sample holder and the pressed cooling contacts were simulated together to ensure proper thermal connection. Also, the uniformity of the temperature distribution in the ceramic sample holder was verified under a modest heat load.

With conductive components, analysis of the induced eddy current losses is necessary in addition to the thermal considerations. The pressed cooling

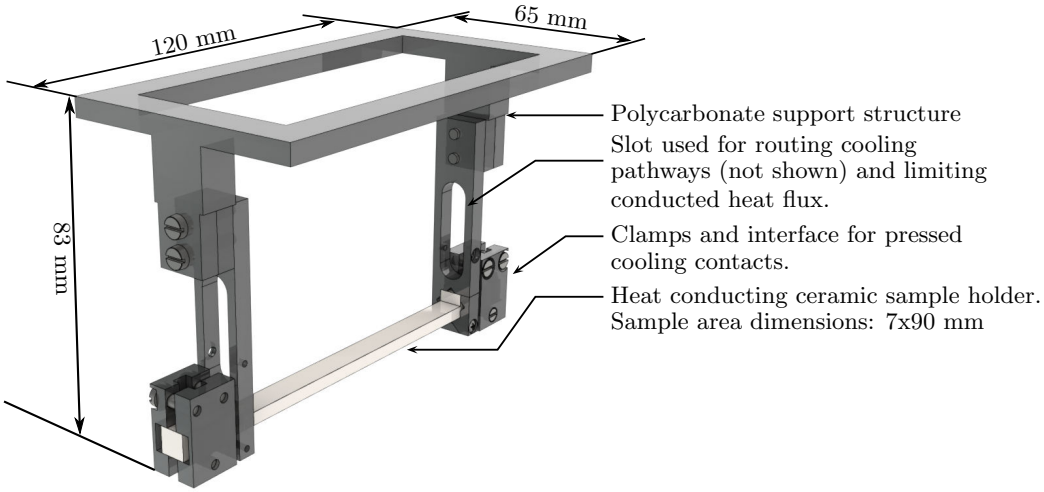

Figure 5.8: Sample holder and support structure. Cooling pathways have been omitted for clarity.

contacts proved to be challenging components as controlling the eddy current losses had to be balanced against good heat transfer. The components had to be manufactured from a solderable metal with reasonable thermal conductivity for ensuring acceptable heat transfer from the ceramic holder to the cooling conductors. However, with most metals thermal and electrical conductivity are closely related and high thermal conductivity implies high electrical conductivity.

5.3.4 Instrumentation

A key component in the measurement system is the Lock-In Amplifier. There are two major suppliers of these apparatus, and for this system, a dual phase, digital signal processing Model 7265 from Ametek Signal Recovery [71] was selected. This particular device was chosen over other alternatives, as it was offered with comprehensive LabView [55] drivers for easy integration into existing laboratory software. In the measurement procedure, the LIA is used for controlling the coil power supply and for measuring the output signal from the measurement coils as well as the coil current using the signal from the Rogowski coil. The variable gain amplifier used for compensating the imbalance of the inductive signals, see figure 5.1, was constructed using a low-noise wide band operational amplifier TL071.

Temperature monitoring and control is achieved using a temperature controller ITC 503 from Oxford Instruments [59]. The device can monitor three temperature sensors simultaneously, while using PID-control for setting the temperature using a resistive heating element. One Cernox CX-AA and one smaller Cernox CX-SD[2] temperature sensors were placed in the system. The CX-AA was placed at the cryocooler 2nd stage interface and the CX-SD at the sample holder. A cartridge heater was used as the heating element for temperature control and it was mounted to the cryocooler 2nd stage.

5.4 Measurement procedure

The sensitive nature of the measurement principle requires a carefully defined measurement procedure. While great care was taken in the design and construction, the two coils are not completely identical. Also, the structures of the conduction-cooled sample cryostat are only visible to one of the two coils. These two nonidealities cause an offset signal to be registered along with the desired loss signal from the sample. Therefore, a system baseline, must be measured before experiments with superconductors can take place.

Additionally challenges were discovered during the commissioning of the system, when it was observed that the baseline drifted between consecutive measurement runs. Further analysis revealed that the reason for the drifting offset was the change in the coil wire resistance as the two coils warmed up during a measurement run. In Section 5.3.1, it was stated, that the coil resistance does not effect the measurement output. While this statement still holds, it is only valid for the resistive losses due to the coil transport current I_{coil}. Here, the observed change in the output were caused by eddy current losses induced to the loops formed in the coil due to compromised insulations. The defects of the excitation coils are further discussed in Section 5.6. Here, it is should be noted that, the drifting offset makes analyzing the results very challenging.

Before superconducting samples can be tested, the system baseline curve needs to be recorded at each of the three operating frequencies. The baseline needs to be updated, if changes are made into the system setup e.g. conductive components are added to the vicinity of the system or the coil cryostats are moved to another location. Location of the cryostats is significant since e.g. the steel reinforcement used in concrete floors can be registered as a loss signal during a measurement.

[2]Hermetic ceramic package, rectangular 3.175 x 1.905 x 1.080 mm (WxDxH).[43]

To make the measurement reliable and repeatable, the system is controlled using a software constructed with LabView. The software is also responsible for the data acquisition. The previously described heating problem was alleviated by implementing a cool-down period in to the software between the acquisition of two consecutive data points. Also, computer control allows all operations related to data acquisition and excitation current control to be performed in the same manner each and every time. Manual user input is required for adjusting the power supply selectors used for choosing the correct compensation capacitance and in setting the desired operation temperature into the temperature controller.

The measurement procedure for a single measurement run consist of four phases. First, primary settings, like operation frequency, LIA sensitivity, input gain, output filters etc., are configured with the user interface. Second, a power supply calibration for determining the correct control signal level is performed. Also in the second step, the reference phase of the LIA is set to match the phase of the Rogowski coil signal. In the third step, secondary settings, like the maximum excitation coil current, the number of data points, the number of measurements per data point and cool-down period, are defined. During the fourth step, the software executes the measurement according to the set parameters.

5.5 Operation verification and example results

Before proceeding with the experiments using the conduction-cooled cryostat, we chose to first verify the correct operation of the coil and data collection systems as these components were ready for operation several months before the conduction-cooled cryostat. Also, this allowed us to replicate the experiment performed on known sample originally tested at Slovak Academy of Sciences (SAS) [72, 79]. Therefore, these initial tests were performed with HTS and copper samples in an open LN_2 bath.

First, the proper operation was verified by constructing a rectangular loop from $\varnothing 0.25$ mm copper wire shown in figure 5.9 as item A). When the dimensions of the loop are known, it was possible to analytically calculate the resistive losses dissipated in the loop when it was placed in an alternating magnetic field. Using Faraday's law of induction, the induced electromotive force ϵ is

$$\epsilon = -\frac{\mathrm{d}\Phi}{\mathrm{d}t} = -\frac{\mathrm{d}BA_{\mathrm{loop}}}{\mathrm{d}t}, \tag{5.1}$$

where Φ is the magnetic flux, B the magnetic flux density and A_{loop} the area

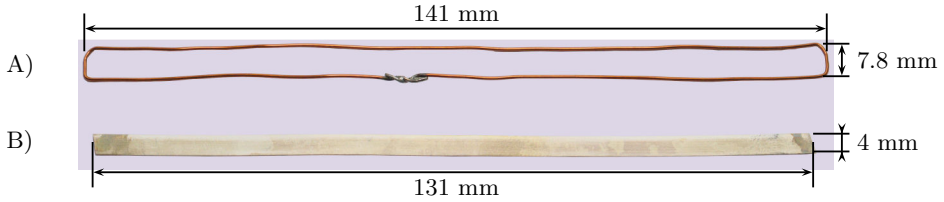

Figure 5.9: Photograph of benchmark samples. Item A) is the closed Cu-loop and B) the BSCCO superconductor.

of the surface enclosed by the Cu-loop. The rms value of ϵ causes an alternating current I_{rms} to be induced into the loop. Consequently, the loss can be computed as

$$P_{\mathrm{loop}} = \epsilon_{\mathrm{rms}} I_{\mathrm{rms}} = \frac{\epsilon_{\mathrm{rms}}^2}{R_{\mathrm{loop}}} = \frac{\epsilon_{\mathrm{rms}}^2}{\rho_{\mathrm{cu}} \frac{l_{\mathrm{loop}}}{A_{\mathrm{cuwire}}}}, \tag{5.2}$$

where ρ_{cu} is the copper wire resistivity, l_{loop} the loop perimeter and A_{cuwire} the area of wire's cross-section.

Small error is introduced as the ends of the loop were soldered together, but the effect was expected to be negligible as the computed resistance of joint[3] is in the range of 2 $\mu\Omega$. The computed resistance for the Cu-loop was 19 mΩ. The measured and computed losses for this sample are shown in figure 5.10. The system seems to work correctly as the predicted and measured values are in good agreement. Next, a benchmark measurement for a HTS conductor was performed.

The second sample to be tested was a BSCCO tape previously characterized in SAS. The sample is displayed in figure 5.9 as item B). Both measurement systems work in the same principle, but as the systems differ in construction, the operation frequencies available generally do not match. However, both system are able to operate at 72 Hz frequency allowing a direct comparison of the results. Furthermore, these measurements were performed in LN_2 without the cryostat structure. The results are illustrated in figure 5.11. The results of this benchmark measurement show good correlation verifying the proper operation of our system.

Experiments with the conduction-cooled cryostat were started by measuring the losses dissipated in the cryostat structures. For this test, the system was cooled to the lowest reachable sample space temperature. During this test,

[3]Bulk solder resistivity at 77 K is 30 $\mu\Omega$mm [18, App 8.1], conduction length i.e. wire separation 0.1 mm, and cross-section, i.e. joint length times conductor diameter, 5·0.25 mm^2

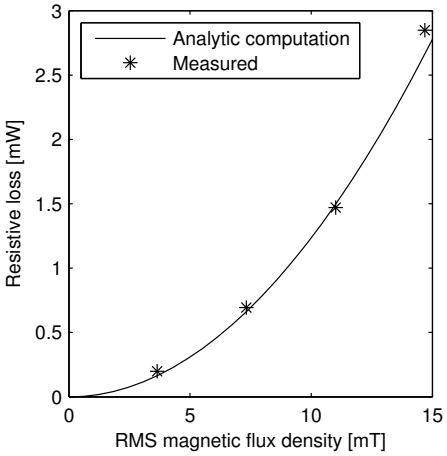

Figure 5.10: Power dissipated due to AC-losses in closed rectangular Cu-loop.

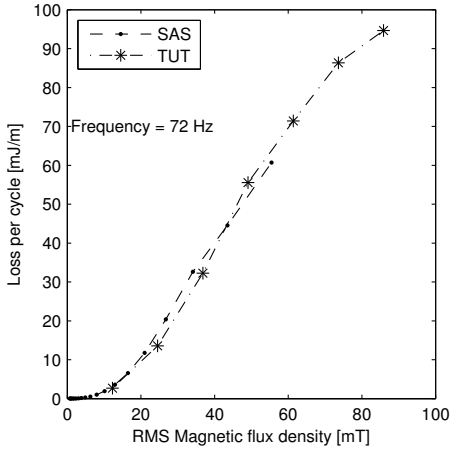

Figure 5.11: AC-loss measured at SAS and TUT for a BSCCO reference sample.

it was discovered that the approach chosen in thermally connecting the sample holder to the cryocooler was inadequate. The lowest temperature reached with the system was 15.5 K in sample space and 6.98 K in the 2nd stage. Therefore, it was not possible to characterize NbTi wires. Also, the opening used for accessing the sample space consistently developed a vacuum leak after 2-2.5 operation hours. These challenges and possible solutions are discussed further in the next section 5.6.

Regardless of the failures in reaching LTS temperatures and leaks in the vacuum seals, the losses of the cryostat and a multifilamentary MgB_2 conductor were successfully measured. With careful preparations, it was possible to obtain sufficient amount of data before the insulating vacuum failed. The losses measured and computed for the MgB_2 sample are reported in figure 5.12. Sample dimensions and current transport properties were listed in the previous Chapter in table 4.1, and the cross-section is presented in figure 2.2(B).

An attempt was also made to obtain measurement results for a second MgB_2 sample. However, during a verification measurement performed with empty sample space implied a significant increase in the losses of the empty cryostat. Further analysis was done and it was determined the coil system did not behave as expected. This implied that the coil system had sustained damage and further measurements were not possible. This topic is discussed further in the next section 5.6.

Based on these three experiments, it can be concluded that the system is

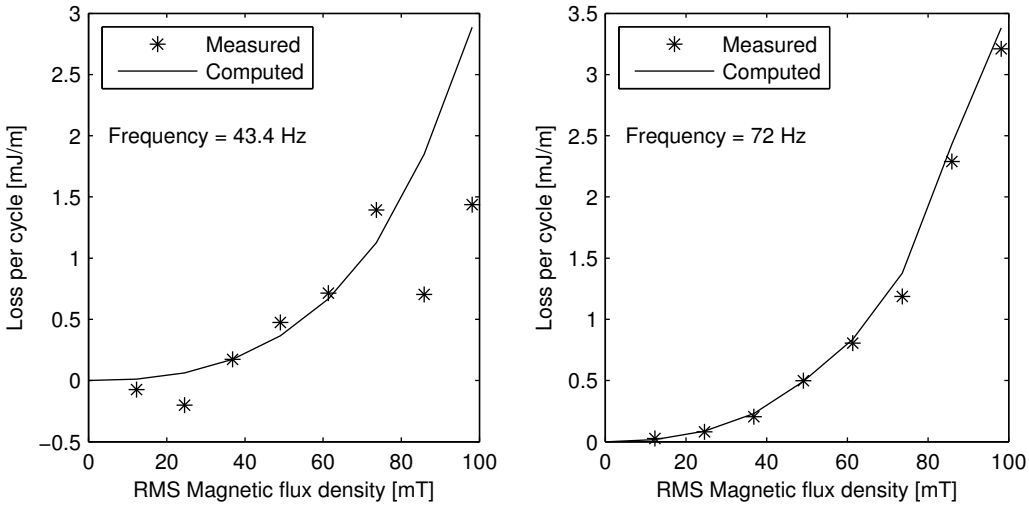

Figure 5.12: Measured and computed AC-loss for 18-filament, copper sheathed MgB_2 conductor. Sample length in measurements was 90 mm.

capable of measuring the AC-loss of MgB_2 and HTS superconductors. However, there are still challenges that require solutions before the system can be declared operational. In the next section I discuss these challenges and required improvements in more detail.

5.6 Lessons learned and solutions for experienced difficulties

Considerable difficulties were experienced in the operation of the measurement system. Even with the careful planning presented here, some of the chosen approaches were discovered to be problematic. This section discusses the discovered challenges and suggests solutions for overcoming them. However, due to time constraints, all of the solutions could not be tested with the real setup.

5.6.1 Excitation coils

Initially, it was considered that winding the coils from a Litz-cable compacted to rectangular cross-section, would be beneficial in achieving high fill-factor and thus coil current density. However, the coil wire provided by an European supplier proved do be of poor quality as even before winding short circuits

between the supposedly insulated strands were observed. It should have been obvious that winding the coils from cable with compromised insulations was a poor choice. Before this project, I only had experience from DC-magnets with less stringent demands for the quality of insulation. Therefore it was deemed adequate that before the winding there were a few intact wires in the Litz-cable. The finished coils also contained at least one insulated wire usable as the pick-up coil.

During the first AC-tests it, was observed that the coils generated more losses than expected. These losses were caused by induced currents flowing in the winding due to the compromised insulations. These losses also proved to be a challenge for the AC-loss measurement, as the losses are registered by the system similarly to the losses generated in the sample. Therefore even a small imbalance in the losses between the two coils is interfering with the measurement. I must emphasize that, the differences between the two coils are extremely small, as the loss voltage signal registered due to this imbalance observed after the anti-series connection of pick-up coils was in the order of 10 mV, or $\sim$ 0.1% of the voltage induced over one pick-up coil. In other words, even 99.9% identical coils do not guarantee a succesful measurement, if the pick-up voltage is used as the criterion.

While valid data was obtained with the system, the system baseline, caused by the inherent imbalance, caused challenges even with the high AC-loss BSCCO and MgB_2 conductors. The baseline interferes with the measurement accuracy as it increases the signal level input to the LIA. This in turn reduces the sensitivity of the LIA as the input and output gains have to be limited to prevent the signal path from overloading. Reducing the sensitivity also reduces the number of significant digits thus making it difficult to detect small changes in the power balance. It is possible, that the low loss LTS conductors could not have been measured due to the high baseline. This, among the aspects discussed in the previous and in the following paragraphs, also implies the necessity of new excitation coils.

As noted, the coil system experienced an unknown failure during an attempt to measure the second MgB_2 sample. A loud snapping sound was heard from the system during a routine removal of the conduction-cooled cryostat for background signal verification. In the following measurements, the failure was detected by comparing the output of the coil system without the conduction-cooled cryostat to the results obtained during previous days. Comparison of this background loss with measurements made during four different days are presented in figure 5.13. It is evident, that some event in the coil system significantly shifted the balance of the system. The energies on the right hand

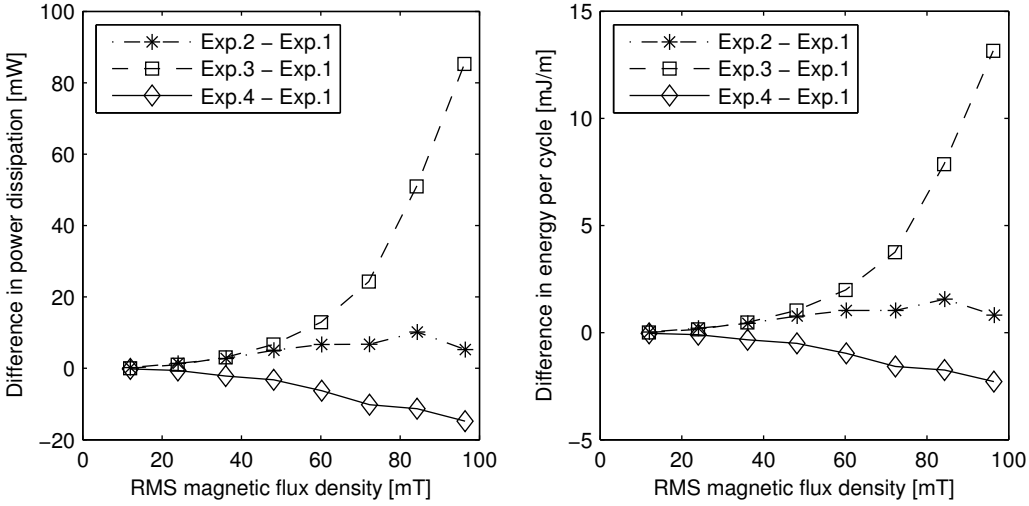

Figure 5.13: Observed difference in coil system output signal using experiment day 1 as reference. On left side difference in measured power dissipation is presented, at right side power dissipation is converted to energy. For right side hypotethical sample length 90 mm was used to enable direct comparison to figure 5.12. System was operated at 72 Hz frequency

side are larger than, or comparable to, the losses reported in figure 5.12. Further measurements are therefore impossible as the system baseline does not remain constant. Possibly the shift was caused by a release of tension by severe cracking of impregnation epoxy, which resulted in wire motion or short circuit during measurement.

The considered solution for this challenge is to construct a new set of coils. With the new coils, the rectangular cross-section cable should not be used. Instead a round cable with insulated strands should be used. This approach removes the step used in forming the rectangular cross-section reducing the likelihood of insulation damages. Also, a stringent requirement for insulation quality and integrity must be placed for the cable supplier. Additional improvement would be to abandon the simple race-track geometry used in the coils. Instead two sets of split-pair racetracks could be used. This configuration increases the surface area of the coils exposed to the LN_2 thus improving thermal management and stabilizing coil temperature.

However, it should be noted that in DC use, there were no problems with the coils. Thus, the short circuits are not between different layers or turns as this would have been detected when the coil constant was determined with a DC measurement. In these tests, both of the coils showed similar bore magnetic

flux density distributions. Therefore, there has to be defects in the coil wire itself creating short circuits between the strands of the Litz wire.

5.6.2 Vacuum leaks in the conduction-cooled cryostat

While considerable effort was taken in minimizing the change of vacuum leaks in the non-conducting components, they were not completely avoided. We experienced leaks in two different locations, at the joint between the sample space and cryostat (figure 5.6) and at the sample space lid. The main cause in both leaks was discovered to be the same i.e. the O-ring seals used at these locations failed after prolonged exposure to temperatures below 0 °C.

The interface between the sample space and the cryostat illustrated in figure 5.6 was problematic from the beginning. The joint contained several small nylon screws used for clamping tight the seal. However, these screws were not strong enough for exerting enough pressure to the sealing o-ring. After replacing the screws with larger ones, the situation improved slightly, but leak tightness in prolonged operation was not achieved. Only after replacing the NBR-rubber O-ring with solid PTFE one, and substituting the nylon screws with ones fabricated from PEEK-plastic, was the interface found to be operational.

The failure of the sample space lid was more subtle and difficult to detect. Failure of the vacuum seal on this location initially only presented itself an increase in sample space temperature and the system could operate at this elevated temperature for a long period of time. No changes were observed in vacuum gauge located a considerable distance away from the cryostat. This behavior was different from the leaks described in the previous paragraph, as that location failed in a much more aggressive manner i.e. the insulating vacuum was lost in a few minutes. The source of the leak was discovered after careful observation of the cryostats top surface. Manipulation of the lid showed that at the O-ring had become rigid therefore losing its sealing ability.

A repair attempt for the cryostat lid was made by placing screws to the four corners of the lid. Slight improvement in the system operation time was observer, but the problem still persisted. The likely cause for this was the nylon screws used in fixing the sample space lid. Nylon screws had to be used as this fix was made during a day between measurements, and using metallic screws might have shifted the system background. Before a new measurement series, the plastic screws will be replaced with stainless steel ones and the o-ring material will be changed.

5.6.3 Insufficient cooling capacity

The lowest obtained temperature of the sample holder was too high for characterizing NbTi. To reach the design goal below T_c of NbTi, i.e. 9 K, modifications for the cooling pathways are required. Currently, the 160 copper strands with ⌀0.25 mm are used in the pathways, providing only 7.8 mm^2 of conduction area for the length of approximately 350 mm between the cryocooler 2nd stage and the ceramic sample holder. The resulting thermal conductance proved to be challenging to estimate, as the purity of the wire material, and thus the thermal conductivity, is unknown. The observation suggest, that it was significantly lower than expected. For the design, material properties of residual resistivity ratio (RRR) 100 were used while the observations suggest the actual RRR to be less than 80. As an example, the corresponding heat transfer rates from 6.5 K to 10 K, with the specified cross-section and length, are 121 and 96 mW, respectively. The realized heat transfer rate is therefore approximately 20% lower than expected.

Improving the situation can be achieved by re-designing the thermal pathways. The suggested solution uses rigid thermal pathways from the cryocooler to the edge of the sample space. The pathways should have a rectangular cross-section of 2x4 mm^2 each, with a total number of four pathways. The long edge should be aligned parallel to the magnetic field lines. The new pathway should be manufactured from copper having RRR more than 100. The original flexible and subdivided wire bundles are used for interfacing with the ceramic sample holder. The two components should be connected together with a pressed joint that can be taken apart for sample change.

The new solution has a total cross-section of 32 mm^2 for the 215 mm long rigid thermal pathways. The flexible wire bundles have the same cross-section of 7.8 mm^2 but length is reduced to 110 mm. The reduction in the overall length is due to the added joint allowing slack to be taken off the flexible conductors. With these parameter, the heat rate transferable from 6.5 K to 10 K increases to 220 mW. Considering the use with LTS, heat rate from 6 K to 8 K can be computed to be 108 mW.

The down side of the new solution is the increase in eddy current losses. FEM simulations performed at maximum flux density and 139.25 Hz frequency for the planned rigid thermal pathway predicted an eddy current loss of 77 mW for each of the four components. Fortunately the loss is distributed and not localized at uncooled end. It is however, possible that the eddy current losses become an issue near the bottom temperature and the coil current has to be reduced. Further, this loss needs to be compensated in the measurement

system as it appears only for one of the coils.

5.7 Remarks

In principle, the calibration free AC-loss measurement is simple. However, the realization of one at conduction-cooled environment proved to be challenging. Even small imperfections in the system result in significant imbalance in the power of the excitation coil system. This imbalance, the system baseline, has a significant effect on the measurement sensitivity. Also, defects in the excitation coils manifested as unpredictable behavior and ultimately made the coil system unusable.

If the system was designed from the beginning, the experienced challenges could have been avoided. The process described in this Chapter illustrates the complicated nature of designing a sensitive scientific apparatus. Even with care and planning taken in this project, the realized system proved to be a initial prototype at best.

However, some of the minor challenges, like the vacuum leak from the seam between the cryostat bottom and sample space, were successfully corrected. For the others, there are viable solutions. Unfortunately, due to time constraints they could not be implemented and tested in the scope of this thesis. Currently the major challenge can be found from the excitation coil system, the most crucial component defining the overall sensitivity of the system. For the coil system, there are no simple fixes. Before further measurements can be performed with the system, new coils must be manufactured. Also, it remains to be seen if NbTi samples can be tested.

Chapter 6

Conclusions

Short sample characterization measurements are the basic tests used for assessing the quality and properties of superconducting wires. The data obtained from the short sample tests are necessary for developing technical superconductors, as a starting point in superconductive system design and as a quality control instrument. Obtaining valid data is therefore crucial.

Conduction-cooling allows the fabrication of dry cryogenic systems cooled with a cryocooler. In these systems, the superconductive component is connected to a thermal interface used for conducting heat to the cryocooler. The advantage of such systems is the simplicity of use. With dry systems, there is no need for cryogenic fluids. Instead, it is possible to construct plug-and-play devices which only require electric power and coolant, water or air, to operate.

In the previous chapters I discussed and demonstrated the positive and negative aspects related to utilizing conduction-cooling in the characterization measurements. The limited cooling capacity was demonstrated to have an effect on the accuracy of the $V(I)$-measurement, if proper precautions are not taken. On the other hand, the nearly adiabatic conditions obtained with a conduction-cooled approach allowed the elimination of the effects caused by convective cooling in the quench propagation and initiation measurements.

For obtaining valid data with a conduction-cooled system, it was demonstrated how the design of the sample holder is a key issue. Also, the considerations of constructing a conduction-cooled cryostat were discussed. In conduction-cooled systems, controlling the heat leaks from ambient temperature to the sample space was shown to be important.

The design process of a cryogenic system, and its difficulties, were discussed using the AC-loss measurement system as an example. It was shown, how the

initial specifications were used in defining the materials and structures of the device. Further, the challenges faced in using materials not commonly used in cryogenic engineering were presented and analyzed.

If the development of the MgB_2 superconductive wires progresses so that they become a competitive alternative to LTS in applications with low to medium strength magnetic fields, it is possible that the application of conduction-cooling will increase in the future. The required operation temperature is easily reached with a cryocooler offering a robust system with a need of very little maintenance.

This thesis consists of six peer-reviewed publications. The outcome of each publication is shortly summarized next.

Publication 1: The quench propagation and initiation at supercritical currents was studied in a conduction-cooled system. With HTS and MgB_2 conductors, it is possible to exceed the I_c for short periods of time. Until now, there has been little research on the thermal stability under such conditions.

Publication 2: Diodes are commonly used for measuring cryogenic temperatures, and a standard Si-diode is known to function as a temperature sensor. However, prior to this publication these common rectifier diodes have not been used for temperature measurements below 50 K. In this publication, the behavior of BAS16 rectifier diode as an interchangeable temperature sensor was studied at temperatures between 15 and 50 K.

Publication 3: Controlling resistive losses is important in conduction-cooled systems as the cooling capacity in such systems is limited. For helping in the design of a conduction-cooled system, this publication presents the computational tools for studying resistive lap-joints between superconducting strands, backed with experimental evidence.

Publication 4: In a conduction-cooled system, the sample holder has to provide interfaces for current supply connection and cooling down the sample, and support the sample against Lorenz forces. In this publication, the aspects of a current/cooling contact used in a conduction-cooled are analyzed. Furthermore, in a short sample testing system, this type of contact can be formed by pressing two surfaces firmly together. The electrical resistance of such joints was studied computationally and experimentally.

Publication 5: The rectifier diodes from **Publication 2** were consider to be suitable for monitoring changes in temperature. For this publication, the sensor response time was improved and magnetic field response measured. Also, the sensors were demonstrated in a thermal stability measurement.

Publication 6: Typically, a conduction-cooled system contains large amount of copper used in the thermal couplings. Therefore, when such a system is experiences alternating magnetic fields, eddy current losses are induced. In this publication, it was shown that it is possible to construct a conduction-cooled cryostat with low AC-losses. The resulting cryostat was successfully demonstrated in a magnetization AC-loss measurement.

Bibliography

[1] Agilent Technologies (Nov. 2014 onwards Keysight Technologies). *Electronic Test & Measurement*. `http://www.agilent.com/` [cited 3.5.2014].

[2] Ansys. *Engineering simulation software*. `http://www.ansys.com/` [cited 30.1.2014].

[3] Autodesk. *Inventor - 3D CAD software for mechanical design*. `http://www.autodesk.com/products/autodesk-inventor-family/overview` [cited 30.1.2014].

[4] N H Balshaw. *Practical Cryogenics*. Oxford Instruments Superconductivity Limited, 2001.

[5] J. G. Bednorz and K. A. Müller. Possible high T_c superconductivity in the Ba-La-Cu-O system. *Z. Phys. B Con. Mat.*, 64:189–193, 1986. 10.1007/BF01303701. doi:10.1007/BF01303701.

[6] Ceramic Substrates & Components Ltd. `http://www.ceramic-substrates.co.uk` [cited 16.4.2014].

[7] W.-K. Chan, P.J. Masson, C. Luongo, and J. Schwartz. Three-dimensional micrometer-scale modeling of quenching in high-aspect-ratio $YBa_2Cu_3O_{7-\delta}$ coated conductor tapes - part i: Model development and validation. *IEEE Trans. Appl. Supercond.*, 20(6):2370–2380, Dec 2010. doi:10.1109/TASC.2010.2072956.

[8] W.-K. Chan and J. Schwartz. Three-dimensional micrometer-scale modeling of quenching in high-aspect-ratio $YBa_2Cu_3O_{7-\delta}$ coated conductor tapes - part ii: Influence of geometric and material properties and implications for conductor engineering and magnet design. *IEEE Trans. Appl. Supercond.*, 21(6):3628–3634, Dec 2011. doi:10.1109/TASC.2011.2169670.

[9] Comsol Multiphysics. *Software solutions for multiphysics modeling*. `http://www.comsol.com/` [cited 30.1.2014].

[10] CONNECTUS. *Consortium of European companies determined to use superconductivity.* `http://www.conectus.org/` [cited 6.2.2014].

[11] T. Coombs, A.M. Campbell, R. Storey, and R. Weller. Superconducting magnetic bearings for energy storage flywheels. *IEEE Trans. Appl. Supercond.*, 9(2):968–971, June 1999. doi:10.1109/77.783459.

[12] Cryomech. *Cryorefrigerator design and manufacturing.* `http://www.cryomech.com/` [cited 6.2.2014].

[13] Curbell plastics. *PEEK-datasheet.* `http://www.curbellplastics.com/technical-resources/pdf/peek-datasheet-curbell.pdf` [cited 28.4.2014].

[14] Dassault Systems. *SolidWorks - 3D CAD software.* `http://www.solidworks.com/` [cited 30.1.2014].

[15] A. Devred. Quench origins. *AIP Conference Proceedings*, 249(2):1262–1308, 1992. doi:10.1063/1.41993.

[16] Dictionary.com Unabridged. Feb 2013. `http://dictionary.reference.com/` [cited 6.2.2013].

[17] W. J. Dixon and A. M. Mood. A method for obtaining and analyzing sensitivity data. *J. Amer. Statist. Assoc.*, 43(241):pp. 109–126, 1948. doi:10.2307/2280071.

[18] J. W. Ekin. *Experimental Techniques for Low-Temperature Measurements.* Oxford: Oxford University Press, 2006.

[19] A. Godeke, M. Dhalle, A. Morelli, L. Stobbelaar, H. van Weeren, H. J. N. van Eck, W. Abbas, A. Nijhuis, A. den Ouden, and B. ten Haken. A device to investigate the axial strain dependence of the critical current density in superconductors. *Rev. Sci. Instrum.*, 75(12):5112–5118, 2004. doi:10.1063/1.1819384.

[20] W. Goldacker, S.I. Schlachter, J. Reiner, S. Zimmer, A. Nyilas, and H. Kiesel. Mechanical properties of reinforced MgB_2 wires. *IEEE Trans. Appl. Supercond.*, 13(2):3261 – 3264, june 2003. doi:10.1109/TASC.2003.812218.

[21] L.F. Goodrich and S.L. Bray. Current ripple effect on superconductive d.c. critical current measurements. *Cryogenics*, 28(11):737 – 743, 1988. doi:10.1016/0011-2275(88)90137-3.

[22] L.F. Goodrich and S.L. Bray. High tc superconductors and critical current measurement. *Cryogenics*, 30(8):667 – 677, 1990. doi:10.1016/0011-2275(90)90229-6.

[23] L.F. Goodrich and S.L. Bray. Integrity tests for high-tc and conventional critical-current measurement systems. *Adv. Cryog. Eng. Mat.*, 36:43–50, 1990. doi:10.1007/978-1-4613-9880-6_6.

[24] L.F. Goodrich, J.W. Ekin, and F.R. Fickett. Effect of twist pitch on short-sample v-i characteristics of multifilamentary superconductors. *Adv. Cryog. Eng. Mat.*, 28:571–580, 1982. doi:10.1007/978-1-4613-3542-9_57.

[25] L.F. Goodrich and F.R. Fickett. Critical current measurements: A compendium of experimental results. *Cryogenics*, 22(5):225 – 241, 1982. doi:10.1016/0011-2275(82)90120-5.

[26] L.F. Goodrich, L.T. Medina, and T.C. Stauffer. High critical-current measurements in liquid and gaseous helium. *Adv. Cryog. Eng. Mat.*, 44:873–880, 1998. doi:10.1007/978-1-4757-9056-6_115.

[27] L.F. Goodrich, A.N. Srivastava, and T.C. Stauffer. Simulators of superconductor critical current - design, characteristics, and applications. *J. Res. Natl. Inst. Stand. Technol.*, 96(6):703–724, 11-12 1991. `http://www.archive.org/details/jresv96n6p703`.

[28] L.F. Goodrich and T.C. Stauffer. Hysteresis in transport critical-current measurements of oxide superconductors. *J. Res. Natl. Inst. Stand. Technol*, 106(4):657–690, July-August 2001. doi:10.6028/jres.106.031

[29] F. Grilli, E. Pardo, A. Stenvall, D.N. Nguyen, Weijia Yuan, and F. Gomory. Computation of losses in hts under the action of varying magnetic fields and currents. *IEEE Trans. Appl. Supercond.*, 24(1):78–110, Feb 2014. doi:10.1109/TASC.2013.2259827.

[30] E. Härö, J. Järvelä, and A. Stenvall. Variation of quench propagation velocities in YBCO cables. *Presented in Applied Superconductivity Conference 10-15.8.2014, Charlotte, NC, USA.* Submitted to *IEEE Trans. Appl. Supercond.*

[31] I. Hiltunen, A. Korpela, H. Laine, J. Lehtonen, M. Lyly, and R. Mikkonen. Measured performance of different solders in Bi2223/Ag current leads. *IEEE Trans. Appl. Supercond.*, 18(2):1427 –1430, june 2008. doi:10.1109/TASC.2008.920618.

[32] I. Hiltunen, J. Lehtonen, R. Mikkonen, and A. Stenvall. Method to determine critical current of poorly cooled short sample. *Physica C*, 469(22):1987 – 1990, 2009. doi:10.1016/j.physc.2009.07.007.

[33] I. Hiltunen, J. Lehtonen, A. Stenvall, and R. Mikkonen. Influence of self-heating on measured *n*-value. *IEEE Trans. Appl. Supercond.*, 20(3):1597 –1600, june 2010. doi:10.1109/TASC.2010.2042156.

[34] Y. Iwasa *Case Studies in Superconducting Magnets.* New York NY: Springer Science+Business Media, 2nd. edition, 2009.

[35] IEEE-SA. IEEE standard for high-voltage testing techniques. *IEEE Std 4-2013 (Revision of IEEE Std 4-1995)*, pages 1–213, 2013. doi:10.1109/IEEESTD.2013.6515981.

[36] Eckels Engineering Inc. Cryo comp software v.5.2, 2012.

[37] J. Järvelä., A. Stenvall, and R. Mikkonen. Considerations for designing a conduction-cooled sample holder. *IEEE Trans. Appl. Supercond.*, 23(2):9500309, April 2013. doi:10.1109/TASC.2012.2237511.

[38] Y. Kamihara, T. Watanabe, M. Hirano, and H. Hosono. Iron-based layered superconductor La[O1-xFx]FeAs (x = 0.05-0.12) with $T_c = 26$ K. *J. Am. Chem. Soc.*, 130(11):3296–3297, 2008. doi:10.1021/ja800073m.

[39] J. E. Kunzler, E. Buehler, F. S. L. Hsu, and J. H. Wernick. Superconductivity in Nb_3Sn at high current density in a magnetic field of 88 kgauss. *Phys. Rev. Lett.*, 6:89–91, Feb 1961. doi:10.1103/PhysRevLett.6.89.

[40] C. Lacroix, J.-H. Fournier-Lupien, K. McMeekin and F. Sirois. Normal zone propagation velocity in 2G HTS coated conductor with high interfacial resistance. *IEEE Trans. Appl. Supercond.*, 23(3):4701605, June 2013. doi: 10.1109/TASC.2013.2239696

[41] The method was suggested by the pre-examiner C. Lacroix in his report on this thesis' manuscript.

[42] Lake Shore Cryotronics. *Instructions, Cernox Resistance Temperature Sensor Installation, Model CX-10XX-AA Package.* `http://www.lakeshore.com/Documents/F014-00-00.pdf` [cited 28.4.2014].

[43] Lake Shore Cryotronics. *Instructions, Cernox Resistance Temperature Sensor Installation, Model CX-10XX-SDPackage.* `http://www.lakeshore.com/Documents/F017-00-00.pdf` [cited 28.4.2014].

[44] Lake Shore Cryotronics. *Measurement and control solutions.*, 8 2012. `http://www.lakeshore.com` [cited 23.8.2012].

[45] J. Lehtonen, R. Mikkonen, and J. Paasi. A numerical model for stability considerations in HTS magnets. *Supercond. Sci. Tech.*, 13(3):251, 2000. doi:10.1088/0953-2048/13/3/301.

[46] Y. Lvovsky, E. W. Stautner, and T. Zhang. Novel technologies and configurations of superconducting magnets for MRI. *Supercond. Sci. Tech.*, 26(9):093001, 2013. doi:10.1088/0953-2048/26/9/093001.

[47] N. Magnusson and S. Hörnfeldt. Calorimetric apparatus for alternating current loss measurements on high-temperature superconductors. *Rev. Sci. Instrum.*, 69(9):3320–3325, 1998. doi:10.1063/1.1149096.

[48] A.P. Martinelli and S.L. Wipf. Investigation of cryogenic stability and reliability of operation of Nb_3Sn coils in helium gas environment. *IEEE Proc. Appl. Superconduc. Conf., Annapolis, 1972*, page 331, 1973.

[49] E. Martínez, F. Lera, M. Martínez-López, Y. Yang, S I Schlachter, P Lezza, and P Kováč. Quench development and propagation in metal/MgB_2 conductors. *Supercond. Sci. Tech.*, 19(1):143, 2006. doi:10.1088/0953-2048/19/1/024.

[50] E. Martínez, E. A. Young, M. Bianchetti, O. Mu noz, S I Schlachter, and Y Yang. Quench onset and propagation in cu-stabilized multifilament MgB_2 conductors. *Supercond. Sci. Tech.*, 21(2):025009, 2008. doi:10.1088/0953-2048/21/02/025009.

[51] M. Masti, J. Lehtonen, R. Perälä, W. Nah, and J. Kang. Comparison of voltage-current characteristics of high quality Bi-2223 tapes with hall-sensor measurements and computed current density distributions. *Physica C*, 401(1-4):155 – 159, 2004. doi:10.1016/j.physc.2003.09.028.

[52] K.-H. Mess, P. Schmüser, and S. Wolff. *Superconducting accelerator magnets*. Singapore: World Scientific Publishing, 1996.

[53] R Mikkonen, T Kalliohaka, A Korpela, J Lehtonen, and R Perälä. A 0.2 mj cryogen free Nb_3Sn smes in UPS application. *Supercond. Sci. Tech.*, 16(8):946, 2003. doi:10.1088/0953-2048/16/8/321.

[54] J. Nagamatsu, N. Nakagawa, T. Muranaka, Y. Zenitani, and J. Akimitsu. Superconductivity at 39 K in magnesium diboride. *Nature*, 410:63–64, March 2001. doi:10.1038/35065039.

[55] National Instruments. *LabVIEW System Design Software*. http://www.ni.com/labview/ [cited 16.4.2014].

[56] S. Nishijima, S. Eckroad, A. Marian, K. Choi, W. S. Kim, M. Terai, Z. Deng, J. Zheng, J. Wang, K. Umemoto, J. Du, P. Febvre, S. Keenan, O. Mukhanov, L. D. Cooley, C. P. Foley, W. V. Hassenzahl, and M. Izumi. Superconductivity and the environment: a roadmap. *Supercond. Sci. Tech.*, 26(11):113001, 2013. doi:10.1088/0953-2048/26/11/113001.

[57] Nobel Media. *All Nobel Prizes in Physics*. http://www.nobelprize.org/nobel_prizes/physics/laureates/ [cited 25.4.2014].

[58] AGA OY A Member of Linde Group. Specialty gas - private communication, 3 2014.

[59] Oxford Instruments plc. http://www.oxford-instruments.com/ [cited 16.4.2014].

[60] Paramed medical systems. *The MROpen MRI-system*, 4 2014. http://www.paramedmedicalsystems.com/medical-systems/open-sky-0000111.html [cited 22.4.2014].

[61] R. L. Powell and A. A. Aboud. Electrical contact resistance of copper-copper junctions at low temperatures. *Rev. Sci. Instrum.*, 29(3):248–249, 1958. doi:10.1063/1.1716164.

[62] J. J. Rabbers, B. ten Haken, and H. H. J. ten Kate. Advanced ac loss measurement methods for high-temperature superconducting tapes. *Rev. Sci. Instrum.*, 72(5):2365–2373, 2001. doi:10.1063/1.1367361.

[63] M. Razeti, S. Angius, L. Bertora, D. Damiani, R. Marabotto, M. Modica, D. Nardelli, M. Perrella, and M. Tassisto. Construction and operation of cryogen free MgB_2 magnets for open mri systems. *IEEE Trans. Appl. Supercond.*, 18(2):882–886, June 2008. doi:10.1109/TASC.2008.920661.

[64] A.P. Rijpma and H.J.M. ter Brake. Cryogenic thermometry with a common diode: Type BAS16. *Cryogenics*, 46(1):68 – 69, 2006. doi:10.1016/j.cryogenics.2005.11.009.

[65] H. Rogalla and P. H. Kes, editors. *100 years of superconductivity*. CRC Press, 2012.

[66] C. Schmidt. The induction of a propagating normal zone (quench) in a superconductor by local energy release. *Cryogenics*, 18(10):605 – 610, 1978. doi:10.1016/0011-2275(78)90188-1.

[67] C. Schmidt, K. Itoh, and H. Wada. Second VAMAS a.c. loss measurement intercomparison: a.c. magnetization measurement of hysteresis and coupling losses in NbTi multifilamentary strands. *Cryogenics*, 37(2):77 – 89, 1997. doi:10.1016/S0011-2275(96)00110-5.

[68] B. Seeber, D. Uglietti, V. Abächerli, P.-A. Bovier, D. Eckert, G. Kübler, P. Lezza, A. Pollini, and R. Flükiger. Critical current versus strain measurement up to 21t and 1000a of long length superconducting wires and tapes. *Rev. Sci. Instrum.*, 76(9):–, 2005. doi:10.1063/1.2018608.

[69] NXP semiconductors. Package outline - sot23. `http://www.nxp.com/documents/outline_drawing/sot023_po.pdf`.

[70] K. Seo, M. Morita, S. Nakamura, T. Yamada, and Y. Jizo. Minimum quench energy measurement for superconducting wires. *IEEE Trans. Magn.*, 32(4):3089–3093, 1996. doi:10.1109/20.511529.

[71] Signal Recovery - Part of AMETEK Advanced Measurement Technology. `http://www.signalrecovery.com/` [cited 16.4.2014].

[72] Slovak Academy of Sciences. *Institute of Electrical Engineering, Superconductor Physics*. `http://www.elu.sav.sk/en-oddelenia/fyziky-supravodicov.html` [cited 28.4.2014].

[73] A. Stenvall. *An Electrical Engineering Approach to the Stability of MgB_2 Superconductor*. PhD thesis, Tampere University of Techonolgy, 2008.

[74] A. Stenvall, A. Korpela, J. Lehtonen, and R. Mikkonen. Formulation for solving 1D minimum propagation zones in superconductors. *Physica C*, 468(13):968 – 973, 2008. doi:10.1016/j.physc.2008.04.011.

[75] A. Stenvall, R. Mikkonen, and P. Kováč. Comparison of 1d, 2d and 3d quench onset simulations. *Physica C: Superconductivity*, 470(22):2047 – 2050, 2010. doi:10.1016/j.physc.2010.09.010.

[76] Sumitomo Heavy Industries. *Cryogenics Group - Cryocoolers, Pulse Tubes, Cryopumps and Compressors*. `http://www.shicryogenics.com/` [cited 6.2.2014].

[77] Sumitomo Heavy Industries. *RDK-408S2 10K Cryocooler Series*. `http://www.shicryogenics.com/products/specialty-cryocoolers/rdk-408s2-10k-cryocooler-series/` [cited 3.5.2014].

[78] Tektronix. *Test and measurement equipment.* `http://www.tek.com/` [cited 16.4.2014].

[79] J. Šouc, F. Gömöry, and M. Vojenčiak. Calibration free method for measurement of the ac magnetization loss. *Supercond. Sci. Tech.*, 18(5):592, 2005. doi:10.1088/0953-2048/18/5/003.

[80] Vishay. *Thermal management in surface-mounted resistor applications.* Technical report, Vishay Beyschlag, February 2011. `http://www.vishay.com/docs/28844/tmismra.pdf`.

[81] M. Vojenčiak. *Influence of ferromagnetic material on performance of high temperature superconductor in form of tape.* PhD thesis, Slovak Academy of Sciences, Institute of Electrical Engineering, 2010.

[82] M. Vojenčiak, F. Grilli, A. Stenvall, A. Kling, and W. Goldacker. Influence of the voltage taps position on the self-field DC and AC transport characterization of HTS superconducting tapes. *Cryogenics*, 57(0):189 – 194, 2013. doi:10.1016/j.cryogenics.2013.08.001.

[83] H. Wada, C.R. Walters, L.F. Goodrich, and K. Tachikawa. Vamas intercomparison of critical current measurements on nb3sn superconductors: A summary report. *Cryogenics*, 34(11):899 – 908, 1994. doi:10.1016/0011-2275(94)90076-0.

[84] M. N. Wilson. *Superconducting magnets.* Oxford: Oxford University Press, 1983.

[85] M.N. Wilson and Y. Iwasa. Stability of superconductors against localized disturbances of limited magnitude. *Cryogenics*, 18(1):17 – 25, 1978. doi:10.1016/0011-2275(78)90132-7.

[86] R. Yamada, E. Marscin, Ang Lee, M. Wake, and J.-M. Rey. 2-d/3-d quench simulation using ANSYS for epoxy impregnated Nb_3Sn high field magnets. *IEEE Trans. Appl. Supercond.*, 13(2):1696–1699, June 2003. doi:10.1109/TASC.2003.812870.

[87] H.-K. Yeom, Y.J. Hong, S.J. Park, T.-B. Seo, K.C. Seong, and H-J Kim. Study of cryogenic conduction cooling systems for an hts smes. *IEEE Trans. Appl. Supercond.*, 17(2):1955–1958, June 2007. doi:10.1109/TASC.2007.898491.

Publication 1

Järvelä J, Stenvall, A and Mikkonen, R 2009
IEEE Trans. Appl. Supercond. **19** 3511
Quench development at supercritical currents in low n-value superconductors
doi:10.1109/TASC.2009.2018528

Publication 2

Järvelä J, Stenvall A, and Mikkonen R 2010
J. Phys.: Conf. Ser **234** 032026
Common rectifier diodes in temperature measurement applications below 50 K
doi:10.1088/1742-6596/234/3/032026

Publication 3

Järvelä J, Stenvall A, Mikkonen R and Rindfleisch M 2011
Cryogenics **51** 400
Contact resistance simulations and measurements of MgB_2-MgB_2 lap joints
doi:10.1016/j.cryogenics.2011.04.003

Publication 4

Järvelä J, Stenvall A and Mikkonen R 2013
IEEE Trans. Appl. Supercond. **23** 9500309
Considerations for designing a conduction-cooled sample holder
doi:10.1109/TASC.2012.2237511

Publication 5

Järvelä J, Stenvall A and Mikkonen R 2013
IEEE Trans. Appl. Supercond. **23** 9000305
Common rectifier diodes in thermal stability characterization measurements
doi:10.1109/TASC.2012.2231453

Publication 6

J. Järvelä, M. Lyly, A Stenvall, R. Juntunen, J. Šouc and R Mikkonen 2014
IEEE Trans. Appl. Supercond. Accepted for publication, August 20, 2014.
Design, fabrication and testing of a low AC-loss conduction-cooled cryostat for magnetization loss measurement apparatus
doi:10.1109/TASC.2014.2357754

Tampereen teknillinen yliopisto
PL 527
33101 Tampere

Tampere University of Technology
P.O.B. 527
FI-33101 Tampere, Finland

ISBN 978-952-15-3387-7
ISSN 1459-2045